Sublimation of water ice mixed with silicates and tholins: evolution of surface texture and reflectance spectra, with implications for comets

Olivier Poch[1]*, Antoine Pommerol[2], Bernhard Jost[2], Nathalie Carrasco[3,4], Cyril Szopa[3] and Nicolas Thomas[2]

[1] Center for Space and Habitability, Universität Bern, Sidlerstrasse, 5, 3012 Bern, Switzerland

[2] Physikalisches Institut, Universität Bern, Sidlerstrasse, 5, 3012 Bern, Switzerland

[3] Université Versailles St-Quentin ; Sorbonne Universités, UPMC Univ. Paris 06 ; CNRS/INSU, LATMOS-IPSL, 11 Boulevard d'Alembert, 78280 Guyancourt, France

[4] Institut Universitaire de France, 103 Bvd St-Michel, 75005 Paris, France

*To whom correspondence should be addressed:

Physikalisches Institut, Universität Bern

Sidlerstrasse, 5

CH-3012 Bern, Switzerland

olivier.poch@csh.unibe.ch

+44 31 631 33 93

Manuscript accepted for publication in *Icarus*

Abstract

The surfaces of many objects in the Solar System comprise substantial quantities of water ice sometimes mixed with minerals and/or organic molecules. The sublimation of the ice changes the structural and optical properties of these objects. We present laboratory data on the evolution of the structure and the visible and near-infrared spectral reflectance of icy surface analogues of cometary ices, made of water ice, complex organic matter (tholins) and silicates, as they undergo sublimation under low temperature (<-70°C) and pressure (10^{-5} mbar) conditions inside the SCITEAS simulation chamber. As the water ice sublimated, we observed *in situ* the formation of a porous sublimation lag deposit, or sublimation mantle, at the top of the ice. This mantle is a network of filaments made of the non-volatile particles. Organics or phyllosilicates grains, able to interact via stronger inter-particulate forces than olivine grains, can form a foam-like structure having internal cohesiveness, holding olivine grains together. As this mantle builds-up, the band depths of the sub-surface water ice are attenuated until complete extinction under only few millimeters of mantle. Optically thick sublimation mantles are mainly featureless in the near infrared. The absorption bands of the minerals present in the mantle are weak, or even totally absent if minerals are mixed with organics which largely dominate the VIS-NIR reflectance spectrum. During sublimation, ejections of large fragments of mantle, triggered by the gas flow, expose ice particles to the surface. The contrast of brightness between mantled and ice-exposed areas depends on the wavelength range and the dust/ice ratio considered. We describe how the chemical nature of the non-volatiles, the size of their particles, the way they are mixed with the ice and the dust/ice mass ratio influence the texture, activity and spectro-photometric properties of the sublimation mantles. These data provide useful references for interpreting remote-sensing observations of comets and also icy satellites or trans-neptunian objects.

Keywords: Ices; Comets, dust; Comets, nucleus; Trans-neptunian objects; Spectroscopy

1. Introduction

Sublimation of ices, the direct transition from solid to gas phase, is a significant process at the surface of many Solar System objects. It is particularly active on air-less bodies where ices are directly exposed to solar radiation. Examples include cometary nuclei, satellites of giant planets, objects of the outer Solar System, and even locally on some objects of the inner Solar System such as Mars, the Moon and Mercury. Sublimation is responsible for shaping these surfaces and changing their reflectance properties. Indeed, if the ice is initially mixed with refractory non-volatiles made of minerals, salts, or organics, its sublimation will produce a residue, or sublimation lag, consisting of an ice-free layer made of the non-volatiles. Understanding the consequences of the sublimation process on the structure and on the spectro-photometric properties of icy surfaces is of prime interest to interpret past, current and future remote sensing observations of these objects.

Sublimation and its resulting lag deposit are particularly important in the case of comets, because these ice-rich bodies approach the Sun periodically and a large amount of ice sublimes at each perihelion passages. The surfaces of comet nuclei appear to be largely covered with an extremely dark material which could be a result of sublimation (sublimation lag deposit, or dust layer formed by re-deposition of dust lifted by cometary activity), and/or a product of the irradiation of ices by cosmic rays and solar energetic particles (Hartmann *et al.*, 1987; Jewitt, 2015; Johnson *et al.*, 1988). This surface layer probably contains complex organic matter and mineral grains (Capaccioni *et al.*, 2015; Fomenkova, 1999; Jessberger *et al.*, 1989; Kuppers *et al.*, 2005). Therefore, studying in the laboratory the build-up and evolution of sublimation lag deposits consisting of similar materials may help to understand the properties of cometary surfaces, and by extension of other icy bodies (Jewitt *et al.* 2007).

Several laboratory simulations have already been performed in the past to study the sublimation of ices mixed with non-volatiles. In the 70's, at the Ioffe Institute in Leningrad and at the Institute of Astrophysics in Dushanbe, E. Kajmakov and co-workers prepared mixtures of ice and minerals and/or organics and observed the formation –and outbursts– of a porous ice-free matrix after sublimation of ices at 10^{-5}-10^{-6} mbar and 180-240 K (Dobrovolsky and Kajmakow, 1977). In the 80's, at the Jet Propulsion Laboratory in Pasadena, Saunders *et al.* (1986) studied the sublimation of water ice samples prepared from a suspension of phyllosilicates and later of other types of silicates, including also organic matter

(Storrs *et al.*, 1988). They noticed that some classes of phyllosilicates and organics were able to form fluffy Filamentary Sublimate Residues (referred to as "FSR"), whereas most classes of silicates were not. Later, in the 80's and 90's, the Comet Simulation (KOSI) project conducted a total of 11 experimental simulations over 7 years, considerably enhancing our understanding of the sublimation of cometary material (Ratke and Kochan, 1989; Thiel *et al.*, 1989 and see Sears *et al.*, 1999 for a review). Many different properties of the samples as well as the evolved gases were studied in detail. The reflectance (in the 0.5 to 2.5 μm wavelength range) of the surfaces were measured before and after the simulations, revealing their darkening and the decrease of the water and carbon dioxide absorptions due to the formation of a sublimation residue on top of the ice (Oehler and Neukum, 1991). However, no surface photometric measurement was performed *in situ*, during the simulation, and the *ex situ* analyses suffered from water frost contamination. More recently, Bar-Nun *et al.* studied the degassing and evolution of amorphous ice under sublimation (Pat-El *et al.*, 2009), while Kossacki *et al.* studied the thermal evolution of the vertical stratification of ice samples upon sublimation (Kossacki *et al.*, 1997). Finally, at the Technical University of Braunschweig, Gundlach *et al.* (2011) retrieved the sublimation coefficient of water ice under various conditions, among other experiments of significance.

The Laboratory for Outflow Studies of Sublimating Materials (LOSSy) was developed at the University of Bern over the past few years, with the aim of complementing past studies by offering detailed spectro-photometric characterization of the evolution of large icy analogue samples during sublimation. The laboratory comprises facilities to produce icy surface analogues (water ice particles, pure or mixed with mineral or organic non-volatiles) and two setups aimed at characterizing the scattering of light by these surfaces: (1) the PHIRE-2 (PHysikalisches Institut Radiometry Experiment) radio-goniometer, (Pommerol *et al.*, 2011), and (2) the SCITEAS (Simulation Chamber for Imaging the Temporal Evolution of Analogue Samples) simulation chamber (Pommerol *et al.*, 2015a). The PHIRE-2 radio-goniometer measures the bidirectional reflectance of cm-sized icy samples over a wide range of incidence, emission and phase angle in the visible and near infrared (0.4-1.1 μm). The SCITEAS thermal vacuum chamber enables *in situ* monitoring and spectro-photometric analyses of ice samples during its sublimation at low pressure and temperature conditions found at the surface of icy Solar System objects (i.e. $T < -70°C$ and $P < 10^{-5}$ mbar). The effects of textural and compositional changes of the sample (sublimation, sintering, formation of an upper desiccated layer etc.) on its reflectance properties can thus be characterized *in*

situ. In Poch *et al.* (2016) we have studied the textural and spectro-photometric properties of different mixtures of water ice and analogues of complex extra-terrestrial organic matter (tholins) during sublimation inside the SCITEAS chamber. We observed the formation of a sublimation lag deposit made of a water-free porous network of organic filaments on top of the ice, and the ejection of mm to cm-sized fragments of the deposit in outbursts-like events. Depending on the type of mixture and the size of the ice particles, we obtained remarkable differences in term of mantle structure, speed of mantle build-up, rates and surface area of mantle ejections, resulting in noticeable effects on reflectance features such as the visible red slope and the water absorption bands.

In the present study we extend this work to water ice mixed with minerals. We study the sublimation of mixtures of water ice and pure minerals (olivine or montmorillonite, a subclass of smectite phyllosilicates) and of a more complex mixture of water ice, organics and minerals (olivine, montmorillonite and tholins) representative of those potentially present in comets. The choice of these materials is supported by the composition of comet nuclei inferred by remote and *in situ* observations, sample return missions, or analysis of interplanetary dust particles. Silicates are one of the major components of comet nuclei. Both crystalline and amorphous silicates appear to be present (Hanner, 1999). Evidence for Mg- and Fe-rich olivines, as well as Mg-, Fe-, and Ca-rich pyroxenes, were found in the grains collected by Stardust (Brownlee *et al.*, 2006; Zolensky *et al.*, 2006). Layered silicates, or phyllosilicates, are hypothesized to be present in comet nuclei, but their presence has not been confirmed. Lisse *et al.* (2007) and Lisse *et al.* (2006) fitted Spitzer Space Telescope spectra obtained after the Deep Impact encounter with comet 9P/Tempel 1 by considering 8% smectite phyllosilicates by surface area of all silicates. Remote infrared observations and *in situ* analyses of 1P/Halley dust composition are also consistent with about 10% layered silicates (Fomenkova *et al.*, 1992; Jessberger *et al.*, 1988; Rietmeijer *et al.*, 1989). Phyllosilicates are also found in some interplanetary dust particles (IDPs) (from 5 to 11%), which may have originated from comets (Bradley, 1988; Nakamura *et al.*, 2005). However, the dust grains of 81P/Wild 2 collected by Stardust do not contain any phyllosilicate (Brownlee *et al.*, 2006; Wozniakiewicz *et al.*, 2010). Phyllosilicates have been detected in CM/CI carbonaceous chondrite meteorites, but their presence on comets is controversial because it would imply that cometary silicates have been aqueously altered, challenging the common conception of these bodies as objects frozen since their accretion (Wooden, 2008; Wozniakiewicz *et al.*, 2010). Previous cometary simulation experiments (Saunders *et al.*,

1986) have shown that mixtures of ice and phyllosilicates can produce sublimation residues having a porous and cohesive structure which could be of particular interest for cometary or planetary surfaces. Consequently, we chose to perform experiment with phyllosilicates to investigate the spectro-photometric properties of such sublimation residues. Finally, comets possess a high mass ratio of organics compared to minerals: estimates of organics/minerals ratio range from 0.3 to 1 (Fomenkova, 1999; Huebner, 2003; Jessberger *et al.*, 1989). This high content of organics may be inherited from icy dust particles that formed in the pre-solar nebula, and in which organics are readily synthesized inside an ice shell surrounding the dust particles (Herbst and Van Dishoeck, 2009). So for this study we have produced tholins, which are analogues of this complex organic matter produced by energy deposition in gases or ices in extraterrestrial environments (Sagan and Khare, 1979).

Many different scenarios have been proposed to explain the formation of comets and how the non-volatile and the volatile components are mixed (Belton *et al.*, 2007; Gombosi and Houpis, 1986; Greenberg, 1998; Greenberg and Li, 1999; Weissman, 1986). Moreover, on every icy surface of the Solar System including comets, the way the non-volatiles and the ice are mixed together will depend on the processes that have affected each particular surface, from its formation through its subsequent evolution to the present day. So in the present study, our goal is to further investigate the influence of the way in which the water and these non-volatile compounds are mixed together on the properties of the sublimation residues, and particularly their reflectance. How do these properties change when the non-volatiles are present as inclusions within water ice grains (intra-mixture), or when the non-volatiles are mixed with pure water ice particles (inter-mixture)? How are the reflectance features of the water and non-volatiles influenced by the texture of the sublimation residue? How do the properties in term of grain size and physico-chemistry of the non-volatile constituents influence the properties of the sublimation residues? Finally, we also want to assess the influence of the concentration of the non-volatiles on the evolution of the ice samples upon sublimation.

Space missions exploring comets, and especially the Rosetta mission, have provided a tremendous amount of data. The experimental results reported here are helpful to interpret this dataset (Pommerol *et al.*, 2015b). Although we selected specific materials in order to mimic a cometary nucleus composition, some of the results presented here can also be applied to other icy bodies.

2. Materials and methods

2.1 SCITEAS

The simulations were performed with the SCITEAS experimental setup. This simulation chamber, its imaging system and the procedure for data retrieving are briefly described in the paragraphs below. A more detailed description can be found in Pommerol *et al.* (2015a).

The SCITEAS thermal-vacuum chamber is designed to accommodate at its centre a sample contained in a 120×60 mm rectangle 20 mm deep. Inside the chamber, the sample is maintained at cold temperature by a continuous circulation of liquid nitrogen in a cylindrical shroud. The reflectance of the sample is continuously monitored in the 0.4 to 2.3 μm wavelength range by a hyperspectral imaging system through a fused quartz window. In the present study, the surface of the sample is constantly heated by infrared radiation produced by the window positioned 70 mm above.

The SCITEAS Imaging System consists of a monochromatic light source which illuminates the entire surface of the sample and two cameras covering the visible and the near-infrared spectral ranges, looking at the sample at an angle of about 13° from the nadir direction. The hyperspectral cubes were acquired with a spectral sampling of 20 nm from 0.38 to 0.96 μm and 10 nm from 0.96 to 2.30 μm in order to better resolve the shape of the absorption bands in the near infrared spectra. In the reduced dataset, absolute uncertainty on the calibrated reflectance factor is ±0.1 and the spatial variability of the reflectance across the field of view is of the order of 10%. During the course of the experiments, the infrared signal suffered from fluctuations. The relative uncertainty of reflectance factor introduced by these fluctuations is estimated to be around ±0.05, but the data presented in Supplementary Figure 8 and Supplementary Figure 9 suffered from a higher noise. However, the long term trends of the reflectance are still reliable and can be compared from a sample to another.

2.2 PHIRE-2

Some measurements presented in this paper were acquired using the PHIRE-2 radio-goniometer. This setup, its calibration and the measurement procedure are explained in detail in Jost *et al.* (2015) (sections 2.1.2 to 2.1.5), and only briefly summarized below. This goniometer, located inside a freezer, enables measurements of samples at -35°C (ice samples) or at room temperature (mineral powders, water-free sublimation residues). The signal of the reflected light from the samples was measured using a bandpass filter at 0.75 μm by scanning from *e*=-80° to *e*=+80° at fixed incidence directions (0 and 60°). The data calibrated in units of the radiance factor (RADF) were systematically converted to the "reflectance factor" (REFF), as defined by Hapke (1993).

2.2 Sample preparation

We have prepared samples of water ice particles mixed with olivine (forsterite), a smectite phyllosilicate (Na-montmorillonite) and complex organic matter (tholins). We have mixed the non-volatile components with the water ice in two different ways (intra-mixture and inter-mixture), and for each of these mixtures we have prepared two samples at different concentrations (0.1 and 1 wt.% of non-volatiles relative to water ice) (see Table 1 for a summary).

2.2.2 Forsterite

Forsterite (Mg_2SiO_4), the magnesium endmember of olivine, was purchased from Alfa-Aesar (ref. 42639). The initially greenish grains, of 1.5-4.8 mm size, were grounded into a white powder. The grains smaller than 80 μm were extracted by dry-sieving and used for the mixtures with the water ice. The obtained forsterite grains were imaged by scanning electron microscope, as seen in Supplementary Figure 6b showing the size and shape of the final particles.

2.2.3 Montmorillonite

Montmorillonite is a subclass of smectite phyllosilicates, which are layered aluminosilicate minerals consisting of an octahedral alumina layer fused between two tetrahedral silica layers (about 1 nm thick). The montmorillonite was purchased from the

Source Clays Repository of the Clay mineral Society (reference Srce_Clay_SWy-2). It was extracted from the Crook County (Wyoming) and has the chemical formula [$Si_{7.89}$ $Al_{3.34}$ $Fe_{0.42}$ $Mg_{0.56}$ $Ca_{0.52}$ $Na_{0.14}$ $K_{0.01}$] (Mermut and Cano, 2001). The original powder was sieved and only the fraction ≤ 80 μm was used. The extracted montmorillonite grains were imaged by scanning electron microscope, as seen in Supplementary Figure 6a. When dispersed in liquid water, the grains are exfoliated into individual mineral layers, called platelets, which are about 1 nm thick and 72 nm diameter (Weber *et al.*, 2014).

2.2.4 Tholins

In this study, we used tholins previously studied in Poch *et al.*, (2016). They were produced in a plasma of 95% N_2 and 5% CH_4, using the PAMPRE setup (Gautier *et al.*, 2011; Szopa *et al.*, 2006). These tholins are made of a complex mixture of molecular and macromolecular material composed of aliphatic hydrocarbons, nitriles, imines, amines or N-bearing aromatic compounds (Bernard *et al.*, 2006; Carrasco *et al.*, 2009; Pernot *et al.*, 2010; Quirico *et al.*, 2008). Bonnet *et al.* (2015) showed they are interesting precursors for the simulation of cometary N-rich refractory organics (before thermal heating). These organic molecules are arranged in high porosity spherical grains having a mean diameter of 315±185 nm (Carrasco *et al.*, 2009) (see also Figure 4c,d). Their optical indices have also been measured (Table A1 of Mahjoub *et al.*, 2012) as well as their reflectance spectra (Figure 4 of de Bergh *et al.*, 2008). They exhibit a strong red slope from 0.2 to 1.0 μm, attributed to n → σ* transitions of amine groups (–NH_2) (Mahjoub *et al.*, 2012).

2.2.5 Mixture types and production of water ice particles

2.2.5.1 Mixture types

In order to obtain reference laboratory data that could apply to diverse surface types and histories, we have prepared two types of mixture:

(1) an **intra-mixture**, in which the non-volatiles are present as inclusions within the water ice grains.
(2) an **inter-mixture**, in which the grains of non-volatiles are intimately mixed with the pure water ice particles at the level of the individual grains.

For each type of mixture, two samples having a mass ratio of non-volatiles to water of 0.1 wt.% and 1 wt.%, respectively, were produced to investigate the influence of the concentration on the sublimation. In order to assess the influence of each of the non-volatile components on the structure and spectro-photometric properties of the sublimation residue, we have first mixed each of the components with water ice separately: tholins (experiments presented in Poch *et al.*, 2016), olivine (experiment n°1), smectite (experiment n°2). And we finally performed the complete mixture of all the components (tholins, olivine and smectite with water ice) in the experiment n°3. In total, for each contaminant, four types of samples have been investigated. Table 1 shows a summary of the prepared samples, named "**(olivine/smectite/tholins-minerals)-(intra/inter)-mixture-(0.1/1) sample**". For example "**olivine-intra-mixture-0.1 sample**" designates the sample of water ice mixed with 0.1 wt.% olivine in an intra-mixture. Inter- and intra- mixtures of 0.1 % pure tholins with water ice have already been studied and presented in Poch *et al.* (2016).

These dust/ice mass ratios (from 0.001 to 0.016, see Table 1) may be very small compared to actual mass ratios in icy extraterrestrial environments, especially on comet nuclei where the dust/ice mass ratio is expected to be larger than 1 (Kuppers *et al.*, 2005), or between 1 and 6 (Kofman *et al.*, 2015). These low dust/ice mass ratios were dictated by the limited amount of tholins available. The minerals were also used at low concentrations because we chose an organics/minerals mass ratio of 0.45, comprised in the range inferred for comets (from 0.3 to 1) (Fomenkova, 1999; Huebner, 2003; Jessberger *et al.*, 1989). Moreover, we aimed to perform a systematic study, varying the composition of the samples while keeping the same concentrations of minerals (see Table 1).

2.2.5.2 Production of water ice particles

The water ice particles were produced with the SPIPA (Setup for the Production of Icy Planetary analogs) setup developed in the LOSSy laboratory (Yoldi *et al.*, 2015). The inter-mixture samples were prepared by introducing 40 g of fresh water ice particles in an aluminium bottle and adding 0.04 mg or 0.4 mg of non-volatiles for the 0.1 wt.% or 1 wt.% mixture respectively. The bottle was then closed and stirred using a Vortex-Genie2 mixer at full speed for 15 seconds and repeated 3 times. During the weighing and the mixing, the aluminium bottle was repeatedly plunged into liquid nitrogen to ensure the preservation of the ice particles at very low temperature and thus to limit thermal metamorphism.

The intra-mixture samples, in which the non-volatiles are included within the ice particles, were prepared from suspensions of the non-volatiles in water. Suspensions of 0.1 and 1 wt.% montmorillonite and forsterite (≤ 80 μm grains) in liquid water were maintained under magnetic agitation for at least 2 hours. In the case of the tholins-mineral 1% sample, 0.35 g of tholins were dispersed in 70 mL liquid water via ultrasonication as described in Poch *et al.* (2016) prior to the introduction of 0.7 g forsterite and 0.07 g montmorillonite powders in the suspension. Then, the suspensions were put in a spray bottle equipped with a 2 mm diameter tube connected to a Hielscher 200Ht ultrasonic unit equipped with a S26d18S sonotrode for spraying and nebulizing. The liquid pumped from the bottle is injected into the sonotrode where it spreads out as a thin film on the nozzle surface. The ultrasonic vibrations delivered to the sonotrode nozzle disintegrate the liquid film into micro-droplets. This nebulization took place inside a freezer cooled down to -60°C, above a stainless steel vessel filled with liquid nitrogen. The droplets ejected by the sonotrode nozzle fall into the liquid nitrogen where they rapidly freeze into ice particles. This method is used for the production of both the pure and the intra-mixed water ice particles. In both cases, the ice particles produced by this method are spherical and have a diameter of 67±31μm as measured by cryo-SEM.

		Forsterite (≤80μm)	**Na-montmorillonite** (≤80μm)	**Tholins** (0.31±0.18μm)
Mixture type with water ice particles (67±31 μm)	**Samples names:**	Concentrations (wt.% compared to water):		
Inter-mixture	tholins-inter-mixture-0.1*			0.1
	olivine-inter-mixture-0.1	0.1		
	olivine-inter-mixture-1	1		
	smectite-inter-mixture-0.1		0.1	
	smectite-inter-mixture-1		1	
	tholins-minerals-inter-mixture-0.1	0.1	0.01	0.05
	tholins-minerals-inter-mixture-1	1	0.1	0.5
Intra-mixture	tholins-intra-mixture-0.1*			0.1
	olivine-intra-mixture-0.1	0.1		
	olivine-intra-mixture-1	1		
	smectite-intra-mixture-0.1		0.1	
	smectite-intra-mixture-1		1	
	tholins-minerals-intra-mixture-0.1	0.1	0.01	0.05
	tholins-minerals-intra-mixture-1	1	0.1	0.5

Table 1 : Summary of the composition, concentrations and mixture types studied here. Each sample is designated by its abbreviated "Sample name" in the text and figures. Two types of mixture have been studied: **intra-mixtures**, in which the non-volatiles are present as inclusions within water ice grains, or **inter-mixtures**, in which the non-volatiles are deposited as a coating around the pure water ice particles. For each of these types of mixture, various compositions of non-volatiles have been prepared: pure organics (**tholins**) (*see Poch *et al.*, 2016), pure minerals (**olivine** or **smectite**) (experiments n°1 and n°2), and a mixture of organics, olivine, and smectite (named "**tholins-minerals**" mixtures) (experiment n°3). The concentration of these non-volatiles in mass relative to the water ice (dust/ice ratio) is given.

2.2.6 Deposition of the ice samples into the sample holder

Three simulation experiments were conducted inside the SCITEAS chamber on a total of 12 samples. For each experiment, a rectangular 120×60 mm sample holder 20 mm thick was divided in four equal compartments and each compartment was filled with a different sample. This enabled us to compare the evolution of different ice mixtures exposed to the same pressure and temperature conditions over the whole simulation. Prior to the deposition of the samples, the sample holder was cooled around -100°C. The samples were deposited by direct sieving through a 400 μm sieve, to avoid introducing into the samples some large agglomerates produced during the mixing in the aluminium bottle. This deposition method resulted in samples having a homogenous surface and having all the same density (0.5 g cm^{-3}). This sample deposition took place in a freezer cooled at -60°C, followed by a rapid transfer of the sample into the SCITEAS chamber.

2.3 Sample characterization

The morphology of the non-volatile grains, the evolving ice samples, and the dry sublimation residues, were characterized by various imaging and microscopy techniques.

Scanning Electron Microscopy (SEM): The particles sizes and microscopic structures of the pure powders (olivine, smectite, tholins), as well as the structure of some sublimation residues were investigated with a scanning electron microscope FEI Quanta 250 FEG with Gatan 3View2XP operated at 10kV and at chamber pressure of about 10^{-5} mbar. Prior to the SEM analysis, the sample material was sputter-coated with some nanometers of gold to make it

electrically conducting. Ice particles produced by the SPIPA setup were also imaged by cryo-SEM.

Optical microscopy: At the end of the experiments, the samples were removed from the SCITEAS chamber and the sublimation residues were imaged using a digital optical microscope GE5 (Aigo).

In situ high resolution and high speed imaging: During the evolution of the samples inside the SCITEAS simulation chamber, the sample surfaces were imaged using a compact digital camera, providing a diagnostic of the surface texture at a higher spatial resolution than the SCITEAS Imaging System. In order to measure the speed of the material ejected by some samples, we mounted the camera at a fixed position on top of the SCITEAS window and recorded high-speed videos at 100 fps and 200 fps.

In situ Optical Coherence Tomography: An Optical Coherence Tomography (OCT) instrument performs an interferometric analysis of the light backscattered by a surface sample. It enables one to image the 3D structure of the subsurface at a resolution of a few micrometers and down to a depth of a few hundreds of micrometers depending on the scattering properties of the surface material. We used a Thorlab's Ganymede OCT instrument working at 930 nm to measure the backscattering properties and the roughness of the sample surfaces as they evolved inside the SCITEAS simulation chamber. The OCT measurements were performed by temporarily fixing the head of the OCT instrument on top of the window of the SCITEAS chamber, and by moving up the sample holder so that the surfaces of the samples were about 2 cm below the window.

2.4 Simulation sequence in the SCITEAS chamber

2.4.1 Experimental conditions: pressure and temperature profiles

The profiles of pressure (measured at the periphery of the chamber) and sample holder temperature through the entire experiment are presented on Figure 1 and Supplementary Figure 1. In the three experiments, the temperature of the sample holder reached about 180K and the pressure 2.10^{-5} mbar, two hours after the closing of the chamber. The temperature

profiles of the sample holders show a continuous and logarithmic-shaped increase from 180 K to about 210 K until around 30 hours. At the same time, the pressure is almost constant (from 1.10^{-5} to 2.10^{-5} mbar). After about 38 hours, the temperature starts to increase above 210 K and simultaneously the pressure starts to decrease more rapidly, because most of the water ice initially present in the sample had already sublimated away. Overall, from 0 to 40 hours, the temperature and pressure variations were quite similar for all experiments, as for the experiments reported in Poch *et al.* (2016) and Pommerol *et al.* (2015a). As described in Pommerol et al. (2015), the sample holder temperature is not actively controlled and it tends to the equilibrium temperature of the chamber itself. This situation is very different from that of a cometary nucleus where steep temperature gradients are expected. The pressure curves in Figure 1 and Supplementary Figure 1 show bumps from 0 to 10 hours, which probably originate from the sublimation and re-deposition of water frost from the sample holder structure to the cold shroud surrounding the chamber. Shorter variations of pressure are also seen over the whole elapsed time. These pressure spikes have typical durations of a few minutes only. Some of these spikes can be correlated with events affecting the surface of the samples as discussed in section 3.1.

2.4.2 Dataset description

The data acquisition was similar for experiments n°1, n°2 and n°3, as well as for the experiments reported in Poch *et al.* (2016) and Pommerol *et al.* (2015a). The acquisition of visible images of the sample started as soon as it was placed inside the SCITEAS chamber. One image was taken every minute with the ambient light of the laboratory turned on. About 0.5 to 1 hour after the start of each experiment, the ambient light of the laboratory was turned off and the long-term spectro-photometric measurements sequence started. Monochromatic images at 600 nm were acquired every minute and hyperspectral cubes were measured every 40 minutes. Black and white monochromatic images at 600 nm and visible images taken with the ambient light were assembled to create videos of the evolution of the samples. Colour composites were produced from the monochromatic images acquired using the visible CCD (Figure 2). All colour composites were also assembled to create videos. Finally, we performed a supplementary experiment to reproduce the evolution of the tholins-minerals-intra-mixture-1 and tholins-minerals-inter-mixture-1 samples in order to record OCT data of the surfaces and high speed videos of the ejection events.

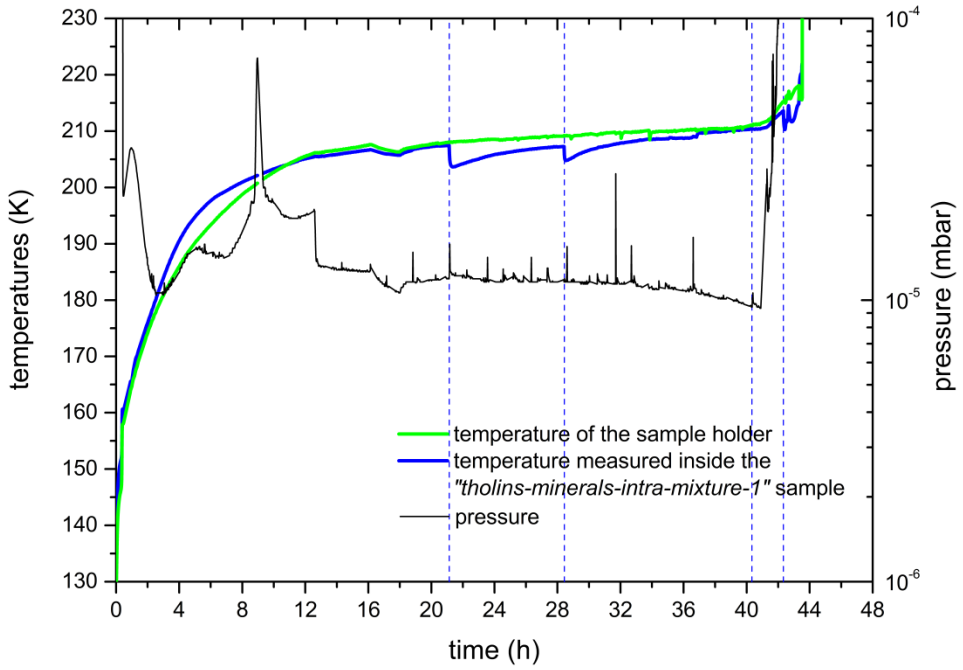

Figure 1 : Temperature (green and blue curves) and pressure (black curves) measured inside the chamber during the experiments n°3. The vertical dashed blue bars indicate the time during which an ejection event occurred on the tholins-minerals-intra-mixture-1 sample. The first two events can be correlated to a drop of the temperature measured by a sensor positioned inside the sample and to a pressure spike (see section 3.1.1). These data are also shown for experiments n°1 and 2 in Supplementary Figure 1 (For interpretation of the references to colour in this figure legend, the reader is referred to the web version of this article)

3. Results of sublimation experiments

3.1 Evolution of the surface morphology

Figure 2 presents visible colour composites of the studied samples, showing the evolution of their surfaces from the beginning to the end of the simulations. Moreover, Videos 1, 2 and 3 depict the detailed evolution of the samples during experiment n°1, 2 and 3 respectively. Supplementary Figure 2 shows schematic timelines of all the major events occurring during the videos. It allows a simultaneous comparison of the evolution of the surface morphology of all the samples. A detailed analysis of these videos is provided in the Supplementary Material document Appendix B and is briefly summarized below.

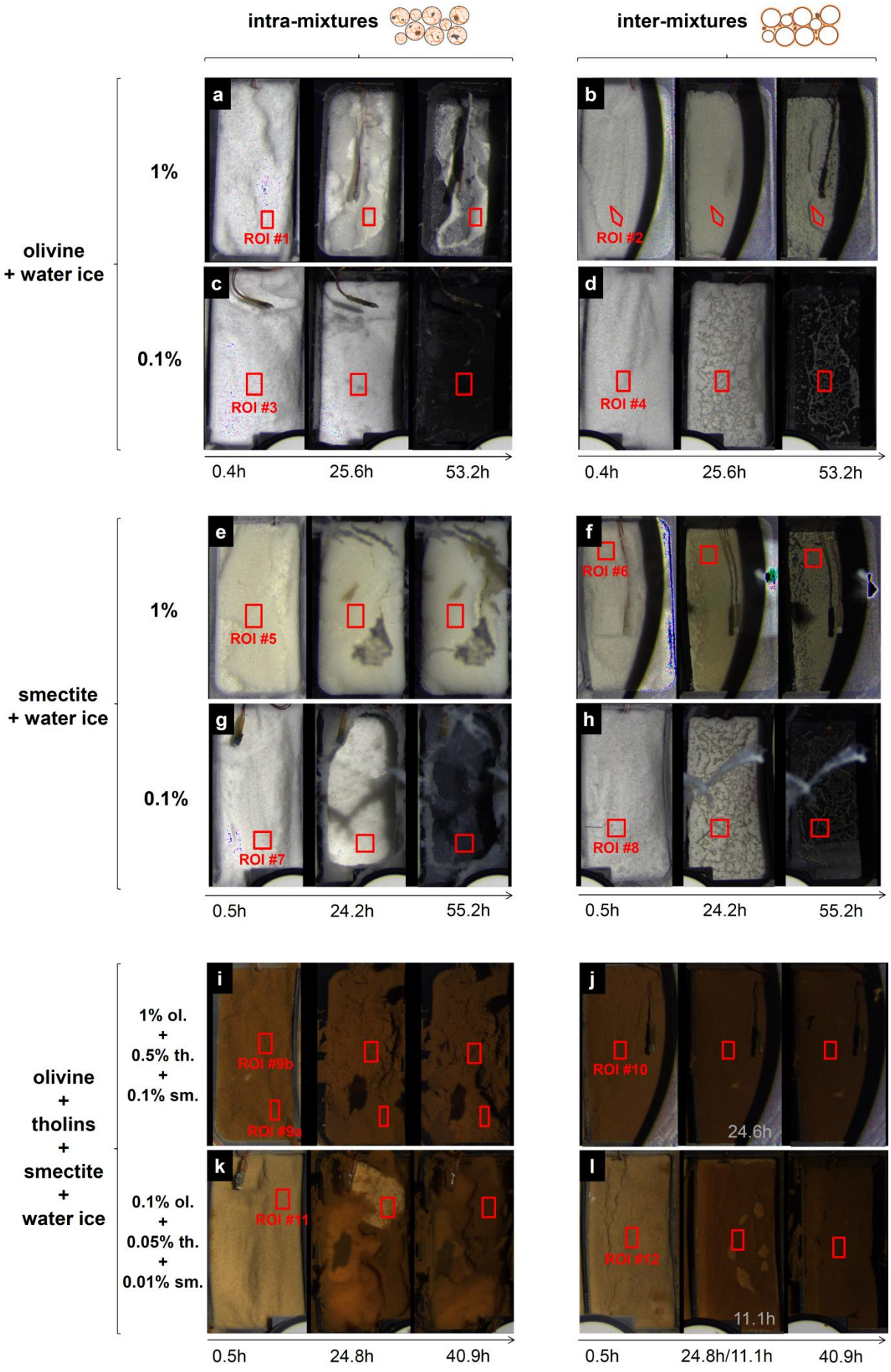
intra-mixtures
inter-mixtures
olivine + water ice
1%
0.1%
a
b
c
d
ROI #1
ROI #2
ROI #3
ROI #4
0.4h
25.6h
53.2h
smectite + water ice
e
f
g
h
ROI #5
ROI #6
ROI #7
ROI #8
0.5h
24.2h
55.2h
olivine + tholins + smectite + water ice
1% ol. + 0.5% th. + 0.1% sm.
0.1% ol. + 0.05% th. + 0.01% sm.
i
j
k
l
ROI #9b
ROI #9a
ROI #10
ROI #11
ROI #12
24.6h
11.1h
0.5h
24.8h
40.9h
24.8h/11.1h

Figure 2 : Colour composites showing the evolution of the surface of each sample from the beginning to the end of the experiment. One should appreciate the diversity of morphologies produced by the sublimation process just by changing the mixture type or nature of the non-volatile contaminant. The Regions Of Interest (ROI) indicated in red in each image have been used to retrieve the spectro-photometric data presented in Figure 5, Figure 6, Supplementary Figure 8, Supplementary Figure 9 and Supplementary Figure 10 which are discussed in section 3.2. The images appear close to natural colours, relatively similar to what the human eye would see, although no special calibration was performed to retrieve the true colours. To produce these VIS colour composite, monochrome images acquired at 0.40, 0.52, and 0.60 μm were used, for the blue, green, and red channel, respectively. Videos 4, 5 and 6 show all the colour composites separating each of these three images. (For a colour version of this figure, the reader is referred to the web version of this article)

3.1.1 Common trends

Build-up of a sublimation mantle: As the water ice sublimes, a deposit made of the non-volatile compounds initially present in the ice builds up at the surface of the samples, causing changes of colour and texture. This deposit is designated as the "sublimation mantle" or the "sublimation lag deposit" in the following paragraphs. This sublimation mantle is made of a network of filaments. The properties (size of the filaments, internal cohesiveness, etc.) of the network are strongly dependent on the mixture type, composition and concentration of the non-volatiles, as detailed below.

Sudden changes of the surface, ejections or subsidences: Sudden releases of fragments of sublimation mantle occur at the surface of some samples, designated as "ejection events" in the following paragraphs. In the areas from where the material is released, the water ice particles, initially located below the sublimation mantle, are re-exposed at the surface. This ice then sublimes away, progressively rebuilding the sublimation mantle at the surface. Some of these ejection events are correlated to a spike or an increase of pressure in the chamber (see Figure 1). Samples not showing ejection events can show sudden "subsidence events", during which a part of the sublimation mantle suddenly collapses because of the release of the gas pressure below it (see the olivine-intra-mixture-1), or because of voids formed below the mantle by the sublimation of the ice (see the olivine-inter-mixture-1). The samples that do not show sudden surface changes during experiments n°1, 2 or 3, can exhibit such changes when irradiated with the a higher thermal input, providing a higher sublimation rate as we tested for tholins-minerals 1% samples during the supplementary experiment (see Supplementary Videos 4, 5, 6 and 7).

3.1.2 Differences between samples

Differences of formation of sublimation mantles: As the sublimation goes on, intra-mixtures-1 samples get covered by a foam-like (see Figure 2e and Figure 3e,i) or veil-like (see Figure 2a and Figure 3a) sublimation mantle. At the lower concentration of 0.1%, all mantles resemble thin veils whatever their composition (see Figure 3c, g, k). On inter-mixtures 0.1% samples, the surface gets covered by millimetre-sized dots that progressively increase in size and connect to each other, forming a network of filaments over the ice. As the sublimation continues, the thickness and the length of these filaments increase. At higher concentration (1%) or in presence of tholins, no individual filaments are clearly seen at a macroscopic scale, but they are still present at a microscopic scale. Specifically for the olivine-inter-mixture-1 sample, the deposit of olivine produced after sublimation is a very uniform and flat layer, resembling a crust (see Figure 3b and central part of Figure 2b). This "crusty" mantle of olivine reduces the sublimation rate of the ice located beneath it and causes the ice to sublimate preferentially from the periphery to the centre of the sample holder whereas the opposite direction is observed for all the other samples. A mesa-like feature is formed and reduces in size by sublimation and collapse of the mantle on its rims.

Differences in term of activity: From all the mixture types, the intra-mixture samples were more active than their inter-mixture counterparts, exhibiting more ejections of mantle during their sublimation (see Supplementary Figure 2). We also observed that low concentration of non-volatiles leads to a more active surface (see the differences between 0.1% and 1% intra-mixtures on Supplementary Figure 2). During the supplementary experiment (see Videos 7, 8 and 9), the fragments ejected from the tholins-minerals-intra-mixture sample were larger (roughly by a factor of 5 to 10) and had a velocity (0.4 ± 0.1 m s^{-1}) 2 to 3 times lower than those produced by the inter-mixture (1.0 ± 0.1 m s^{-1}). This size difference of the ejected fragments indicates that mantles formed after the sublimation of intra-mixtures have a higher internal cohesiveness than those formed from inter-mixtures. For intra-mixtures of pure minerals (smectite or olivine) at concentration of 1%, no ejection event occurred. Mineral sublimation lag underwent deformations, subsidence and/or fracturation events. But when tholins are added to olivine grains, ejection events are observed. This indicates that the mantles built in presence of tholins are more cohesive and consequently more easily lifted by

the gas flow than those of pure olivine grains. This easier lifting leads to a higher upward force applied on the mantle, resulting in its breakup and ejection of mantle fragments.

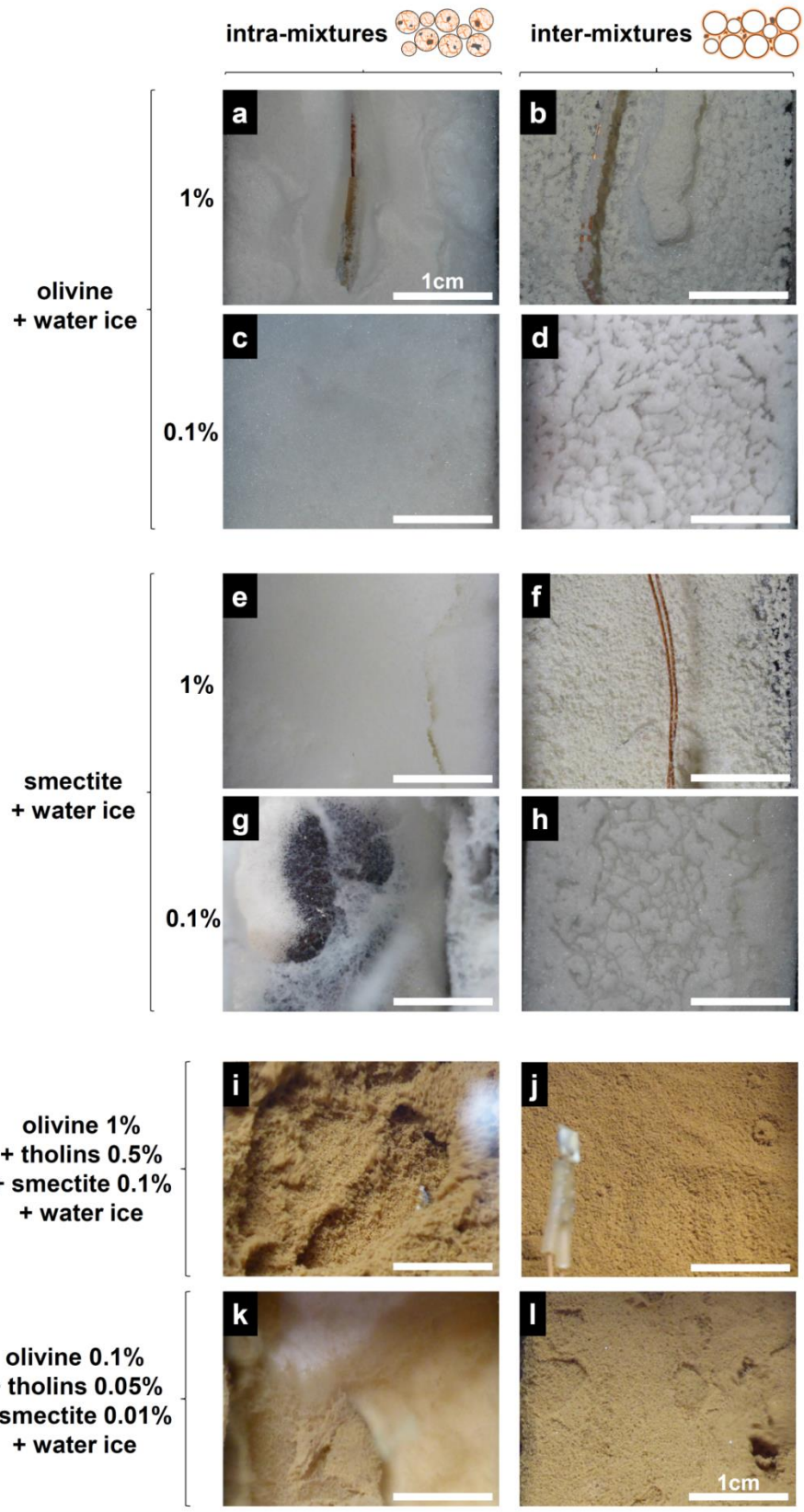

Figure 3 : High resolution images of the surfaces of the samples after sublimation, showing veils, filaments, crust or foam-like structures. These images were taken *in situ*, while the sample were sublimating inside the simulation chamber at around -70°C and 10^{-5} mbar.

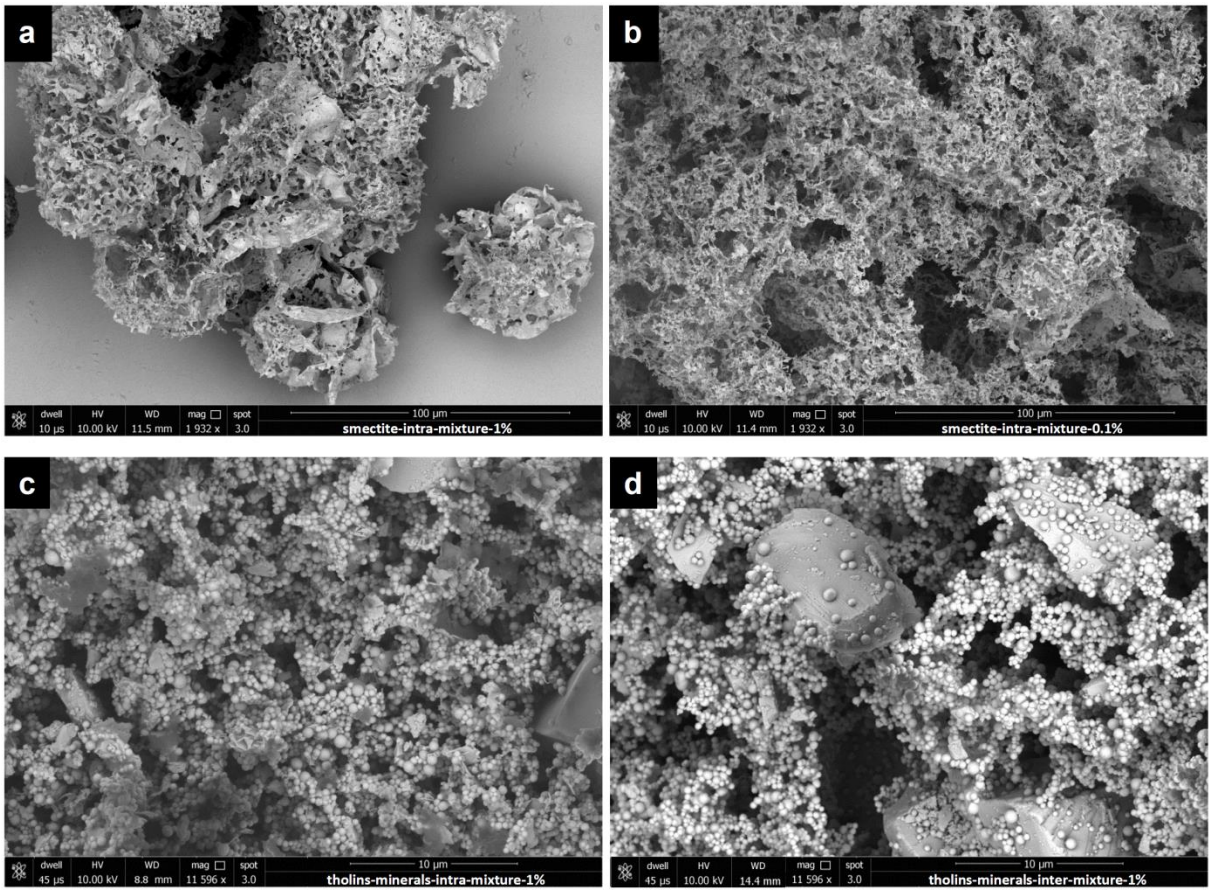

Figure 4: Scanning Electron Microscope images of the water-free sublimation residues of **(a)** an intra-particle mixture of water ice and smectite at a concentration of 1% (smectite-intra-mixture-1) and **(b)** 0.1%, (smectite-intra-mixture-0.1), **(c)** an intra-particle mixture of water ice with olivine (1%), tholins (0.5%) and smectite (0.1%) (tholins-minerals-intra-mixture-1) and **(d)** an inter-mixture of pure water ice particles with olivine (1%), tholins (0.5%) and smectite (0.1%) (tholins-minerals-inter-mixture-1).

3.1.5 Morphology and physical properties of the sublimation lag deposits

Figure 3 shows *in situ* high-resolution images of the sublimation residues, or "mantles", obtained at the surface of each sample. Supplementary Figure 3 shows more detailed images of the same residues obtained *ex situ* (i.e. after the samples were extracted from the simulation chamber) by visible microscopy. Finally, Figure 4 provides even more

details on the microscopic structure of some sublimation residues, obtained *ex situ* by scanning electron microscopy.

3.1.5.1 Intra-mixtures. Low concentration intra-mixture samples (0.1%) form residues having filamentous veil-like structures (Figure 3c, g, k), with filaments a few microns thick (Supplementary Figure 3c, g). At higher concentration (1%), most intra-mixture samples form foam-like structures that retain the initial spherical shape of the water ice particles (see Figure 3e, i, Supplementary Figure 3e, i and Figure 4a for the foam-like structures and Figure 1b in Poch *et al.* (2016) for the initial ice particles). However, an intra-mixture of olivine and water does not produce such structure. Instead, olivine sublimation mantle resembles a thick veil-like structure (Figure 3a) composed of filaments (Supplementary Figure 3a). We observed that the filaments obtained from pure olivine are the most fragile (as seen on Supplementary Figure 3c). Weak interactions between olivine grains could explain why they are not able to form a cohesive mantle. When some amount of tholins and smectite are added to the olivine grains (as in the tholins-minerals-intra-mixture-1 sample), a foam-like sublimation mantle having a higher internal cohesion is built. Figure 4c shows the sublimation residue of the tholins-minerals-intra-1 sample observed with scanning electron microscope. The spherical particles of tholins are associated to some smectite layers and are bounded to each other, forming a three dimensional network binding the olivine grains together, and thus providing internal cohesion to the residue.

The foam-like residue obtained from the pure smectite sample has a different structure, as seen in Figure 4a. It consists of “ribbons” of smectite layers, which have clearly retained the spherical shapes of the initial water ice particles. This structure may have formed during the freezing of the droplets of the smectite suspension in liquid nitrogen. As the water froze, the individual smectite platelets (~1 nm thick and 72 nm diameter) concentrated at the interfaces between the growing water crystals (because impurities are expulsed out of the crystal structure while they grow: this mechanism, known as "zone refining", was proposed by Saunders *et al.*, 1986). The “ribbons” observed in Figure 3 are likely to be the relics of the crystal interfaces (see section 4.2.1 for a detailed discussion). The bounding of the smectite platelets together may have occurred during the crystallisation or during the sublimation.

The foam-like structure obtained from the tholins samples probably also formed in a similar way. Pictures of the tholins sublimation residues taken *in situ* clearly show the “ghost”

spherical shape of the water ice particles (Figure 3i and Supplementary Figure 7e). However this spherical shape is less obvious on the images taken *ex situ* (Supplementary Figure 3i and Figure 4c) possibly because of the rearrangement of the tholins network during its manipulation outside the simulation chamber.

Knowing the thicknesses of the samples and their concentration in non-volatiles, the density of the mantle is estimated to be around 5.10^{-3} g cm^{-3} and 8.10^{-3} g cm^{-3} for the smectite-intra-mixture-1 and the tholins-minerals-intra-mixture-1 samples respectively. The initial density of the ice mixtures being of about 0.5 g cm^{-3}, the porosity of these samples is around 90%.***3.1.5.2 Inter-mixtures.*** Concerning the inter-mixtures, low concentration samples (0.1%) form residues consisting of filaments (Figure 3d, h, l) around 100 to 200 μm thick for smectite and olivine particles (Supplementary Figure 3d, h) and around one order of magnitude thinner in the case of tholins particles (Figure 3l). The final thickness of the filaments appears linked to the original size of the individual dust particles: smectite and olivine particles are ≤80 μm particles while tholins are around one order of magnitude smaller particles (~0.3 μm). At higher concentration (1%), inter-mixture samples form homogenous deposits having a variable amount of voids in their structure (Figure 3b, f, j). In the case of the olivine-inter-mixture-1 sample, a dense crust (with no void) is formed over the ice. The fact that olivine grains built such a crust whereas smectite grains did not could be explained by the presence of more grains in the very small size-range fraction for olivine, as seen by SEM in Supplementary Figure 6b. During the formation of the mantle, smaller grains efficiently fill the gaps between the bigger grains, building a denser crust over the ice.

Contrary to the intra-mixtures, the residues produced from the sublimation of inter-mixtures do not retain the shape of the initial ice particles, as shown by comparing Supplementary Figure 3e, f, Supplementary Figure 3i, j and Supplementary Figure 7a, b. At the microscopic scale (Figure 4d), the mantle produced from the tholins-minerals-inter-mixture-1 sample is made of aggregates of tholins bridging together mineral grains. At this scale, the differences compared to the intra-mixture (Figure 4c) are the higher thickness of these filaments (composed of larger aggregates of tholins particles), the presence of larger voids between the filaments, and the absence of a smectite layer within the tholins bridges (because smectite was present as grains, not as platelets). The estimation of the density from thickness measurements gives 2.10^{-2} g cm^{-3} for the sublimation mantle of the tholins-inter-mixture-1 sample. The

deposit obtained from an inter-mixture is thus 2.5 times denser than the one obtained from an intra-mixture.

The optical coherence tomography (OCT) images of the surface of the intra- and inter-mixtures of tholins and minerals enable to link the texture of the mantles to their optical properties. Supplementary Figure 7 reveals that in a dense residue the light is mainly scattered close to the surface whereas in a more porous one the scattering is more evenly distributed in the first tenths of micrometers below the surface.

3.1.6 Texture of the remaining ice after the experiments

Just after their preparation, all the samples had the same granular texture, given by the individual ice particles, similar to fine sand. At the end of the experiment n°3, the samples were removed from the chamber and the texture of their remaining ice was manually probed using a steel spatula. This very qualitative test revealed some stunning texture differences between samples.

The ice particles of the tholins-minerals-intra-mixture-1 sample appear to have a fluid texture similar to the initial sample below a thin (1-2 mm) crust. But the ice particles of the tholins-minerals-inter-mixture-1 sample have lost their initial fluidity: they appear to be strongly consolidated. This consolidation probably comes from the re-condensation of the water between the ice particles or sintering, building bonds that connect the ice particles together and provide solidification of the whole sample. We plan to quantify the compressive strengths of these ice samples with a dedicated device in future experiments.

This test was only performed after experiment n°3, because at the end of the experiments n°1 and n°2, the ice was almost completely sublimated, so no texture test could be performed on the samples made of pure smectite or olivine.

3.2 Evolution of the spectro-photometric properties of the samples

The spectro-photometric characteristics of the surfaces of the samples are studied as a function of time through the detailed analysis of the hyperspectral cubes acquired during the experiments. Figure 5 and Figure 6 present a subset of the hyperspectral data acquired with the SCITEAS imaging system (see also Supplementary Figure 8, Supplementary Figure 9 and Supplementary Figure 10) and Videos 4, 5 and 6 depict the evolution of the samples over each Regions of Interest.

3.2.1 Comparison of the reflectance spectra before/after sublimation

Regions of Interest (ROIs): *The reflectance of the samples surfaces was extracted from the hyperspectral images only at some limited areas, called Regions of Interest (ROIs), indicated in Figure 2. Extracting the average spectra of the whole samples surfaces was not possible because of the presence of external elements in the images: mainly fragments of sublimation mantle stuck on the window of the chamber hiding some parts of the sample and casting shadows on other parts, and temperature sensors and their shadows.*

Figure 5 presents, for each of the most concentrated samples (all "1%" mixtures), the initial (black line) and final (red line) reflectance spectra averaged over the ROI #1, #2, #5, #6, #9a and #10. To facilitate the interpretation of these spectra, reference spectra of each of the elements of the mixtures are also shown: pure water ice, pure olivine, pure smectite and pure tholins, all measured with the SCITEAS setup.

3.2.1.1 Spectra of the ice samples before sublimation

All initial ice samples clearly exhibit the water ice absorption bands at 1.02, 1.26 and 1.51 μm. For a given concentration of non-volatiles (1%), intra-mixture samples have a higher level of reflectance than inter-mixture samples from 0.4 to 1.4μm (+50%, +25% and +20% at 0.7 μm for olivine, smectite and tholins-minerals samples respectively). Similarly, the water bands of intra-mixture samples (Figure 5a, c, e) have deeper band depths than inter-mixture samples (Figure 5b, d, f) (+75%, +20% and +15% respectively). These differences between intra and inter mixtures are much more significant for olivine than for smectite and tholins.

Olivine samples: The reflectance spectrum of the pure olivine powder is characterized by a red slope from 0.4 to 0.6μm (charge transfer absorption) and a broad "V-shaped" absorption band centred at 1.0μm (Fe^{2+} absorption) (Clark, 1999). When this olivine powder is mixed

(with a mass ratio of 1%) in an intra-mixture with water ice, none of these spectral features are seen (Figure 5a). However, when mixed as an inter-mixture, some spectral features of the olivine are clearly seen (Figure 5b).

Smectite samples: The reflectance spectrum of the pure smectite powder is characterized by a red slope from 0.4 to 0.6μm (charge transfer absorption) and absorptions bands centred at 1.40 μm (first overtone of the O-H stretching modes), 1.9 μm (combination of structural O-H and adsorbed H-O-H stretching modes) and 2.2 μm (metal-OH band) (Cooper and Mustard, 1999). The red slope of the smectite is clearly seen on the reflectance spectra of both intra- and inter- mixtures with water ice (Figure 5c, d). The OH/H_2O absorption bands are masked by the large absorptions of the water ice at these wavelengths. However, the presence of the smectite clay may induce a slight asymmetry of the 2.0 μm water band, with a maximum of absorption shifted toward 1.9 μm as seen for both intra- and inter- mixtures (see Figure 5c, d).

Tholins samples: Pure tholins are characterized by a strong red slope in the visible from 0.4 to 1.3 μm and by some broad and low intensity absorption bands in the near infrared at around 1.5, 1.95 and 2.2 μm. The intra- and inter- mixtures of tholins with water ice have reflectance spectra characterized by a red slope from 0.4 μm to about 0.95 μm, due to the presence of tholins, followed by water ice absorption bands at 1.02, 1.26 and 1.51 μm.

3.2.1.2 Spectra of the sample surfaces after sublimation

Most of the final reflectance spectra, obtained after sublimation of the samples (red lines in Figure 5) do not show the water ice absorption bands at 1.02, 1.26 and 1.51 μm because there is no more ice in the sample (this is the case for the smectite samples, Figure 5c, d) or because the ice is masked by an optically thick water-free mantle (as it is the case for the tholins-minerals samples, Figure 5e, f). However, spectra of olivine samples still exhibit very broad and low intensity absorptions at 1.02, 1.26 and 1.51 μm (Figure 5a, b) due to the presence of water ice less than around 3 mm below the mantles of olivine.

For all the samples, the comparison of the initial spectra of the ices and the final spectra indicate (1) a decrease of the reflectance in the visible range (due to the deposition of the non-volatiles at the surface of the samples) and (2) an increase of the reflectance in the near infrared (above 1.4 μm) (due to the masking or absence of water ice) (see Figure 5).

The mantles deposited at the surface of the samples after the sublimation of the ice are made of the non-volatiles with which the ice was mixed with. However, the reflectance spectra of these mantles are generally very different from the reflectance spectra of the pure non-volatiles (dotted and dashed lines in Figure 5).

Intra-mixtures: The reflectance spectra of the mantles obtained from intra-mixtures show absent or very faint absorption features of the non-volatiles in the near infrared. The spectral features of olivine are absent on the reflectance spectrum of the mantle of the olivine-intra-mixture-1 sample (Figure 5a). For the mantle of the smectite-intra-mixture-1 sample, the typical OH/H_2O absorption bands of smectite at 1.4, 1.9 and 2.2 μm are hardly detectable, and only the red slope from 0.4 to 0.6 μm is clearly present (Figure 5c). The spectrum exhibits a featureless blue slope from 0.7 to 2.2 μm. For the mantle of the tholins-minerals-intra-mixture-1 sample, the reflectance spectra is clearly dominated by the tholins with a marked red slope from 0.4 to 1.0 μm, a featureless blue slope from 1.1 to 2.2 μm and a faint absorption band at 1.95 μm (Figure 5e). The absorption features of the minerals are absent of the spectrum. In particular, the olivine absorption at 1.0 μm is invisible, although olivine is present at a concentration of 1%, i.e. twice the concentration of tholins in mass. The absence of absorption bands and the origin of the featureless blue slope in the near infrared seen for the smectite-intra-1 and tholins-mineral-intra-1 samples is discussed in section 4.2.1. Finally, between 39.8 and 40.9h, the mantle over the ROI #9a (tholins-minerals-intra-mixture-1) is ejected and water ice is re-exposed to the surface, as shown by the red dashed spectrum on Figure 5e.

Inter-mixtures: The reflectance spectra of the mantles obtained from inter-mixtures show more spectral signatures of the non-volatile components, although these signatures are mostly still fainter than those of the original powders. The spectrum of the mantle of the olivine-inter-mixture-1 sample (Figure 5b) clearly exhibits the red slope from 0.4 to 0.6 μm and the blue side of the absorption band centred at 1.0μm. The spectrum of the mantle of the smectite-inter-mixture-1 sample (Figure 5d) exhibits the red slope from 0.4 to 0.6 μm and OH/H_2O absorption bands of lower intensity than the initial smectite powder. The band depths of absorptions at 1.4, 1.9 and 2.2 μm are respectively reduced by 70%, 80% and 50% compared to the initial smectite powder. The low intensity of these bands may be due to the low amount of smectite present in the deposit, or to the way the smectite grains are agglomerated together (see Supplementary Figure 3f) that reduces the penetration of light compared to the raw

powder used to acquire the “pure smectite” spectrum. The fact that the most important reduction of band depth is observed for the H_2O stretching mode at 1.9 μm probably indicates that a significant fraction of the water contained in the smectite grains was released during the evolution of the sample under vacuum. One should note that this desorption of water is probably very favoured by the high porosity of the material formed by sublimation, compared to raw smectite powders exposed to vacuum (see Pommerol *et al.*, 2009 and Beck *et al.*, 2010). Finally, the spectrum of the mantle of the tholins-minerals-inter-mixture-1 sample (Figure 5f) shows the red slope of the tholins from 0.40 to 0.95 μm and no other obvious spectral signature. Only very faint absorptions can barely be distinguished from the noise at 1.0 μm (possible olivine absorption), and between 1.88-2.03 μm and 2.13-2.30 μm (possible tholins absorptions). One should note that contrary to intra-mixtures, inter-mixture mantles do not exhibit a continuous blue slope in the near-infrared.

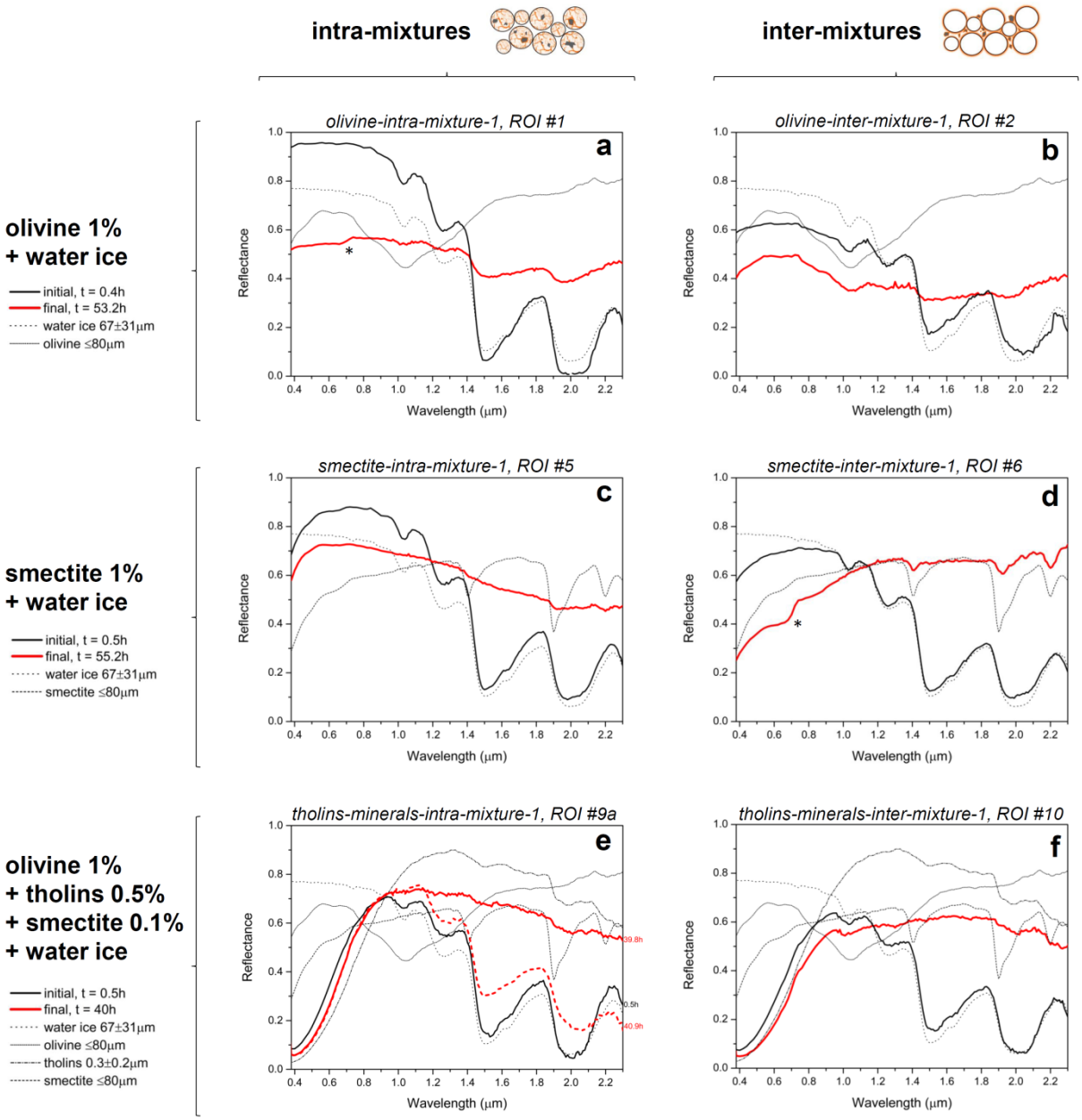

Figure 5 : Reflectance spectra of the sample surfaces in the ROI #1 **(a)**, ROI #2 **(b)**, ROI #5 **(c)**, ROI #6 **(d)**, ROI #9a **(e)** and ROI #10 **(f)** indicated in Figure 2. The reflectance spectra measured ~30 minutes after the start of the simulation (black line) can be compared to the ones measured 40 to 55 hours later (red line) when a sublimation mantle has formed on top of the samples. To facilitate the interpretation of these spectra, reference spectra of pure water ice and pure tholins are also shown in dotted and dashed black lines respectively (these spectra were measured separately, during previous experiments). A detailed interpretation of these spectra is provided in section 3.2.1. Reflectance spectra from all the ROIs of all the other samples are presented in Supplementary Figure 10. *Artefact originating from the strong red slope at 0.7 µm of the aluminium oxide coating the sample holder (For interpretation of the references to colour in this figure legend, the reader is referred to the web version of this article)

3.2.2 Comparison of the *in situ* spectral evolutions of the samples

The whole sequence of hyperspectral cubes acquired during the experiments allows us to study the dynamic of the evolution of the samples' reflectance as the sublimation goes on. We perform here the detailed analysis of the spectral evolution on the tholins-minerals samples only, because they exhibit the strongest spectral feature (the red slope of the tholins) and they are closer in term of composition to the ice mixture of a comet. The detailed spectral evolution of the smectite and olivine samples (without tholins) is discussed in the Appendix C (Supplementary Figure 8 and Supplementary Figure 9).

Figure 6 compiles the temporal evolution of several spectral criteria for the four different tholins-minerals ice samples (ROI #9a, ROI #9b, ROI #11 and ROI #12 from Figure 2).

The spectral criteria plotted in Figure 6 are:

(a) the reflectance at 0.40 μm, located in the tholins absorption band (Figure 6a),
(b) the normalized spectral red slope between 0.40 and 0.94 μm due to the tholins (Figure 6b) (following the definition from Fornasier *et al.*, 2015):

$$Spectral\ Red\ Slope\ (\%/100\,nm) = \frac{R_{0.94\mu m} - R_{0.40\mu m}}{(940-400)\times R_{0.40\mu m}} \times 10^4 \qquad \text{Eq. (1)}$$

(c) and the band depth of the water absorption band centred at 1.51 μm (Figure 6c):

$$Water\ band\ depth\ at\ 1.51\ \mu m = 1 - \frac{R_{1.51\mu m}}{R_{1.35\mu m}} \qquad \text{Eq. (2)}$$

The results shown in Figure 6 are described in the two paragraphs below. Paragraph 3.2.2.1 focuses on the long-term evolution of these spectral features, ignoring the ejection events. Paragraph 3.2.2.2 discusses the impact of activity (ejection events) on the photometry of the surface, focusing on ROI #9b (tholins-minerals-intra-mixture-1 sample) and ROI #11 (tholins-minerals-intra-mixture-0.1 sample).

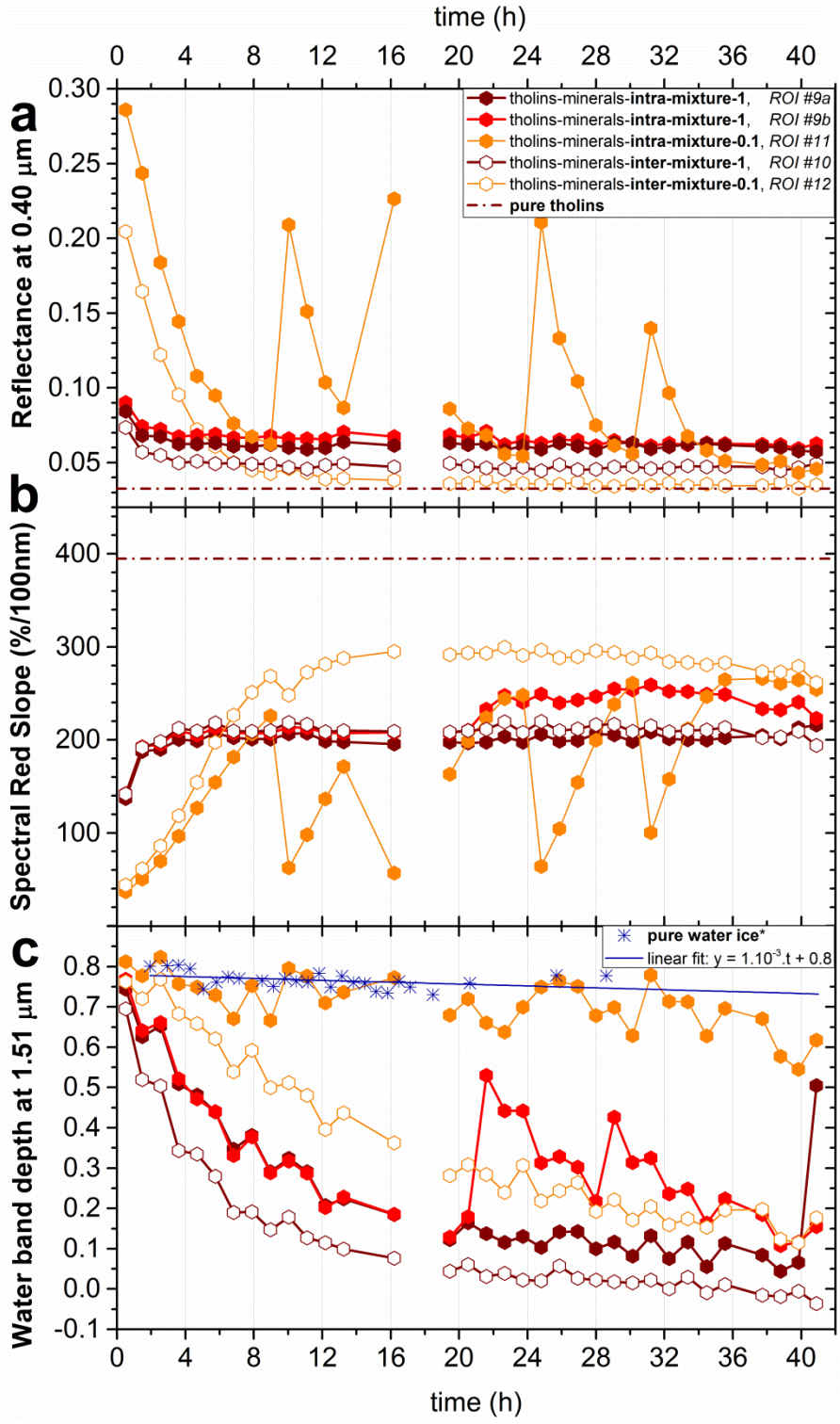

Figure 6 : *In situ* spectral evolution of the samples of tholins, olivine and smectite mixed with water ice particles as intra- or inter- mixtures and at different concentrations. Temporal evolution of **(a)** the reflectance at 0.40 µm where tholins absorb the most, **(b)** the normalized spectral red slope due to tholins between 0.40 and 0.94 µm (see Eq. 1), **(c)** the band depth of the water absorption band at 1.51 µm (see Eq. 2). These data have been obtained from spectra acquired in ROI #9a, #9b (tholins-minerals-intra-mixture-1), ROI #11 (tholins-minerals-intra-mixture-0.1), ROI #10 (tholins-minerals -inter-mixture-1) and ROI #12 (tholins-minerals-inter-mixture-0.1) located in Figure 2i,j,k,l and Video 6 (see Table 1 for the explanation of the samples names). Ejections on mantle fragments occurred on

ROI #11 and ROI #9b (see Video 6), leading to sudden variations of some spectral features. *The pure water ice data are from ROI #0 of Poch *et al.* (2016). (For a colour version of this figure, the reader is referred to the web version of this article)

3.2.2.1 Long-term spectral evolution

Reflectance at 0.40 μm and spectral red slope: As the water sublimates, the reflectance at 0.40 μm decreases for all samples because of the deposition of water-free tholins over the surface (Figure 6a). The largest decrease is observed for the sample having the lowest concentration in non-volatiles: mixtures at 0.1% experienced a decrease of ~80% of their reflectance at 0.40 μm in 9 hours whereas mixtures at 1% only experienced a decrease of around 30%. Following these exponential decreases, the reflectance values of most samples remain relatively stable during the 40 hours of the simulation, only exhibiting a long term trend toward an asymptotic value close to the reflectance of pure tholins (dotted-dashed line in Figure 6a). The tholins-minerals-inter-mixture-0.1 sample reaches a reflectance value close to that of the pure tholins ($R_{tholins}$+10%) after around 20 hours of evolution. The other samples never reach a reflectance value lower than $R_{tholins}$+40% after more than 40 hours of evolution. The tholins-minerals-intra-mixture-1 sample exhibits the highest reflectance at 0.40 μm with values constantly superior by 80% to that of pure tholins.

For all samples, the spectral red slope between 0.40 and 0.94 μm, plotted in Figure 6b, follows opposite variations compared to the reflectance at 0.40 μm, plotted in Figure 6a. After a clear increase of the red slopes, within 4 hours for the mixtures at 1% or 9 hours for the mixtures at 0.1%, a slowing down is observed and the red slopes reach a plateau equal to 53% and 68% of the one of the pure tholins for the mixtures at 1% and 0.1% respectively.

These variations of the reflectance at 0.40 μm and of the visible red slope are due to the increase of the optical thickness of the sample surfaces in the visible wavelengths because of the building of a layer of non-volatile compounds containing tholins. As the tholins accumulate at the surface of the sample, the absorption of the surface at 0.40 μm increases, and consequently the reflectance at 0.40 μm decreases and the spectral red slope (or band depth) increases. The slowing down of these variations few hours after the start of the sublimation indicates that the tholins layer becomes optically thick. By comparing the values of the reflectance and spectral red slope for different sample types and concentrations on

Figure 6a and b, it seems that the evolution of the reflectance at 0.40 μm depends more on the mixture type and the final texture of the sublimation mantle (the one from the inter-mixtures being denser than the one from intra-mixtures), whereas the evolution of the spectral red slope depends more on the concentration of non-volatile compounds in the ice.

Water band depth: The Figure 6c shows the evolution of the depth of the 1.51 μm water ice band for the different tholins-minerals samples, as well as for a pure water ice sample (from ROI #0 on Figure 3 of Poch *et al.*, 2016). During sublimation, the pure water ice exhibits a very slight decrease of the water band depth, maybe due to an increase of the number of bigger ice particles (slower to sublime) as discussed in Poch *et al.*, (2016). The decrease seen for the tholins-minerals samples is much more pronounced. It is explained by the building of the tholins sublimation mantle over the sample surface, masking the water ice particles located underneath. From 0 to 8 hours, the decrease of the water band depth is 14 to 65 times faster for the tholins-minerals samples than for pure water (see Figure 6c). The decrease is faster for the 1% mixtures by a factor of 2 to 4 compared to the 0.1% mixtures. And at equal concentrations, the decrease of the water band depth is faster for the inter-mixtures by a factor of 1.2 to 2 compared to the intra-mixtures.

By comparing the variations of the red slope and the water band depth between 8 and 40 hours for most of the samples, it appears that while the red slope remains constant, the water band depth significantly decreases. This observation indicates that despite the constant value of the red slope (mantle optically thick in the visible), the mantle of tholins and minerals continues to increase in thickness deeper in the sample, reducing the depth of the water absorption bands in the backscattered light.

After nearly 40 hours of sublimation, the water band depths are virtually zero for the intra- and inter- mixtures at 1% (Figure 5e, f). For the inter-mixture at 0.1%, the water bands are still present but have a very low band depth, between 0.1 to 0.2 (Figure 5c). For the intra-mixture at 0.1%, the water bands are still clearly seen, with a band depth around 0.6 after 40 hours of sublimation.

3.2.2.2 Spectral evolution during ejection of fragments of sublimation mantle

As described in section 3.1, the evolution of the samples during their sublimation is characterized by sudden ejections of fragments of mantle. Figure 6 shows the spectral

evolution of the ROI #11 (tholins-minerals-intra-mixture-0.1 sample) and ROI #9b (tholins-minerals-intra-mixture-1 sample) where such events occurred at least twice during the simulation (see Video 6).

Four ejection events occurred in ROI #11, on the tholins-minerals-intra-mixture-0.1 sample, at around 10h, 16h, 24.6h and 30.5h. All are characterized by a sudden:

- surge of reflectance (by +240%, +160%, +290% and +150% respectively),
- drop of the red slope (by -72%, -67%, -74% and -61% respectively),
- increase of the water band depth by no more than +20% (the ejection events correspond to local maxima on the curve in Figure 6c).

These spectral data clearly confirm the ejection of the mantle and the simultaneous exposure of ice particles at the surface of the sample. After each ejection event, the reflectance at 0.40 μm as well as the spectral red slope of ROI #11 are back to their value at t=2h, but never reach again the initial value at t=0h (see Figure 6a, b). Following each ejection event, the reflectance at 0.40 μm and the red slope evolve back toward the values for pure tholins, at the same rates and following exponential-decrease and logarithmic-shaped curves, respectively.

Two ejection events occurred in ROI #9b, on the tholins-minerals-intra-mixture-1 sample, at around 21h and 28h. The first event covers the whole area of the ROI whereas the latter event covers only a portion of the ROI. Both events are characterized by a sudden surge of the water band depth (by +197% and +95% respectively) and a slight increase of the red slope (by about +18%), but no significant variation of reflectance is observed.

On the same sample (tholins-minerals-intra-mixture-1), an ejection event is also seen at t=40.3h on ROI #9a. This event produced a sudden surge of the water band depth by +667%, but very faint variations of the reflectance at 0.40 μm (-7%) and red slope (+1%), confirming the peculiar behaviour of these spectral parameters during ejection events on this intra-mixture-1 sample compared to the intra-mixture-0.1 sample.

These data show that ejection events occurring on 1% intra-mixtures lead to an increase of the water band depth two orders of magnitude higher than those occurring on 0.1% intra-mixtures. Moreover, ejection events on 0.1% intra-mixtures are characterized by

high increase of reflectance in the ultraviolet-visible range and a decrease of the red slope, whereas such effects are practically absent for ejection events occurring on 1% intra-mixtures. For 1% intra-mixtures, the variations of the reflectance and red slope after an ejection event are of very low intensity (one to two orders of magnitude lower than for 0.1% intra-mixtures) and seem to occur in opposite directions: a decrease of the reflectance and an increase of the red slope. This increase of absorption in the visible might be due to the higher roughness of the surface exposed after the ejection events, compared to the flat surface of the initial mantle (see Supplementary Figure 7e and Video 6).

3.2.3 Scattering of the light by a sublimation residue

After the end of the experiment n°2, the sublimation residue obtained from the smectite-intra-mixture-1 sample was extracted from the SCITEAS simulation chamber and its light scattering properties were measured using the PHIRE-2 radio-goniometer. Figure 7 shows measurements of the reflectance factor (REFF) at 0.75 μm for incidence angles of 0° (Figure 7a) and 60° (Figure 7b). As a comparison, the initial smectite powder and the pure water ice particles were also measured. Over most of the phase curves, the scattering properties of the sublimation residue are close to those of initial water ice particles (strong forward scattering), except the lower intensity of the opposition peak. The smectite powder is made of larger aggregates (Supplementary Figure 6a), and thus has a higher roughness, than the smectite sublimation residue which is made of fine clay platelets (Figure 4a). The smectite powder is less bright and less forward scattering because it is rougher than the sublimation residue. Finally, the fact that the sublimation residue has retained the shape of the initial water ice particles probably explains the similarity seen with the phase curve of the water ice surface.

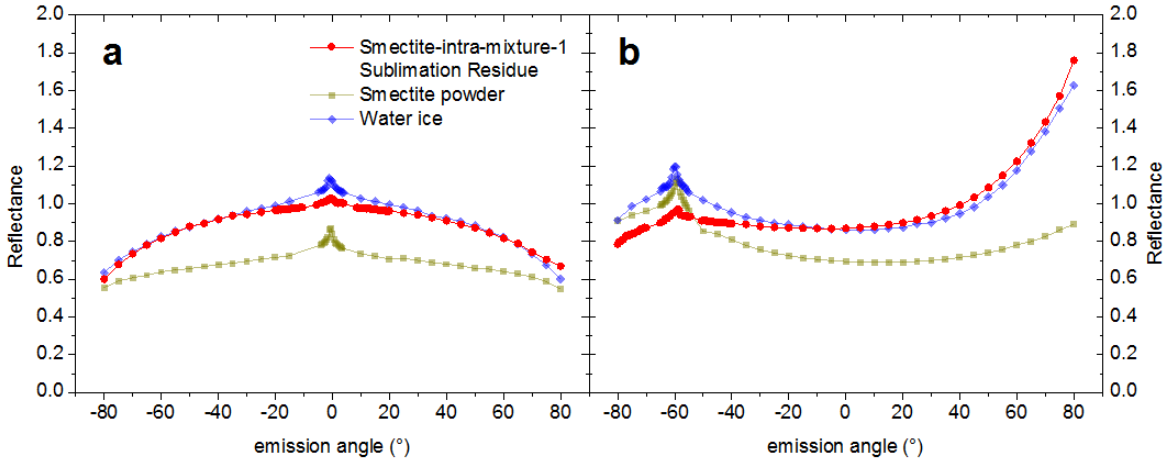

Figure 7 : Phase curves at 0.75 µm and at incidence angles i=0° **(a)** and i=60° **(b)** measured with the PHIRE-2 radio-goniometer for (1) the mantle obtained after the sublimation of the smectite-intra-mixture-1 (seen on Figure 2e, Figure 3e, Supplementary Figure 3e and Figure 4a) (red circles), (2) the initial smectite powder (green squares) and (3) the pure water ice particles. The scattering properties of the sublimation residue are close to those of initial water ice particles, except around the opposition peak where the light intensity is lower. The sublimation residue is strongly forward scattering.

4. Discussion

4.1 Mechanism of mantle build-up and ejection events

We have studied the sublimation of icy samples prepared from different types of mixture, constituents and concentrations and we observed the formation of sublimation lag deposits having diverse morphologies and activities. However, all sublimation lag deposits have in common a structure consisting of filaments made of the non-volatile materials, at the macroscopic or microscopic scale. Figure 8 illustrates the build-up of this sublimation mantle for ice-dust intra-mixture versus inter-mixture. The flow of gas generated by the sublimation of the ice moves the non-volatile particles and makes them collide and aggregate; forming a network of filaments in 2D (see Videos 1 and 2 showing the evolution of the 0.1% inter-mixture samples of pure olivine and pure smectite) or in 3D (see the smectite-intra-mixture-1 and tholins-minerals-intra-mixture-1 samples for example) over the ice surface. The filaments delimit areas (in 2D) or channels (in 3D) where fresh ice is exposed at the surface and from where the gas produced by the sublimation can freely escape the sample. When the network of filaments is denser, the size of these voids decreases and the mantle starts to impose more resistance to the gas flow. As the tortuosity of the path followed by the gas to exit the mantle

layer increases, the force exerted by the gas on the mantle increases up to the point when it reaches the tensile strength of the mantle and breaks it in fragments that are ejected away by the gas flow (see Figure 8). The sudden release of pressure within the ice results in an increase of its sublimation rate and a decrease of its temperature because of latent heat absorption. After the ejection event, the mantle is progressively rebuilt on the surface of the ice. For some samples, we observed that new ejection events occur again preferentially within the same area as the previous ones, probably because of a thinner and consequently more fragile mantle on these areas (see tholins-minerals-intra-mixture-1, tholins-minerals-inter-mixture-1, on Video 7). These samples also exhibit ejected area having quasi-circular shapes.

The building of filamentary structures from the sublimation of ices containing non-volatiles has been reported by several previous studies, from Dobrovolsky and Kajmakow (1977) to Saunders *et al.* (1986). The reports on the KOSI experiments do not explicitly name the structure as "filamentous", but a porous structure made of particles bonded together was described by Ratke and Kochan (1989), Thiel *et al.* (1989), Roessler *et al.* (1990), Thiel *et al.* (1991) and Kömle *et al.* (1991). In another context, the building of filaments and spider web-like structures has also been reported by sublimation of snow-flakes observed under SEM (Rosenthal *et al.*, 2007). Such filaments are formed by coalescence of salts, via surface diffusion driven by the reduction of the total surface energy. We estimate that the formation of such filamentous matrix residues upon sublimation is likely to be a universal process. The observation of outbursts of these sublimation residues was also reported before by Dobrovolsky and Kajmakow (1977) and explained by Thiel *et al.* (1989) and Ratke and Kochan (1989).

Our new observations suggest that the thickness of the individual filaments making up the sublimation residue, the density of the filamentous structure, its strength and the size of the ejected fragments all depend on the concentration, size and physico-chemistry of the non-volatile particles, and on how the ice and the non-volatiles are mixed together. The Table 2 and the paragraphs below provide a summary of the influence of each of these parameters on the texture, and consequently on the spectro-photometric properties of the sublimation residues.

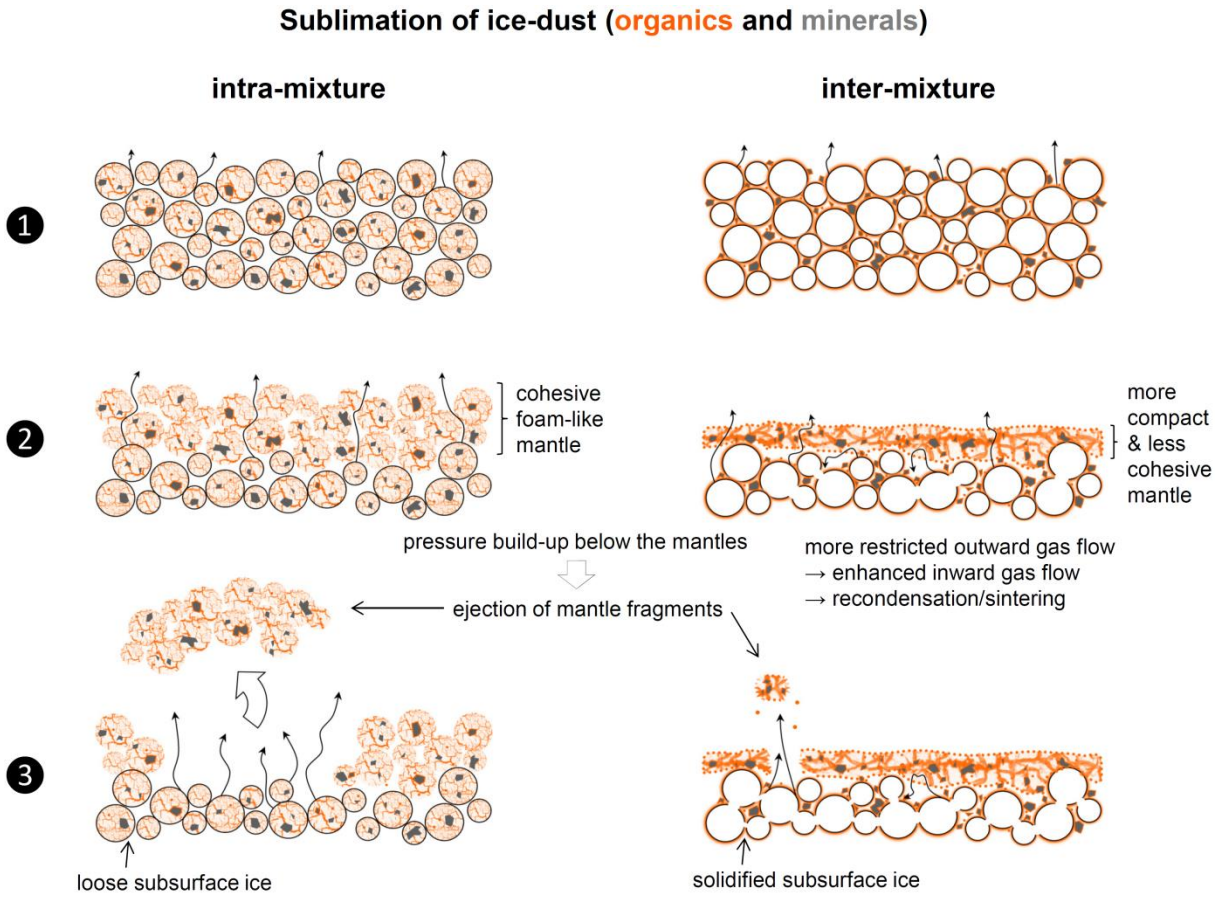

Figure 8 : Sublimation induced processes on ice-dust mixtures for which the non-volatiles are contained inside the ice grains (intra-mixture) or are intimately mixed with pure ice grains (inter-mixture). The dust is here composed of organic matter (orange) and silicate grains (grey).

Mixture type:	**Intra-mixture**							**Inter-mixture**						
Sample name:	**olivine-intra-mixture-0.1**	**olivine-intra-mixture-1**	**smectite-intra-mixture-0.1**	**smectite-intra-mixture-1**	**tholins-intra-mixture-0.1***	**tholins-minerals-intra-mixture-0.1**	**tholins-minerals-intra-mixture-1**	**olivine-inter-mixture-0.1**	**olivine-inter-mixture-1**	**smectite-inter-mixture-0.1**	**smectite-inter-mixture-1**	**tholins-inter-mixture-0.1***	**tholins-minerals-inter-mixture-0.1**	**tholins-minerals-inter-mixture-1**
Composition:	**0.1% olivine**	**1% olivine**	**0.1% smectite**	**1% smectite**	**0.1% tholins**	**0.1% olivine 0.05% tholins 0.01% smectite**	**1% olivine 0.5% tholins 0.1% smectite**	**0.1% olivine**	**1% olivine**	**0.1% smectite**	**1% smectite**	**0.1% tholins**	**0.1% olivine 0.05% tholins 0.01% smectite**	**1% olivine 0.5% tholins 0.1% smectite**
Ice particles size (µm)**:**	67±31	67±31	67±31	67±31	67±31	67±31	67±31	67±31	67±31	67±31	67±31	67±31	67±31	67±31
Density of the ice (g cm^{-3})**:**	0.5	0.5	0.5	0.5	0.5	0.5	0.5	0.5	0.5	0.5	0.5	0.5	0.5	0.5
Sublimation rate (mm/h)**:**	0.58±0.09	0.41±0.05	0.52±0.07	0.27±0.02	0.20±0.05	0.40±0.02	0.14±0.02	0.43±0.06	0.36±0.02	0.48±0.06	0.33±0.03	0.12±0.05	0.34±0.03	0.14±0.02
Structure of the sublimation deposit:	veil-like, 2D network of few µm thick filaments	veil-like, 2D network of few µm thick filaments	veil-like, 2D network of few µm thick filaments	foam-like, 3D network of few µm thick filaments	foam-like, 3D network of few µm thick filaments	veil-like, 2D network of few µm thick filaments	foam-like, 3D network of few µm thick filaments	2D network of 100-200 µm thick filaments	crust-like	2D network of 100-200 µm thick filaments	loose deposit, >200 µm thick filaments	skin/veil-like, 2D network of few µm thick filaments	skin/veil-like, 2D network of few µm thick filaments	loose deposit, 3D network of few µm thick filaments
Density of the mantle (g cm^{-3})**:**	N.D.	N.D.	N.D.	5.10^{-3}	5.10^{-4}	N.D.	8.10^{-3}	N.D.	N.D.	N.D.	N.D.	N.D.	N.D.	2.10^{-2}
Cohesiveness of the mantle:	+	+	+++	++++	+++	+++	++++	-	-	-	-	++	+	+
Structure of the ice beneath the mantle:	N.D.	N.D.	N.D.	N.D.	1 mm hard crust on top of soft ice	1-2 mm hard crust on top of soft ice	1-2 mm hard crust on top of soft ice	N.D.	N.D.	N.D.	N.D.	ice harden at all depths	ice harden at all depths	ice harden at all depths
Spectral properties of the sublimation mantle:	olivine absorption bands undetectable	olivine absorption bands undetectable	very weak smectite absorption in UV	featureless blue slope 0.7-1.9 µm, very weak smectite absorptions	visible red slope, water absorption bands partially masked	visible red slope, water absorption bands partially masked, minerals undetectable	visible red slope, featureless blue slope 1.1-2.2 µm, minerals undetectable	weak olivine absorption bands	olivine absorption bands detectable	very weak smectite absorption in UV	strong absorption in UV but very weak absorption bands in near infrared	visible red slope, water absorption bands partially masked	visible red slope, water absorption bands partially masked, minerals undetectable	visible red slope, water completely masked, minerals undetectable
Surface activity:	ejection events	subsidence events	ejection events	inflation and vibration	ejection events	ejection events	ejection events	no	subsidence events	no	no	ejection events	ejection events	no (exp.3), ejection events (sup. exp.)
Size of the ejected fragments:	~5 mm	N.A.	~10 mm and larger	N.A.	~10 mm and larger	~10 mm and larger	~10 mm	N.A.	N.A.	N.A.	N.A.	~10 mm	~5 mm	~2 mm
Spectral changes after mantle ejection events:														
Reflectance at 0.4 µm:	N.D.	N.A.	N.D.	N.A.	+30 to +160%	+150% to +290%	-7% to 0%	N.A.	N.A.	N.A.	N.A.	+150 to +210%	N.D.	N.D.
Visible red slope (0.40-0.94 µm):	N.D.	N.A.	N.D.	N.A.	-15 to -60%	-61 to -74%	+1% to +18%	N.A.	N.A.	N.A.	N.A.	-60 to -70%	N.D.	N.D.
Water band depth (1.5 µm):	N.D.	N.A.	N.D.	N.A.	+20 to 45%	< +20%	+95 to +667%	N.A.	N.A.	N.A.	N.A.	+10 to +15%	N.D.	N.D.

Table 2 : Summary of the results obtained after sublimation of the ice samples in this study and in *Poch *et al.* (2016). The structural and spectral characteristics of the sublimation mantles are described, as well as the activity observed during sublimation (ejection events etc.). N.D. stands for "Non Determined", N.A. stands for "Not Applicable" and "sup. exp." stands for the "supplementary experiment" shown in Video 7.

4.2 Influence of the sample mixture type, composition, and concentration on the texture and consequently on the spectro-photometric properties of the sublimation residues

4.2.1 Influence of the mixture type (inter- or intra- mixture)

The way the non-volatile components are mixed with the ice has a strong influence on the properties of the sublimation lag deposit produced from the ice mixture. The sublimation of inter-mixtures leads to rather compact and loose deposits on top of the ice, having a weak internal cohesion, whereas the sublimation of intra-mixtures produces much more structured residues, having higher porosity and internal cohesion.

The spectro-photometric properties of the sublimation residues are significantly affected by such differences of structure. The reflectance spectra of residues of inter-mixtures show the absorption bands of the non-volatile compounds, although with a significant reduction of the band depths, possibly in part because of dehydration under vacuum. However, the spectral signatures of the non-volatiles are hardly detectable in the reflectance spectra of residues of intra-mixtures. We explain this disappearance of the absorption bands by the small size of their particles combined with the very porous nature of the sublimation mantles (see Figure 4). As explained by Cooper and Mustard (1999) and Salisbury and Wald (1992), when very fine particles are separated by spaces more than a wavelength in size they scatter the light individually as volume-scattering particles. Whereas in more tightly packed, less porous cases, the particles scatter coherently, behaving as large, surface-scattering particles. As a consequence, the band depths of the materials present in very porous sublimation mantles, as the one obtained from the sublimation of intra-mixtures, are extremely faint or quasi-absent (see Figure 5).

The foam-like residues of intra-mixtures which have conserved the shape of the initial ice particles exhibit a featureless blue slope from about 1 to 2 μm. This featureless blue slope is probably caused by the light scattering within the porous structure of the residues. Brown (2014) used Mie and Rayleigh scattering models to study spectral bluing induced by small particles and found that all sufficiently narrow size distribution of spherical scatterers will cause spectral bluing, regardless of their optical index. In particular, Brown (2014) indicates that the spectral bluing is the strongest for size factors[1] between 0.5 and 1.2. We note that the

[1] The size factor X is defined as $X = \pi.D/\lambda$ with D the diameter of the scatterer's particle and λ the wavelength.

size factor for the spherical tholins particles is 0.5 at 1.1 μm and 0.9 at 2.2 μm, and so it is in the range highlighted by Brown (2014). Several Solar Systems objects exhibit featureless and blue-sloped surface reflectance spectra (Brown, 2014 and references herein) and our data show that the sublimation of intra-mixture ices can produce such spectral feature.

The mixture type also has a strong influence on the activity of the sample surface during sublimation. Both intra- and inter- mixtures show ejection events, but the fragments ejected by intra-mixtures are around 5 times larger than the ones ejected by inter-mixtures. This is due to the higher internal cohesion of intra-mixtures versus inter-mixtures residues. Moreover, the residues from inter-mixtures are denser and are ejected faster than the more porous ones of intra-mixtures.

Finally, the two mixture types lead to very different strength of the ice beneath the sublimation mantle after a few hours of sublimation. The ice remaining below the mantle of inter-mixture samples is significantly harder than the one of intra-mixture samples. This hardening is due to the recondensation or sintering of water between the ice particles. The initial presence of non-volatiles between the individual ice particles may provide pre-existing mechanical linkages which facilitate the recondensation/sintering process. The texture of the sublimation mantle may also play a role in the hardening of the ice, by influencing the temperature or pressure within the ice, and thus the sublimation/recondensation rates as discussed by Prialnik and Mekler (1991). Because the mantle produced from inter-mixtures is more compact, it is possible that it restricts more the flow of gas passing through it, enhancing inward flow and recondensation of water between the ice grains (see Figure 8). Many other cometary simulation experiments by Kochan *et al.* (1989), Ratke and Kochan (1989), Seiferlin *et al.* (1995) and Thiel *et al.* (1989) also observed a solidified crust of ice below an upper mantle.

4.2.2 Influence of the constituents (minerals, organics, and particle size)

Intra-mixture: When mixed as an intra-mixture, we observed that smectite reduced at the size of platelets (~1 nm thick and 72 nm diameter) produce a residue having a stronger internal cohesion (foam-like structure) than the olivine grains (≤ 80 μm) (fragile veil-like structure). The addition of organics (0.3±0.2 μm particles) in the mixture also provides more cohesion.

From these observations, it is clear that the internal cohesiveness strongly depends on the strength of the intermolecular forces engaged between the non-volatile particles (electrostatic forces, Van der Waals forces or hydrogen bonds). Concentrated at the interfaces between the ice crystals during the freezing of the water droplet, the non-volatiles can interact and rearrange. The tholins particles used in this study can interact via hydrogen bonds and electrostatic forces, the montmorillonite platelets via electrostatic bonds, but the olivine grains have much less possibilities to interact strongly enough with other olivine grains to build a cohesive residue. Strong inter-particles interactions promote the building of a highly porous and cohesive sublimation mantle. The reflectance spectra of these residues do not show all the absorption bands characteristic of the material they are made of and in most cases, only the UV-Vis absorptions are still detectable.

Inter-mixture: For this type of mixture, the size of the non-volatile particles is the main factor controlling the structure of the residue of inter-mixtures, rather than their physico-chemistry properties. The smaller the grain size of the non-volatiles, the thinner the filaments and the smaller the voids or channels are between the filaments. For broad size distributions particularly extended toward the small particles, the aggregation of the grains can lead to the reduction of the size and/or number of these voids resulting in the formation of a crust that significantly reduces the sublimation rate of the ice located underneath (as observed for the olivine-inter-mixture-1) (see Table 2).

Finally, for both inter- and intra-mixture, we observed that when tholins particles are present in the mixture, even at a concentration ten times smaller than the mineral grains, the absorption features of the minerals are almost completely masked.

4.2.3 Influence of the concentration of non-volatiles (0.1%, 1%)

Intra-mixture: When the concentration of non-volatiles increases, the cohesion of the final residue increases, resulting in less frequent ejection events but larger ejected fragments. Also, as the concentration increases, the spectral changes after ejection events are less pronounced in the visible wavelengths but more pronounced in the near infrared. This trend is of course largely dependent on the spectral properties of the material, and particularly the organic particles constituting the sublimation deposit. Here we used tholins which are dark in the UV-

Vis (optically thick mantle in the UV-VIS) but very bright in the near infrared (optically thin mantle in the NIR).

Inter-mixture: When the concentration of non-volatiles increases, the filaments formed from the aggregation of the materials dragged by the gas flow increase in thickness, which reduces the area of the voids or channels between the filaments, reducing the sublimation rate (see Table 2).

The extrapolation of these results for higher dust/ice mass ratios, closer to that expected on comets (100 wt.% and more), should be done with caution. On the first hand, one could expect that increasing the concentration of non-volatiles could increase the internal cohesion of the mantle. But on the other hand, decreasing the amount of ice in the sample could reduce the aggregation of the non-volatiles via gas dragging. Future experimental studies of the sublimation of inter- and intra- ice mixtures containing higher concentrations of non-volatiles should provide a more definitive answer to this question.

4.3 Implications for comets and icy bodies

4.3.1 Potential limitations of laboratory simulations compared to icy bodies

First, the extrapolations of the details observed on a scale of centimetres in the laboratory to the larger scales observable by planetary or cometary space instruments is not obvious and should be done with caution. Second, as we mentioned in section 2.4.1, the irradiation source and gradient of temperature inside our samples were very different from an ideal cometary case. The possible consequences of these parameters on the building of sublimation mantles will be addressed in future studies. Third, the gravitational field in the laboratory is about three orders of magnitude stronger than on a comet. However, calculations performed by Kochan *et al.* (1990) and Ratke and Kochan (1989) show that some dust particles lying on top of the ice surface are not gravity force dominated. Figure 10 in Ratke and Kochan (1989) shows that the gas drag dominates by two orders of magnitude over gravity for particles (0.3 g/cm^3) smaller than 10 μm, and that the cohesive forces between particles dominate by several orders of magnitude over gravity. In our experiments, the tholin particles, having a density of that order and a mean diameter of around 0.3 μm, are thus

mainly influenced by the gas drag and the cohesive forces. However, the mineral grains of diameter smaller than 80 μm and of density around ~3 g/cm^3 are probably more subjected to the gravity field in our experiments. Nevertheless, we observed that both olivine and smectite grains rearranged in filamentous structures upon sublimation, like tholins do, indicating that the gas drag still plays a major role during the sublimation. Consequently gravity has probably a negligible impact on the structure of the sublimation residues and their spectro-photometric properties.

4.3.2 The major influence of the inter-molecular forces between non-volatiles

Our results demonstrate that the sublimation process can produce structure similar to that of Interplanetary Dust Particles (Duprat *et al.*, 2010) by the aggregation of fine grain materials forming a matrix that can bound together bigger grains (see Figure 4c). In particular, our results demonstrate the ability of organic matter to act as a glue binding minerals in comatery grains, as proposed by Kissel and Krueger (1987). More generally, the inter-particulate or inter-molecular interactions between the non-volatile components have a major influence on the texture, the activity and the spectro-phometric properties of the sublimation residues. In this regard, one should note that although the tholins we used produced strong internal cohesion, other types of organics may not. Storrs *et al.* (1988) noticed that not all organics have the same abilities to form filamentous residues. The content of hetero-atoms (other than carbon) and hydrogen (H/C ratio) in the chemical structure probably enhances the ability of organic molecules to interact more strongly, and form cohesive sublimation residues.

4.3.3. Application to the interpretation of remote sensing datasets of icy bodies

The results of the experiments presented in this paper constitute reference laboratory data that can be used to interpret remote sensing datasets on icy surfaces, including comets and icy satellites.

The temporal evolution of the spectral properties of the laboratory samples can serve to understand the influence of the sublimation process on the spectral properties of the icy surfaces. For example, our laboratory data on ice-tholins analogue mixtures suggest that variations of the surface reflectance and steepness of the red slope observed on the cometary surface may be indicative of the thickness of the organic mantle covering ice material

(Fornasier *et al.* 2015, Capaccioni *et al.* 2015). For instance, by comparing the spectral ratios between the reflectance spectra obtained before and after the formation of the sublimation mantle with those observed on the comet, Pommerol *et al.* (2015b) showed that the contrasts of brightness and colour seen at the surface of the nucleus were consistent with the result of sublimation process (see Fig. 9 and Fig. 11 in Pommerol *et al.*, 2015b). A similar method could be applied to compare the data obtained from other bodies with our laboratory data. Additionally, the documentation of the evolution of the reflectance of the continuum and the water band depth in the near infrared can also support the interpretation of the data gathered by infrared spectrometers on-board spacecrafts. For such comparison and interpretation purposes (calculation of spectral ratios, calculation of spectral slopes or band depths with other wavelengths or definitions, etc.), the calibrated hyperspectral data of all the ROIs presented in this paper are available upon demand to the corresponding author.

Furthermore, the evolution of the structure and physical properties of the analogue samples during sublimation also provides interesting clues to understand the surface of icy bodies. The ability of non-volatile particles, and particularly organics, to build bounds between them can help to explain the formation and ejection of large dust grains in jets and their deposition as “airfall” on cometary nuclei (Thomas *et al.*, 2015). The hardening of the ice below the sublimation mantle, as observed in laboratory experiments, also provides a plausible mechanism to explain the observation of brittle mechanical behaviour of some regions on the surface of 67P/Churyumov-Gerasimenko (Pommerol *et al.*, 2015b). Moreover, differences seen in term of mantle structure, sublimation speed, speed of mantle building, rates and surface area of mantle ejection, between intra- and inter- mixtures (see Table 2) might provide clues to discriminate between these mixture types on cometary nuclei surfaces or on other surfaces of air-less bodies where dirty ices are sublimating.

5. Conclusion

The sublimation of cometary ice analogues, made of crystalline water ice mixed with olivine, smectite and complex organic matter, has been carried out under low temperature and pressure conditions. The temporal evolutions of the surface texture and surface visible and near-infrared reflectance of the samples were monitored *in situ*. Samples prepared using

different mixture types, compositions and concentrations have been sublimed, and their evolutions have been compared. The main results are summarized below:

- **After few hours of sublimation, a water-free residue, made of the non-volatiles contained in the ice, mantles the top of the samples**. The texture, the activity and the spectro-photometric **properties of this mantle are found to differ strongly** depending on the chemical nature of the non-volatiles, the size of their particles, the way they are mixed with the volatile component and the dust/ice mass ratio. Two types of mixtures of non-volatiles with the ice have been investigated: intra-mixtures and inter-mixtures. The prepared intra-mixture samples are made of ice grains in which the non-volatiles are mainly aggregated at the interfaces between the water crystals, inside the particles. In contrast, the inter-mixture samples are made of particles of pure water ice whose external surfaces have been coated with the non-volatiles (non-volatiles decoupled from the ice). Both of **these mixture types are potential analogues of ices present at the surface or near sub-surface of cometary nuclei** (Lignell and Gudipati, 2014; Protopapa *et al.*, 2014; Sunshine *et al.*, 2007).
- **The sublimation of intra-mixture ices form a residue made of a network of filaments which can be very porous and cohesive if the non-volatile particles have the ability to aggregate via strong inter-particulate interactions (foam-like structure).**
- **The sublimation of inter-mixture ices produces a residue at least twice more compact and less cohesive than intra-mixtures.** The residue has a structure made of aggregates of filaments. The space between the filaments (voids) depends on the concentration, the size distribution and the shapes of the non-volatile particles. For example non-volatile particles having wide size distribution can produce an aggregate with virtually no void, a dense crust, on top of the ice.
- **Non-volatile organic matter plays a major role in the properties of the sublimation residues.** Because of their strong inter-particulate forces, C,H,N-tholins act as a glue bonding mineral grains together and **increasing the internal cohesiveness** of the residues.
- **Sudden ejections of fragments of the mantles, from mm to cm sizes, are observed during the sublimation**, triggered by the force exerted by the gas flow on the mantles. The **internal cohesion of the mantle** is the main parameter controlling the

frequency of the ejection events and the size of the ejected fragments. More cohesive mantles produce larger fragments. Intra-mixtures are much more active than inter-mixtures. The presence of complex organic matter enhances the occurrence of these ejection events by increasing the internal cohesion and the tortuosity of the matrix, making the sublimation residue more impervious to the gas flow.

- **A hardening of the ice is observed in inter-mixture samples after sublimation and formation of a compact mantle above the ice.** Such hardening is much less pronounced for intra-mixture samples. It is due to the recondensation/sintering of the water between the individual ice particles. This hardening may be caused by the initial presence of non-volatiles between the individual ice particles or the texture of the sublimation mantle favouring inward gas flow.
- **The reflectance spectra of the foam-like sublimation residues obtained from intra-mixtures** show some absorption features of the non-volatiles in the visible, whereas in the near infrared range the spectra **exhibit a featureless blue slope in the near infrared,** due to a **peculiar light scattering property** provided by the fluffy filamentous structure of the residue (Brown, 2014).
- **The reflectance spectra of the sublimation residues obtained from inter-mixtures** show more pronounced spectral signatures of the non-volatile components, although these signatures are mostly still fainter than those of the original powders. **These residues do not exhibit a blue slope** in the near-infrared, probably because of their more compact structure.
- **As the ice sublimes and the residue of non-volatiles forms** on top of the ice, the **reflectance at 0.40 µm** (where most of non-volatiles absorb light) **decreases**, as well as the **band depths of the water ice** absorption bands which are masked by the layer of non-volatiles. Simultaneously, the **spectral red slope** due to the absorption of complex organic matter (tholins) in the UV-visible increases. This spectral feature of the organic matter clearly dominates the reflectance spectrum versus the minerals, because the mineral grains are embedded in a matrix of tholins particles.
- The evolution of **the reflectance at 0.40 µm appears to depend more on the mixture type** (intra- or inter- mixture) whereas **the band depths of water ice and the spectral red slope are more sensitive to the concentration** of the non-volatile compounds in the ice.

- Interestingly, we observed that while the depth of the water absorption bands in the infrared continues to decrease, the spectral features of the non-volatiles (reflectance at 0.40 μm and red slope) remain almost constant in the visible. This indicates that **the mantle of tholins and minerals rapidly becomes optically thick in the visible**, stopping any further spectral evolution in this wavelength range while continuing to increase in thickness deeper in the sample.
- **The ejections of large fragments of mantles expose ice particles to the surface of the samples.** This activity can be monitored spectroscopically from **the contrast of brightness between mantled and ice-exposed areas.** However, **the magnitude of this contrast strongly depends on the wavelength range and the dust/ice ratio considered.** The activity of low dust/ice mixtures could be best monitored in the visible (from the contrast of albedo between active and non-active areas) whereas the activity of high dust/ice mixtures could be best monitored in near-infrared. These effects are due to the spectral properties of the tholins used for this study: very absorbent in the UV-visible, but very bright in the near-infrared. Cometary organic matter could probably have less contrasted optical properties and be also absorbent in the near-infrared.
- **The phase curve of the sublimation residue having a foam-like structure is close to that of the initial water ice particles**, but the intensity of the opposition peak is lower.

These data provide useful references for interpreting remote sensing observations of comets and potentially of other icy Solar System surfaces. In particular, they provide some elements of explanation regarding the activity of comet nuclei where sublimation of dirty ices and deposition of organic and mineral dust particles play a major role.

To improve the representativeness of future simulations compared to comets, we are working on extending the capability of our setup for the production of icy analogues to allow the production of intra-mixture ices having higher concentrations in non-volatiles. Furthermore, we will also work on carrying out simulations more representative in term of irradiance and spectral reflectance, by illuminating the sample using a Sun simulator and preparing samples having lower albedo, closer to that of cometary components.

Acknowledgements

The construction of the SCITEAS facility was funded by the University of Bern and by the Swiss National Science Foundation. The NCCR PlanetS is acknowledge for the founding of the Optical Coherence Tomography (OCT) instrument. We thank Adolfo Odriozola, Daniel Studer and Benoît Zuber from the Institute of Anatomy of the University of Bern for their help in the analysis of the samples via Scanning Electron Microscopy. We also thank Klaus Mezger from the Institute of Geological Sciences of the University of Bern for his help regarding the grounding of the mineral powders. We thank Sonia Fornasier for useful discussions. O.P. thanks the Center for Space and Habitability of the University of Bern for funding. Finally, we want to thank two anonymous reviewers for their careful reading of the manuscript and their comments which improved its quality.

Supplementary Materials

Videos can be found on http://dx.doi.org/10.1016/j.icarus.2015.12.017 or can be obtained directly from the author by email (olivier.poch@csh.unibe.ch). The Supplementary Figures are provided in the "Appendix A" below.

Appendix A. Supplementary Figures:

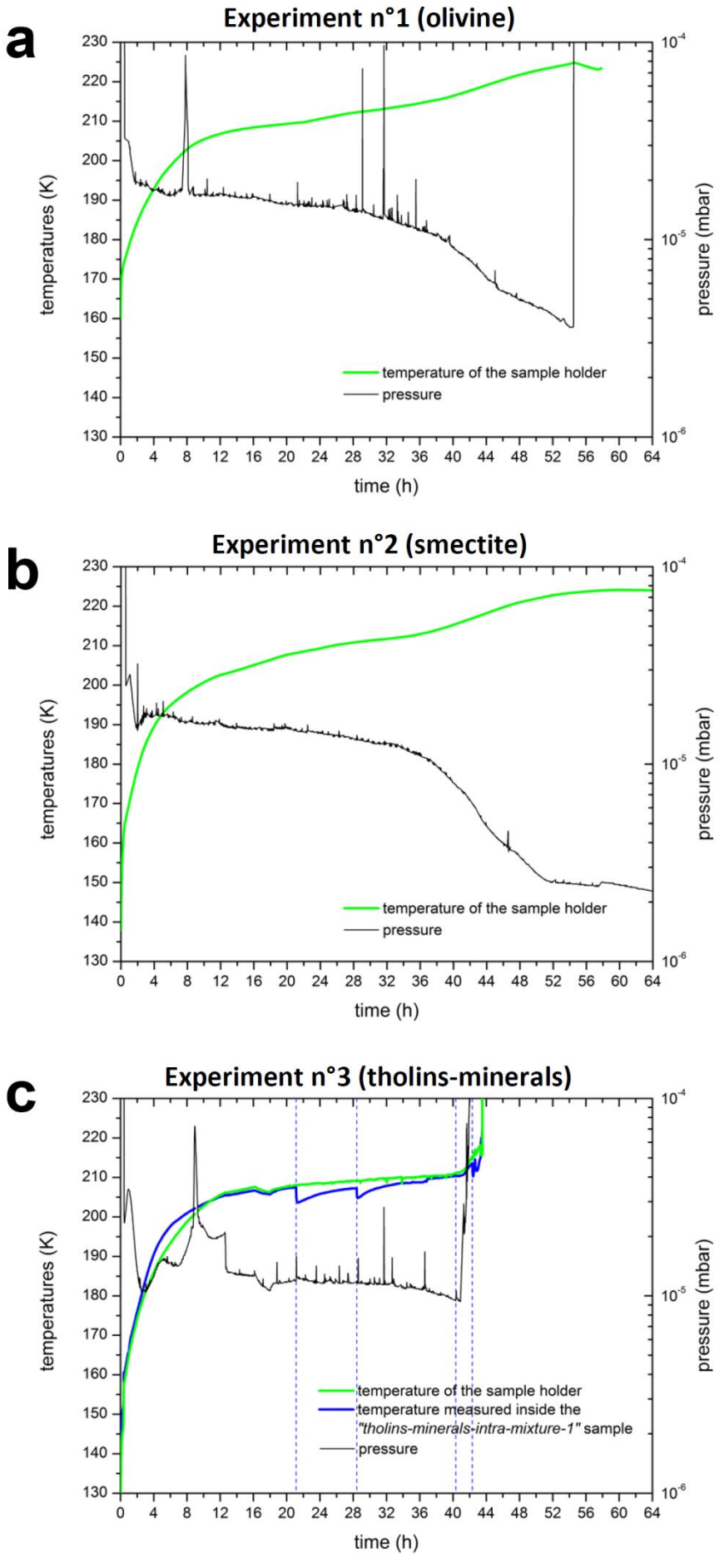
a
Experiment n°1 (olivine)
temperatures (K)
pressure (mbar)
time (h)
temperature of the sample holder
pressure
b
Experiment n°2 (smectite)
temperatures (K)
pressure (mbar)
time (h)
temperature of the sample holder
pressure
c
Experiment n°3 (tholins-minerals)
temperatures (K)
pressure (mbar)
time (h)
temperature of the sample holder
temperature measured inside the
"tholins-minerals-intra-mixture-1" sample
pressure

Supplementary Figure 1 : Temperature (green curves) and pressure (black curves) measured inside the chamber during the experiments n°1 **(a)**, n°2 **(b)** and n°3 **(c)**. In **(c)**, vertical dashed blue bars indicate the time during which an ejection event occurred on the tholins-minerals-intra-mixture-1 sample. The first two events can be correlated to a drop of the temperature measured by a sensor positioned inside the sample (blue curve) and to a pressure spike (black curve) (see section 3.1.1). Experiment n°1 was shorter than the others because the samples were removed from the chamber to test the strength of the ice before it is totally sublimed. (For interpretation of the references to colour in this figure legend, the reader is referred to the web version of this article)

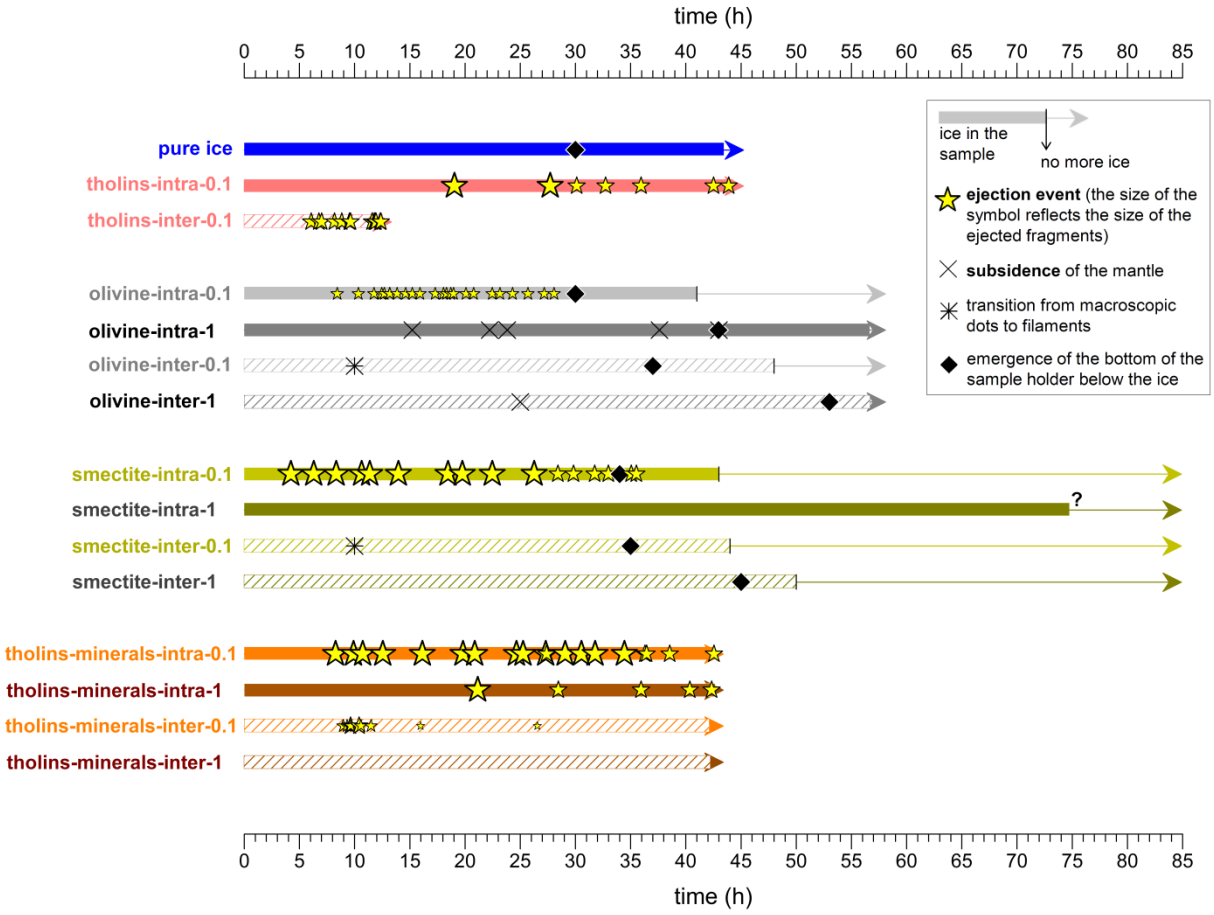

Supplementary Figure 2 : Timelines of the evolution of the surface of all the samples during their sublimation, as seen on Videos 1, 2 and 3. Overall, the temperature and pressure variations were quite similar for all experiments (see Figure 1 and Supplementary Figure 1), allowing a simultaneous comparison of the evolution of the surface morphology of all the samples. The data from “pure ice”, “tholins-intra-0.1” and “tholins-inter-0.1” samples are from Poch *et al.*, (in press).

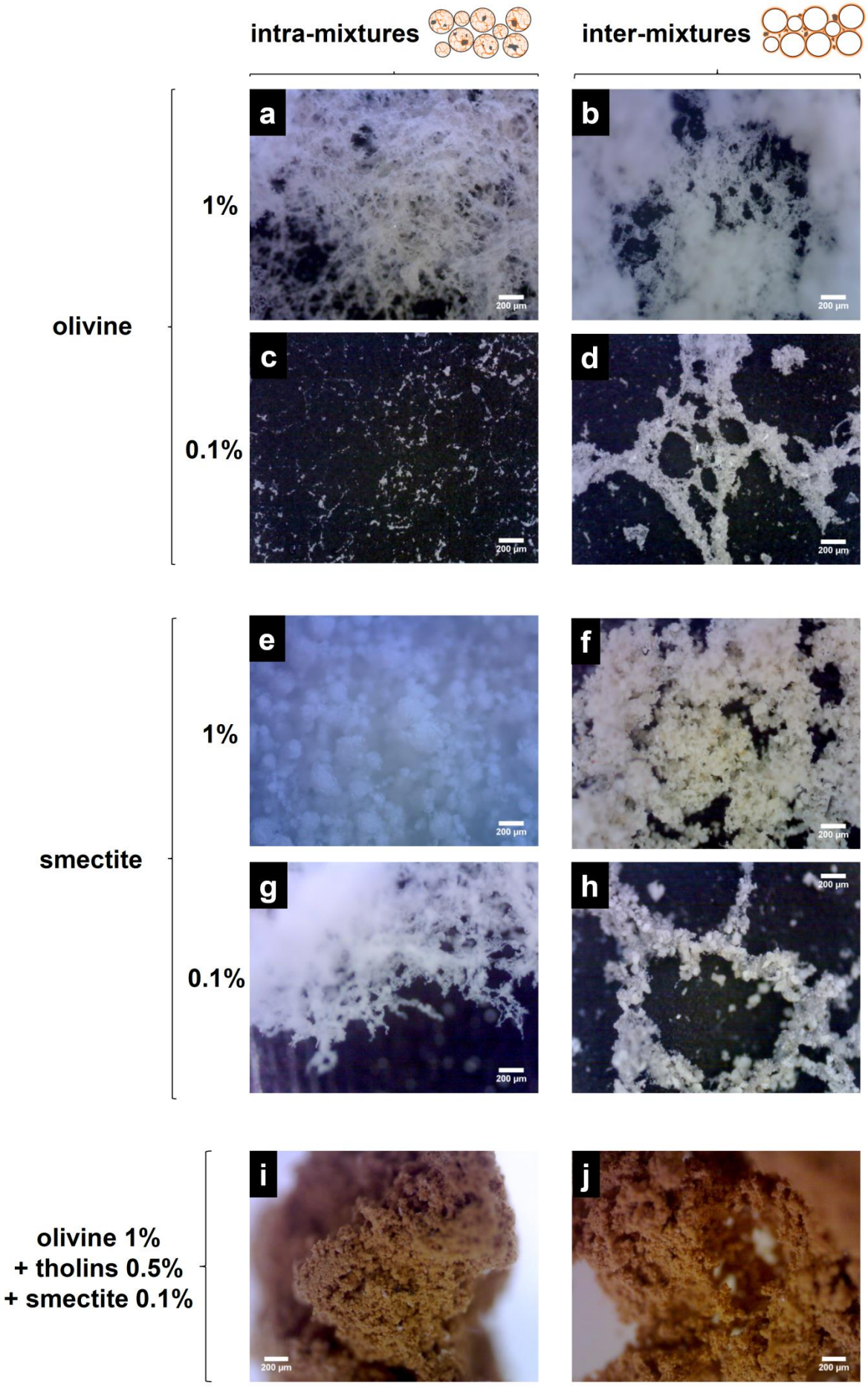
intra-mixtures
inter-mixtures
olivine
1%
0.1%
smectite
1%
0.1%
olivine 1%
+ tholins 0.5%
+ smectite 0.1%
a
b
c
d
e
f
g
h
i
j
200 µm

Supplementary Figure 3 : Visible microscope images of the water-free residues collected after sublimation of the samples in the simulation chamber. These images were taken *ex situ*, after the simulation. Tholins-minerals samples of low concentration (0.1%) have not been imaged by microscopy.

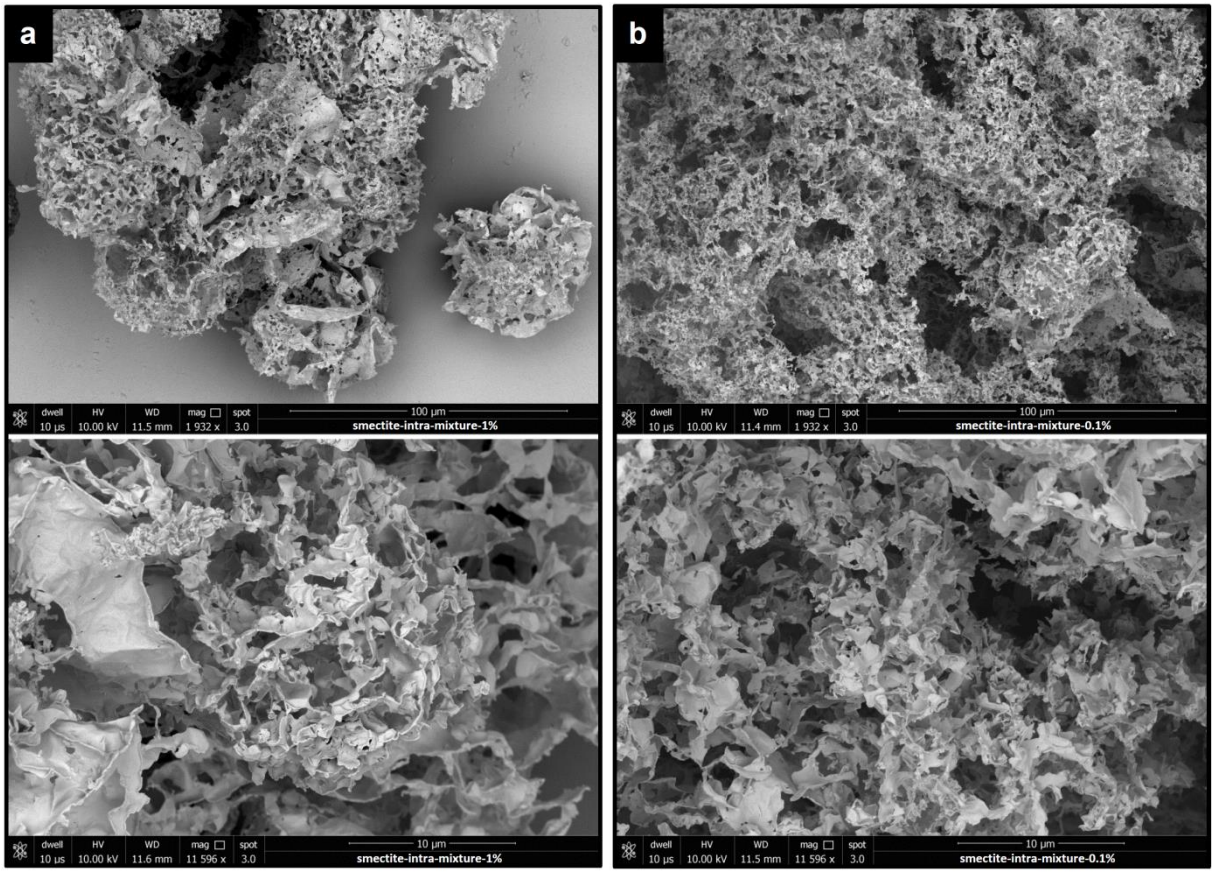

Supplementary Figure 4 : Scanning Electron Microscope images of the water-free sublimation residues of an intra-mixture of water ice particles and smectite (Na-montmorillonite) at a concentration of **(a)** 1% (smectite-intra-mixture-1), and **(b)** 0.1% (smectite-intra-mixture-0.1).

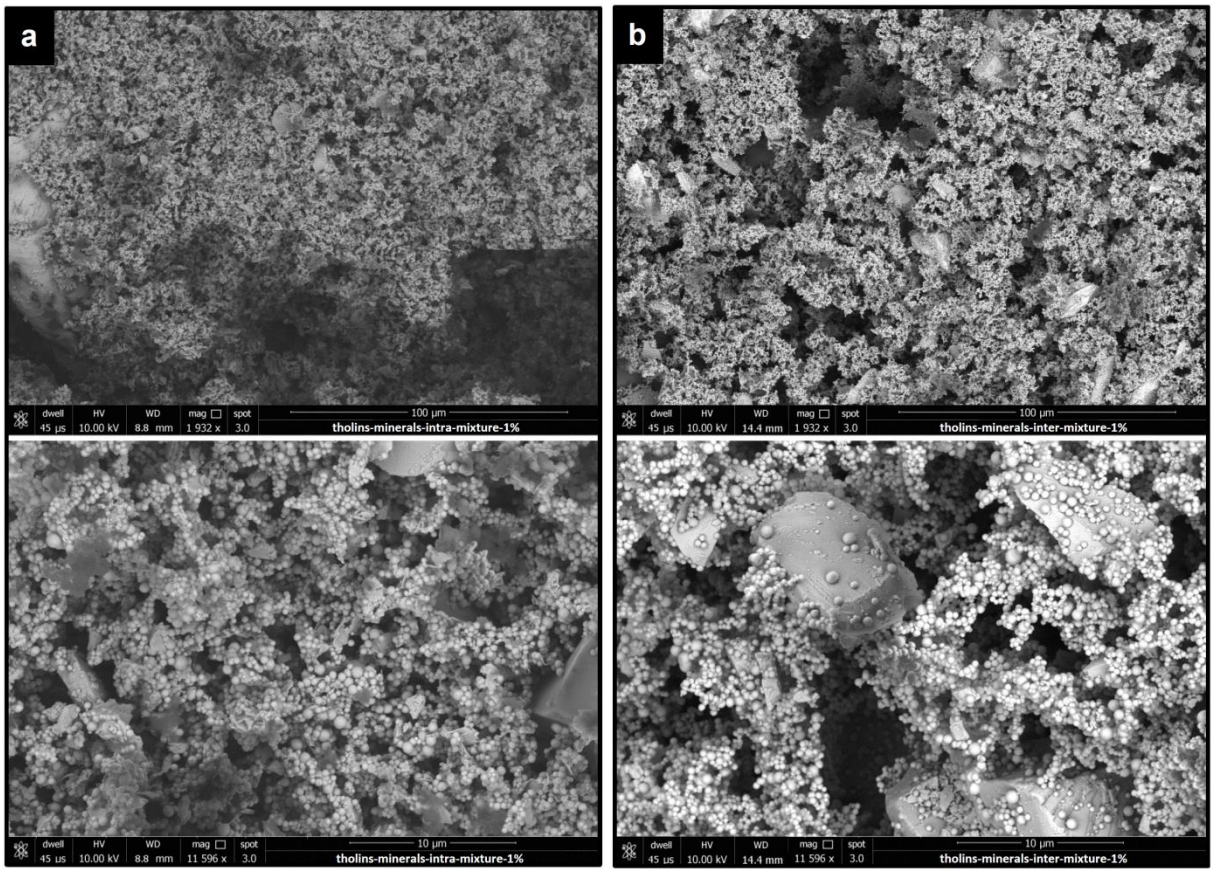

Supplementary Figure 5 : Scanning Electron Microscope images of the water-free sublimation residues of water ice particles mixed with olivine (1%), tholins (0.5%) and smectite (0.1%) as **(a)** an intra-mixture (tholins-minerals-intra-mixture-1) and as **(b)** an inter-mixture (tholins-minerals-inter-mixture-1).

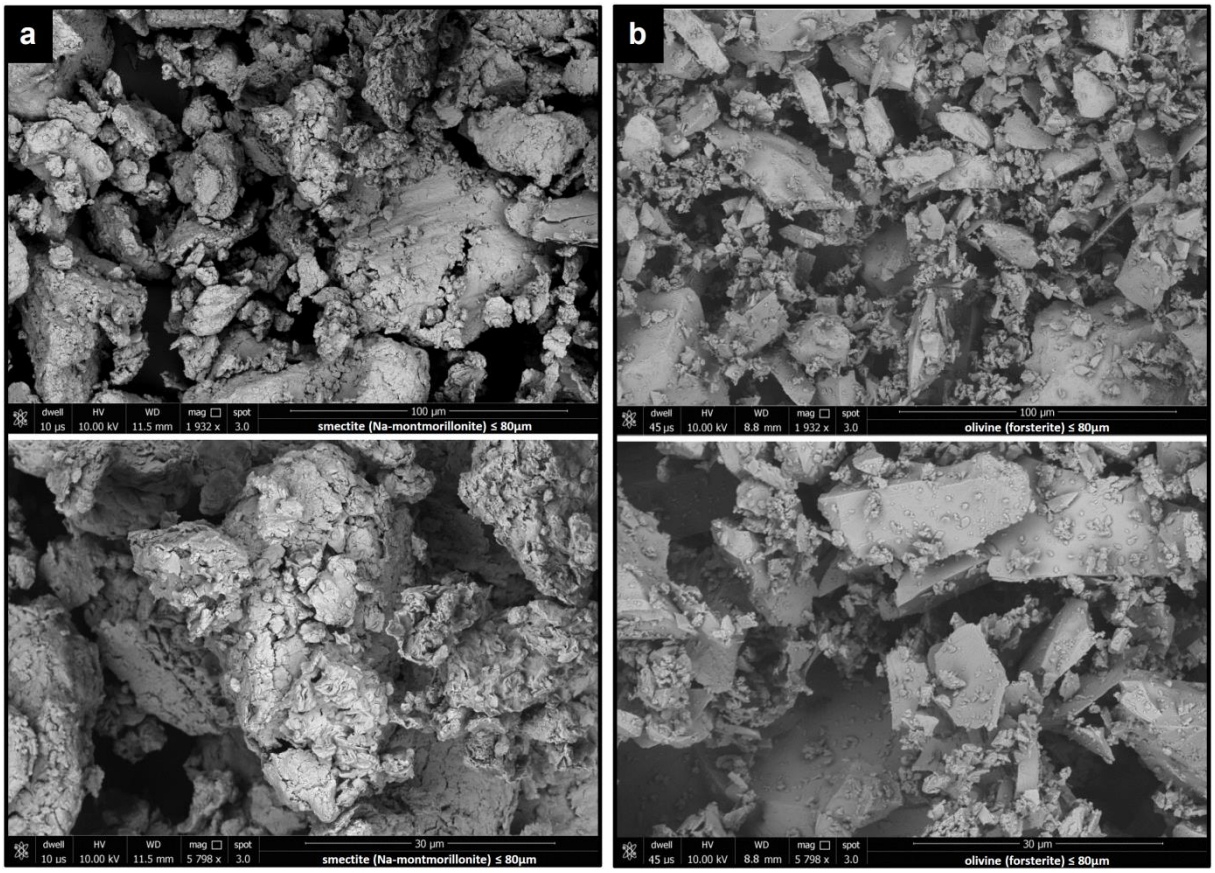

Supplementary Figure 6 : Scanning Electron Microscope images of **(a)** the particles of smectite (Na-montmorillonite) and **(b)** the particles of olivine (forsterite) after grounding and sieving using an 80 µm sieve. The grains of smectite are made of clusters of clay platelets (tactoids). The olivine powder is made of compact grains having a wide size distribution; it contains more small grains than smectite.

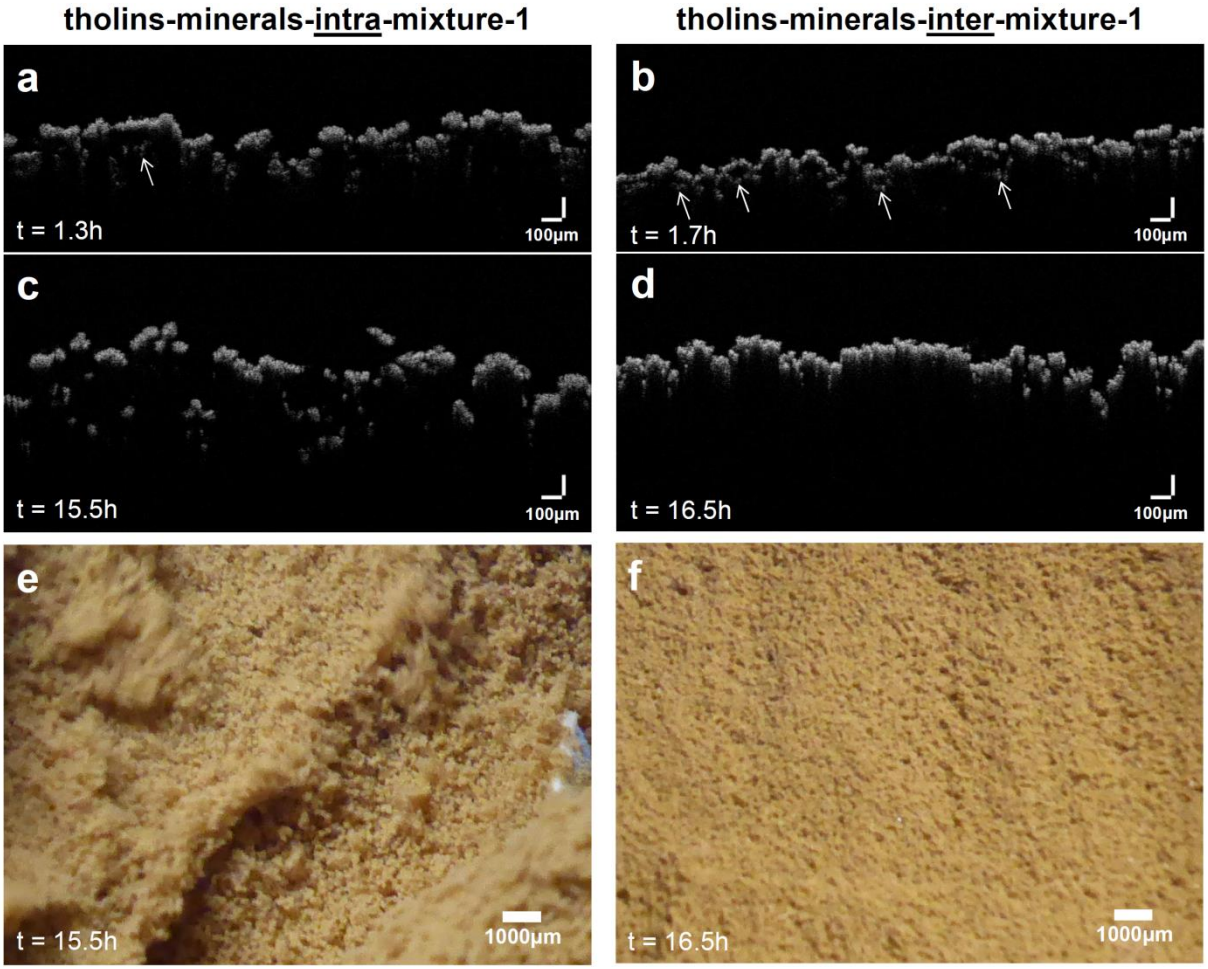

Supplementary Figure 7 : Optical Coherence Tomography images of the surface of the tholins-minerals-intra-mixture-1 (left) and tholins-minerals-inter-mixture-1 (right) samples obtained *in situ* during the sublimation of the samples inside the simulation chamber, at t = 1.3-1.7h **(a,b)** and t = 15.5-16.5h **(c,d)** (see also the Video 11 and 12 showing the 3D reconstruction of the surfaces). At t = 1.3-1.7h the surface of the samples consists of water ice particles and of some layer of sublimation residues. At t = 15.5-16.5h, the surface of the samples is completely water-free: the images show the sublimation residue. High resolution images of the surface of the samples obtained *in situ* are shown in **(e)** and **(f)**. (see Table 1 for an explanation of the sample names and see Appendix B.5 for the interpretation of the data)

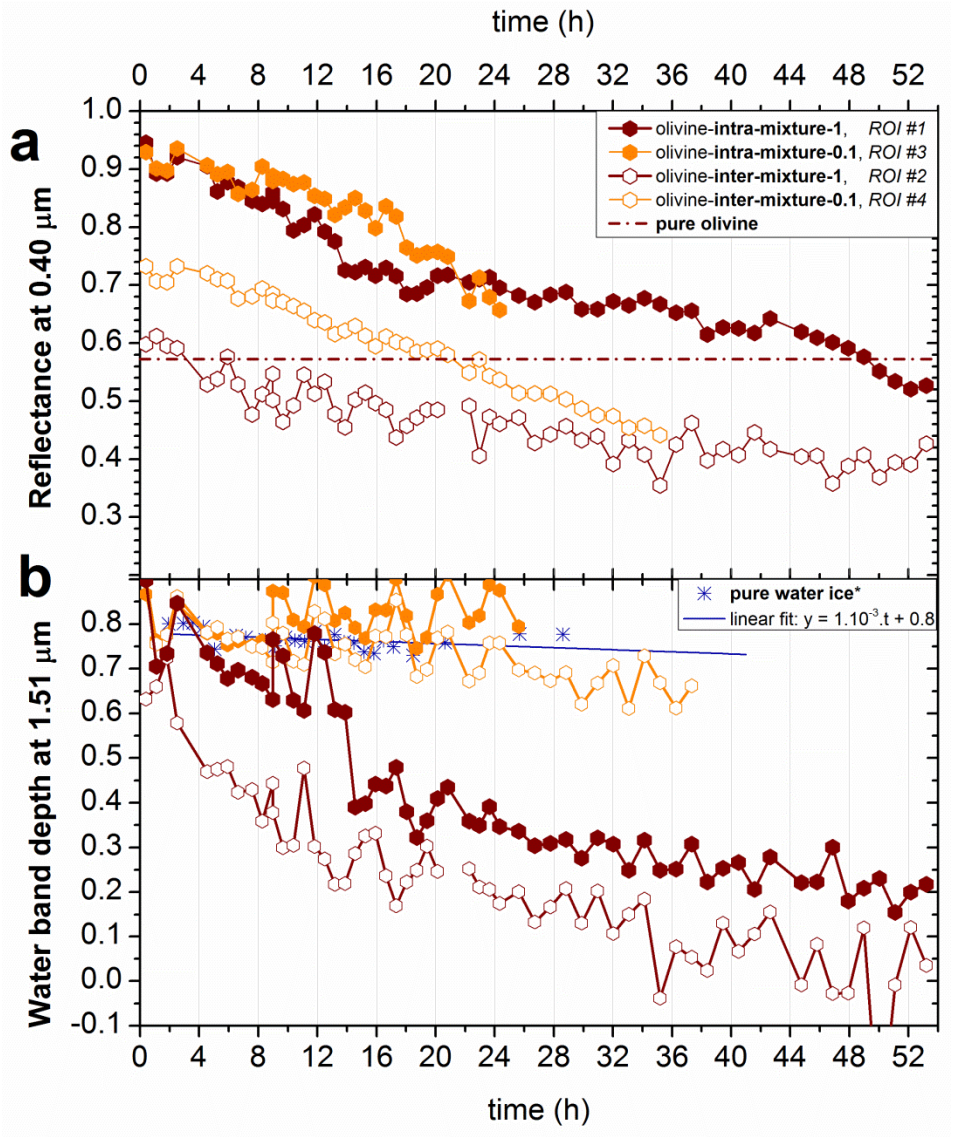

Supplementary Figure 8 : *In situ* spectral evolution of the samples of **olivine mixed with water ice** particles as intra- or inter- mixtures and at different concentrations. Temporal evolution of **(a)** the reflectance at 0.40 µm where olivine absorbs, and **(b)** the band depth of the water absorption band at 1.51 µm (see Eq. 2). These data have been obtained from spectra acquired in ROI #1 (olivine-intra-mixture-1), ROI #3 (olivine-intra-mixture-0.1), ROI #2 (olivine-inter-mixture-1) and ROI #4 (olivine-inter-mixture-0.1) located in Figure 2a,b,c,d and Video 4 (see Table 1 for the explanation of the samples names). *The pure water ice data are from ROI #0 of Poch *et al.* (in press). (For a colour version of this figure, the reader is referred to the web version of this article)

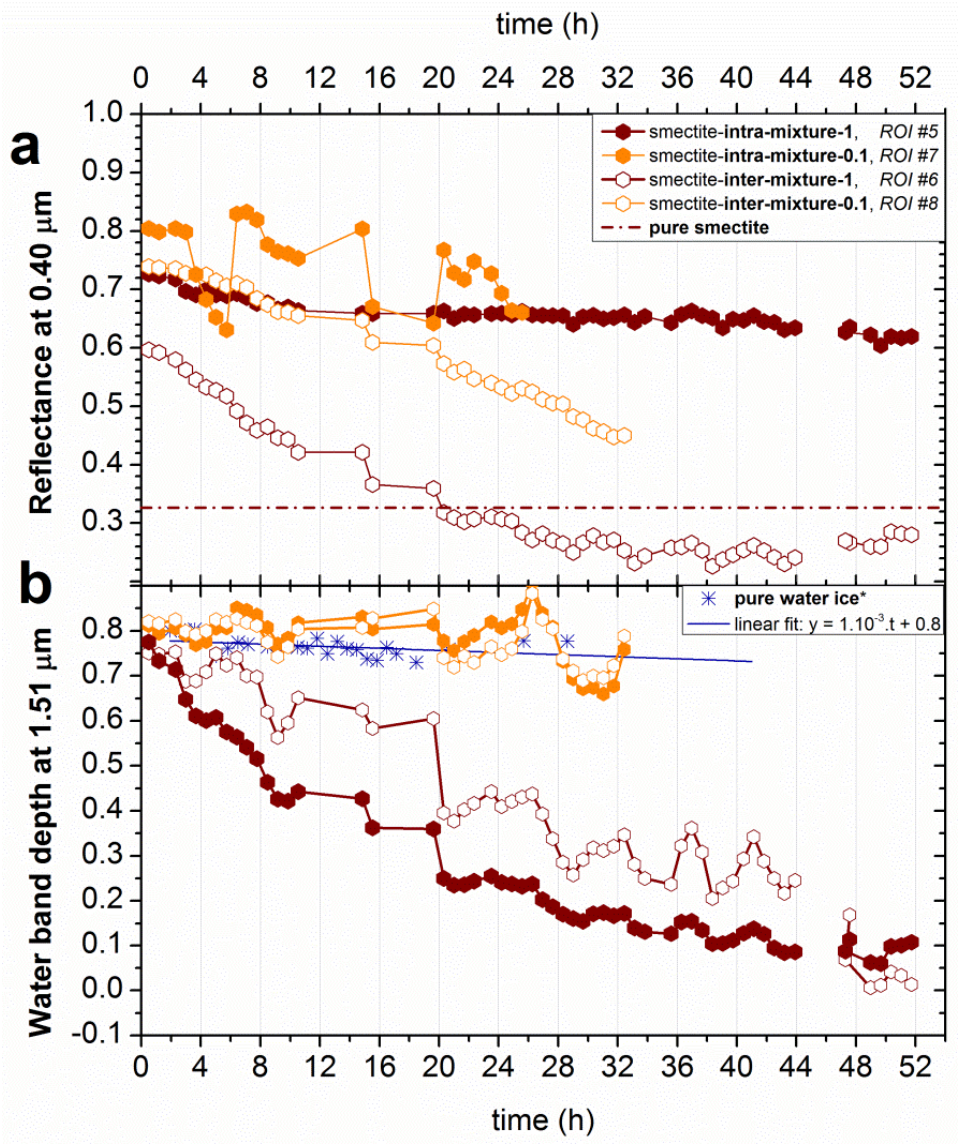

Supplementary Figure 9 : *In situ* spectral evolution of the samples of **smectite mixed with water ice** particles as intra- or inter- mixtures and at different concentrations. Temporal evolution of **(a)** the reflectance at 0.40 µm where smectite absorbs the most, and **(b)** the band depth of the water absorption band at 1.51 µm (see Eq. 2). These data have been obtained from spectra acquired in ROI #5 (smectite-intra-mixture-1), ROI #7 (smectite-intra-mixture-0.1), ROI #6 (smectite-inter-mixture-1) and ROI #8 (smectite-inter-mixture-0.1) located in Figure 2e,f,g,h and Video 5 (see Table 1 for the explanation of the samples names). *The pure water ice data are from ROI #0 of Poch *et al.* (in press). (For a colour version of this figure, the reader is referred to the web version of this article)

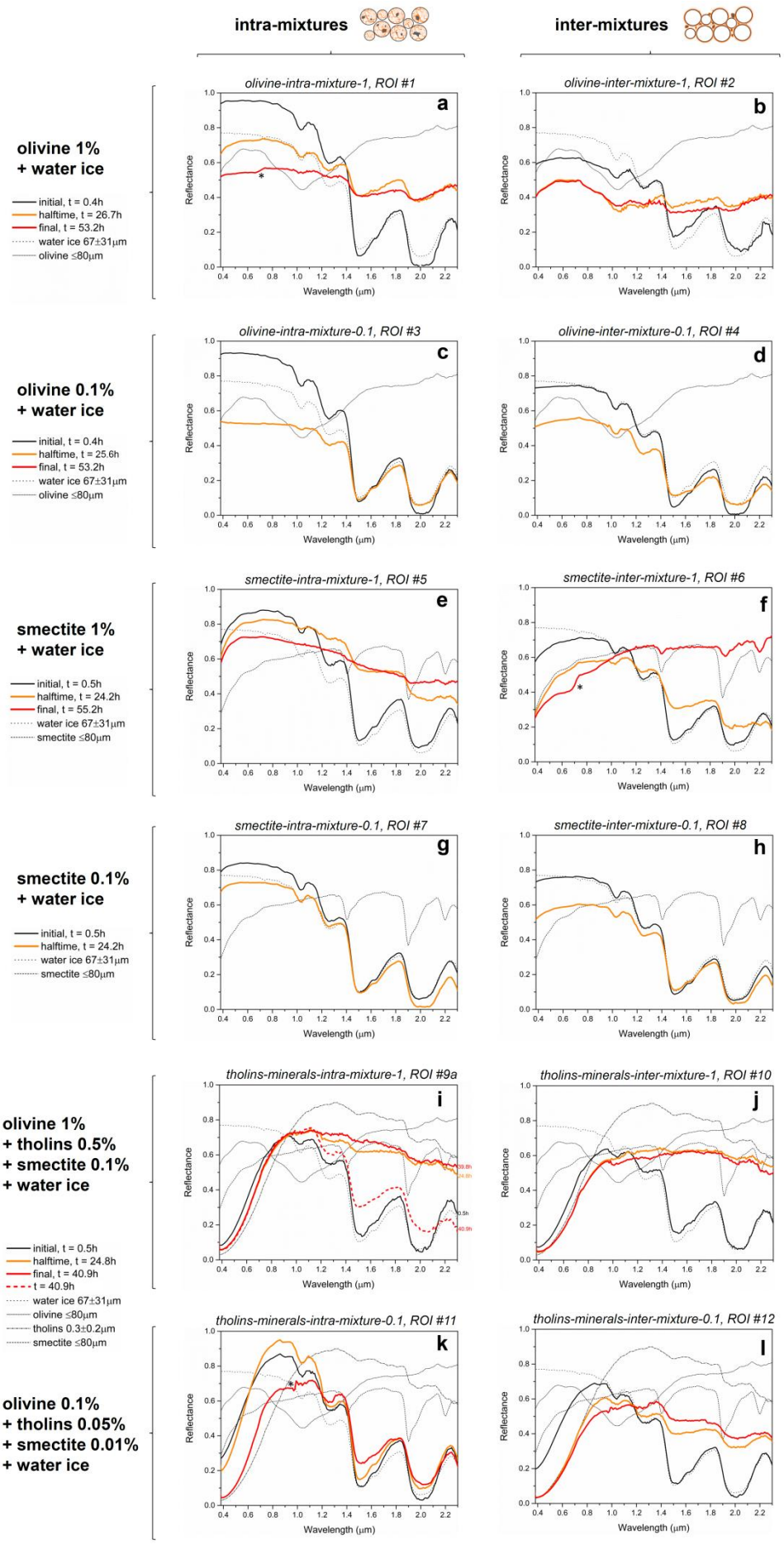
intra-mixtures
inter-mixtures
olivine 1%
+ water ice
initial, t = 0.4h
halftime, t = 26.7h
final, t = 53.2h
water ice 67±31μm
olivine ≤80μm
olivine-intra-mixture-1, ROI #1
a
olivine-inter-mixture-1, ROI #2
b
olivine 0.1%
+ water ice
initial, t = 0.4h
halftime, t = 25.6h
final, t = 53.2h
water ice 67±31μm
olivine ≤80μm
olivine-intra-mixture-0.1, ROI #3
c
olivine-inter-mixture-0.1, ROI #4
d
smectite 1%
+ water ice
initial, t = 0.5h
halftime, t = 24.2h
final, t = 55.2h
water ice 67±31μm
smectite ≤80μm
smectite-intra-mixture-1, ROI #5
e
smectite-inter-mixture-1, ROI #6
f
smectite 0.1%
+ water ice
initial, t = 0.5h
halftime, t = 24.2h
water ice 67±31μm
smectite ≤80μm
smectite-intra-mixture-0.1, ROI #7
g
smectite-inter-mixture-0.1, ROI #8
h
olivine 1%
+ tholins 0.5%
+ smectite 0.1%
+ water ice
initial, t = 0.5h
halftime, t = 24.8h
final, t = 40.9h
t = 40.9h
water ice 67±31μm
olivine ≤80μm
tholins 0.3±0.2μm
smectite ≤80μm
tholins-minerals-intra-mixture-1, ROI #9a
i
tholins-minerals-inter-mixture-1, ROI #10
j
olivine 0.1%
+ tholins 0.05%
+ smectite 0.01%
+ water ice
tholins-minerals-intra-mixture-0.1, ROI #11
k
tholins-minerals-inter-mixture-0.1, ROI #12
l
Reflectance
Wavelength (μm)

Supplementary Figure 10 : Reflectance spectra of all the ROIs of all the samples as shown in Figure 2. The reflectance spectra measured ~30 minutes after the start of the simulation (black line) can be compared to the ones measured about 26 hours later (orange line) and at the end of the experiment (red line) when a sublimation mantle has formed on top of the samples. To facilitate the interpretation of these spectra, reference spectra of pure water ice and pure tholins are also shown in dotted and dashed black lines respectively (these spectra were measured separately, during previous experiments). *Artefact originating from the strong red slope at 0.7 μm of the aluminium oxide coating the sample holder (For interpretation of the references to colour in this figure legend, the reader is referred to the web version of this article)

A.2. Videos:

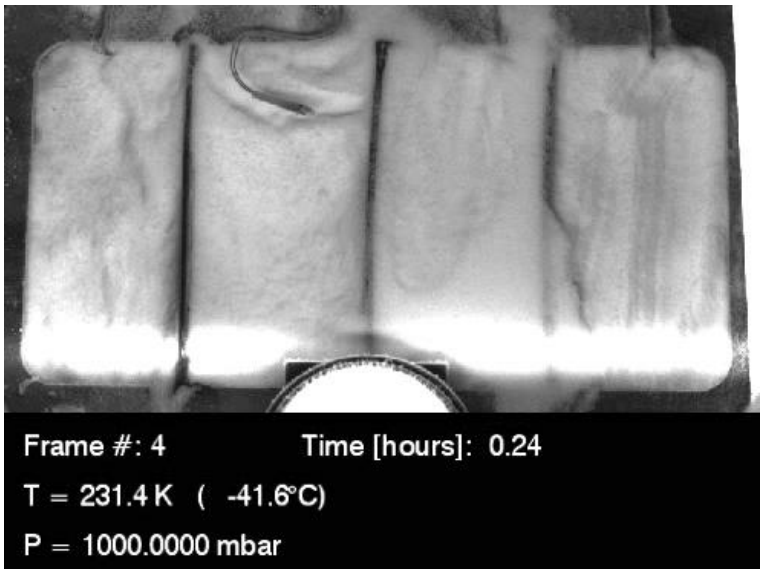

Video 1 : This black and white video shows the evolution of the samples during the experiment n°1: **water ice mixed with olivine**. From left to right are the samples: olivine-intra-mixture-1, olivine-intra-mixture-0.1, olivine-inter-mixture-0.1 and olivine-inter-mixture-1 (see Table 1). Both monochromatic images at 0.60 μm and visible images taken with the ambient light on have been put together in this video. The temperature of the sample holder and the pressure inside the chamber are indicated on each frame (see also Supplementary Figure 1a). A detailed analysis of the events occurring during this video is provided in section 3.1.

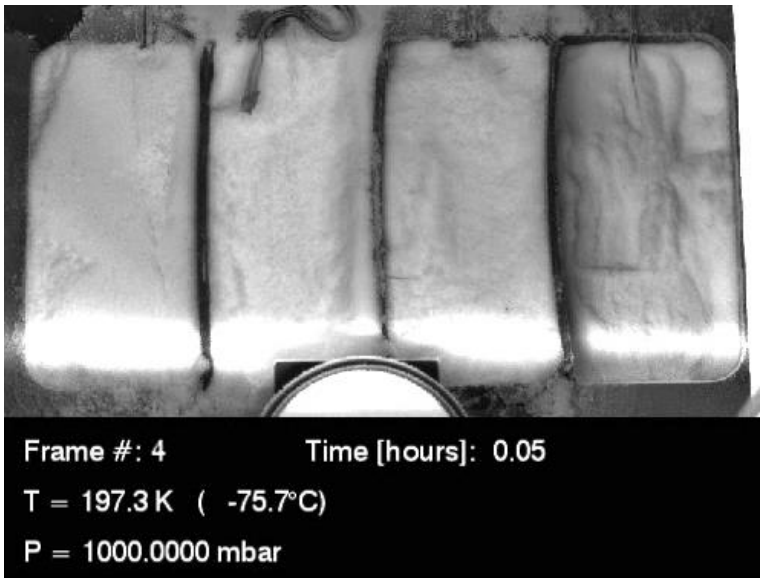

Video 2 : This black and white video shows the evolution of the samples during the experiment n°2: **water ice mixed with smectite**. From left to right are the samples: smectite-intra-mixture-1, smectite-intra-mixture-0.1, smectite-inter-mixture-0.1 and smectite-inter-mixture-1 (see Table 1). Both monochromatic images at 0.60 μm and visible images taken with the ambient light on have been put together in this video. The temperature of the sample holder and the pressure inside the chamber are indicated on each frame (see also Supplementary Figure 1b). A detailed analysis of the events occurring during this video is provided in section 3.1.

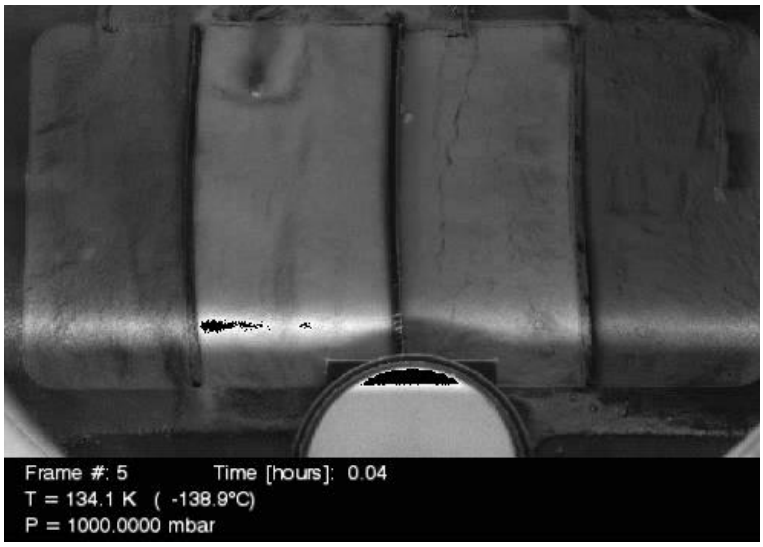

Video 3 : This black and white video shows the evolution of the samples during the experiment n°3: **water ice mixed with olivine, tholins and smectite**. From left to right are the samples: tholins-minerals-intra-mixture-1, tholins-minerals-intra-mixture-0.1, tholins-minerals-inter-mixture-0.1 and tholins-minerals-inter-mixture-1 (see Table 1). Both monochromatic images at 0.60 μm and visible images under ambient light have been put together in this video. The temperature of the sample holder and the pressure inside the chamber are indicated on each frame (see also Figure 1 or Supplementary Figure 1c). A detailed analysis of the events occurring during this video is provided in section 3.1.

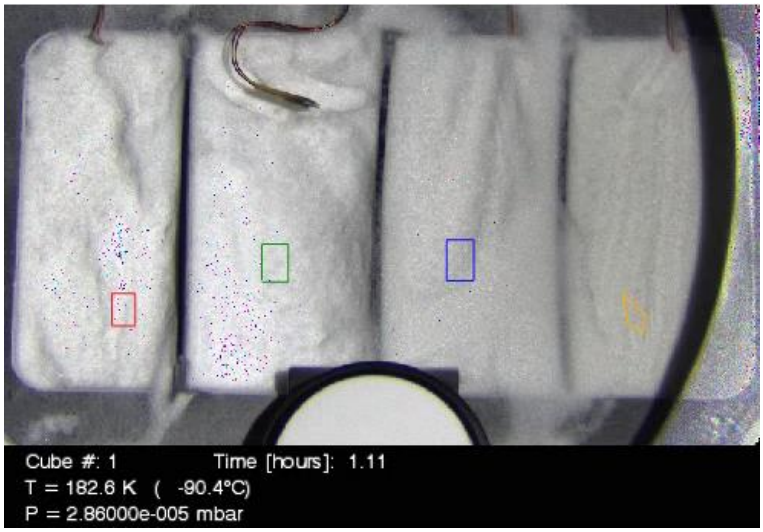

Video 4 : This colour video shows the evolution of the samples during the experiment n°1: **water ice mixed with olivine**. From left to right are the samples: olivine-intra-mixture-1, olivine-intra-mixture-0.1, olivine-inter-mixture-0.1 and olivine-inter-mixture-1 (see Table 1). Each image of this video is a colour composite of three monochrome images acquired at 0.40, 0.52, and 0.60 μm, for the blue, green, and red channel, respectively. The temperature of the sample holder and the pressure inside the chamber are indicated on each frame (see also Supplementary Figure 1a). The Regions Of Interest (ROI) indicated in each frame have been used to retrieve the spectro-photometric data presented in Figure 5a,b and Supplementary Figure 8 (red = ROI #1, green = ROI #3, blue = ROI #4, orange = ROI #2).

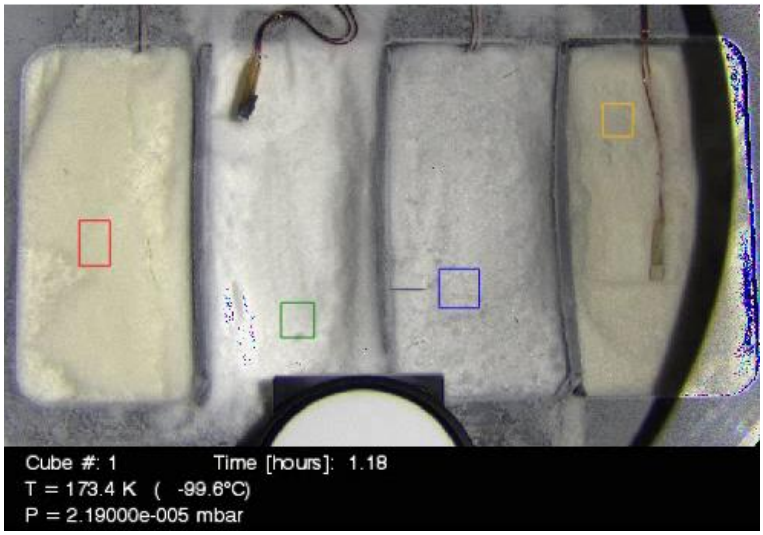

Video 5 : This colour video shows the evolution of the samples during the experiment n°2: **water ice mixed with smectite**. From left to right are the samples: smectite-intra-mixture-1, smectite-intra-mixture-0.1, smectite-inter-mixture-0.1 and smectite-inter-mixture-1 (see Table 1). Each image of this video is a colour composite of three monochrome images acquired at 0.40, 0.52, and 0.60 μm, for the

blue, green, and red channel, respectively. The temperature of the sample holder and the pressure inside the chamber are indicated on each frame (see also Supplementary Figure 1b). The Regions Of Interest (ROI) indicated in each frame have been used to retrieve the spectro-photometric data presented in Figure 5c,d and Supplementary Figure 9 (red = ROI #5, green = ROI #6, blue = ROI #8, orange = ROI #7).

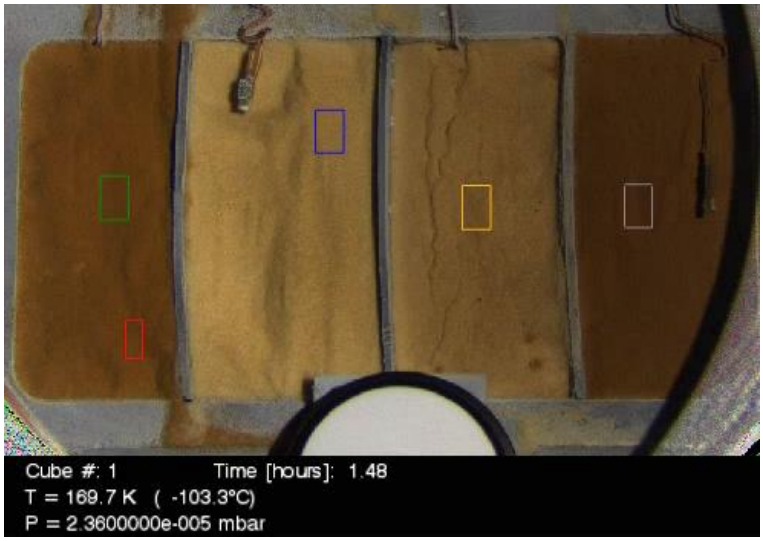

Video 6 : This colour video shows the evolution of the samples during the experiment n°3: **water ice mixed with olivine, tholins and smectite**. From left to right are the samples: tholins-minerals-intra-mixture-1, tholins-minerals-intra-mixture-0.1, tholins-minerals-inter-mixture-0.1 and tholins-minerals-inter-mixture-1 (see Table 1). Each image of this video is a colour composite of three monochrome images acquired at 0.40, 0.52, and 0.60 μm, for the blue, green, and red channel, respectively. The temperature of the sample holder and the pressure inside the chamber are indicated on each frame (see also Figure 1 or Supplementary Figure 1c). The Regions Of Interest (ROI) indicated in each frame have been used to retrieve the spectro-photometric data presented in Figure 5e,f and Figure 6 (red = ROI #9a, green = ROI #9b, blue = ROI #11, orange = ROI #12, grey = ROI #10).

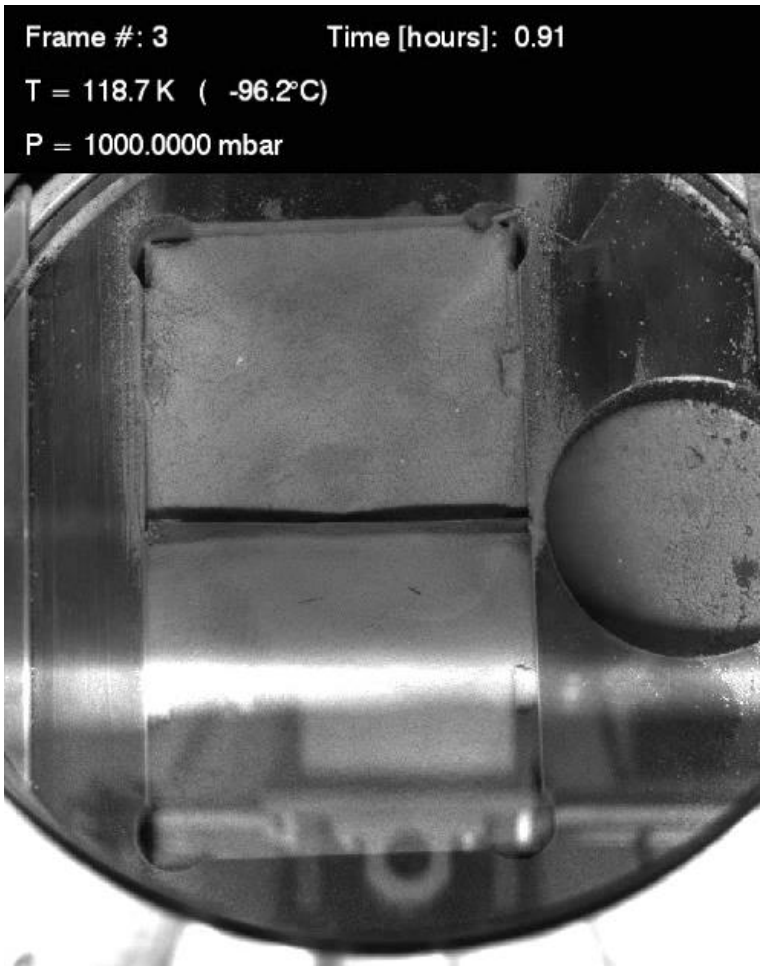

Video 7 : This black and white video shows the evolution of the samples during the supplementary experiment performed with samples of **water ice mixed with tholins, olivine and smectite**: on top of the frame is the "tholins-minerals-intra-mixture-1" sample and at the bottom is the "tholins-minerals-inter-mixture-1" (see Table 1). The temperature of the sample holder and the pressure inside the chamber are indicated on each frame. From t=8h to t=15h, several ejection events occur on the intra-mixture sample, forming quasi-circular depressions which deepen after multiple events. During the simulation, the sample holder has been moved vertically in order to scan the surface of the samples using the OCT instrument (see Supplementary Figure 7, Video 11 and Video 12). During one of the moves, at t=22.2h, the surface of the inter-mixture sample is disrupted and some fragments (<1 mm) of residue are ejected, followed by others, later in the simulation.

Video 8 : Slow motion capture (200 fps) of an ejection event occurring on the sublimation residue of the sample of **water ice intra-mixed with tholins, olivine and smectite** seen on Video 7 (tholins-minerals-intra-mixture-1 sample, cf. Table 1). A around t=3s, one can clearly see the local deformation of the mantle, followed by the ejection of several fragments of several millimeters. The speed of the ejected particles has been estimated to be about 0.4±0.1 m s^{-1}. The video was recorded with a rate of 200 frames per second. So the time separating each frame of this video is 5 ms. The sample holder is 6 cm wide.

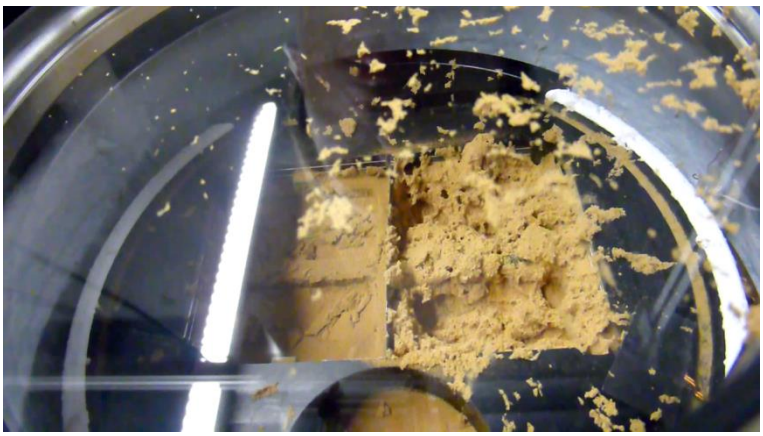

Video 9 : Slow motion capture (100 fps) of an ejection event occurring on the sublimation residue of the sample of **water ice intra-mixed with tholins, olivine and smectite** seen on Video 7 (tholins-minerals-intra-mixture-1 sample, cf. Table 1). The surface of the mantle is seen to vibrate more and more strongly until the ejection of several millimeters to centimeters-sized fragments at around t=5s. The video was recorded with a rate of 100 frames per second. So the time separating each frame of this video is 10 ms. The sample holder is 12 cm long and 6 cm wide.

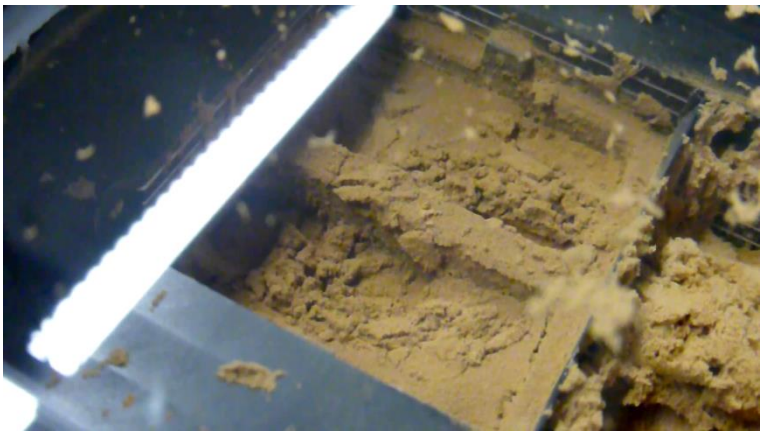

Video 10 : Slow motion capture (200 fps) of an ejection event occurring on the sublimation residue of a sample of **water ice <u>inter</u>-mixed with tholins, olivine and smectite** seen on Video 7 (tholins-minerals-inter-mixture-1 sample, cf. Table 1). The speed of the ejected particles has been estimated to be around 1.0±0.1 m s^{-1}. The video was recorded with a rate of 200 frames per second. So the time separating each frame of this video is 5 ms. The sample holder is 6 cm wide.

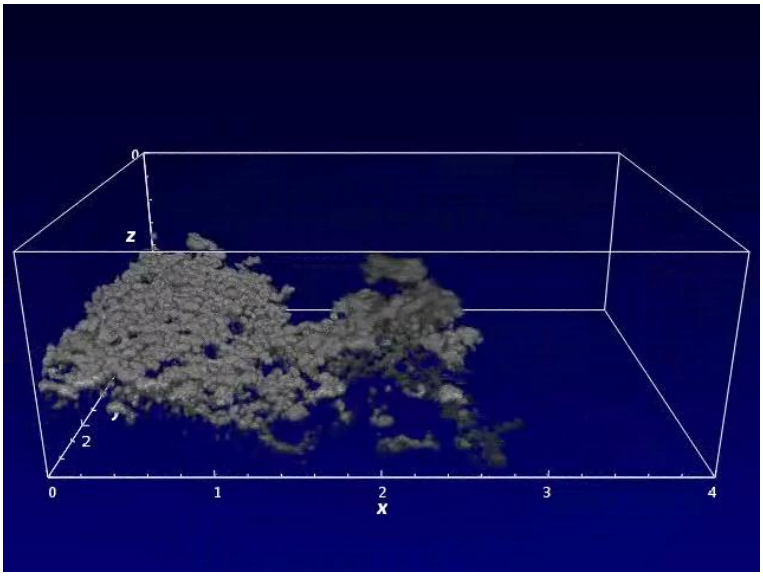

Video 11 : 3D OCT reconstruction of the sublimation residue formed at the surface of the tholins-minerals-intra-mixture-1 sample after 15.5h of sublimation inside SCITEAS. The OCT scan was performed *in situ*, through the window of the simulation chamber. It shows the porous structure of the residue. The volume mapped is 1.4×2.6×4 mm.

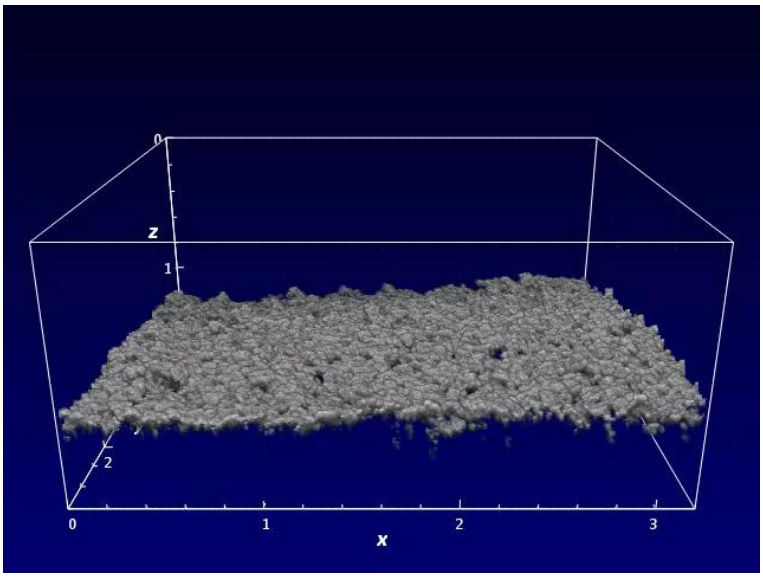

Video 12 : 3D OCT reconstruction of the sublimation residue formed at the surface of the tholins-minerals-inter-mixture-1 sample after 15.5h of sublimation inside SCITEAS. The OCT scan was performed *in situ*, through the window of the simulation chamber. Compared to the residue of the intra-mixture shown in Video 11, this residue has a more compact structure. The volume mapped is 1.4×2.6×3.2 mm.

Appendix B:

Detailed description of the evolution of the surface morphology of the samples

Videos 1, 2 and 3 depict the detailed evolution of the samples during experiment n°1, 2 and 3 respectively. A detailed analysis of these videos is provided below. To facilitate the interpretation of the videos by the reader, the time values given in the text below referred to the time shown on each frame of the videos. Supplementary Figure 2 shows the schematic timelines of all the major events occurring during the videos. It allows a simultaneous comparison of the evolution of the surface morphology of all the samples.

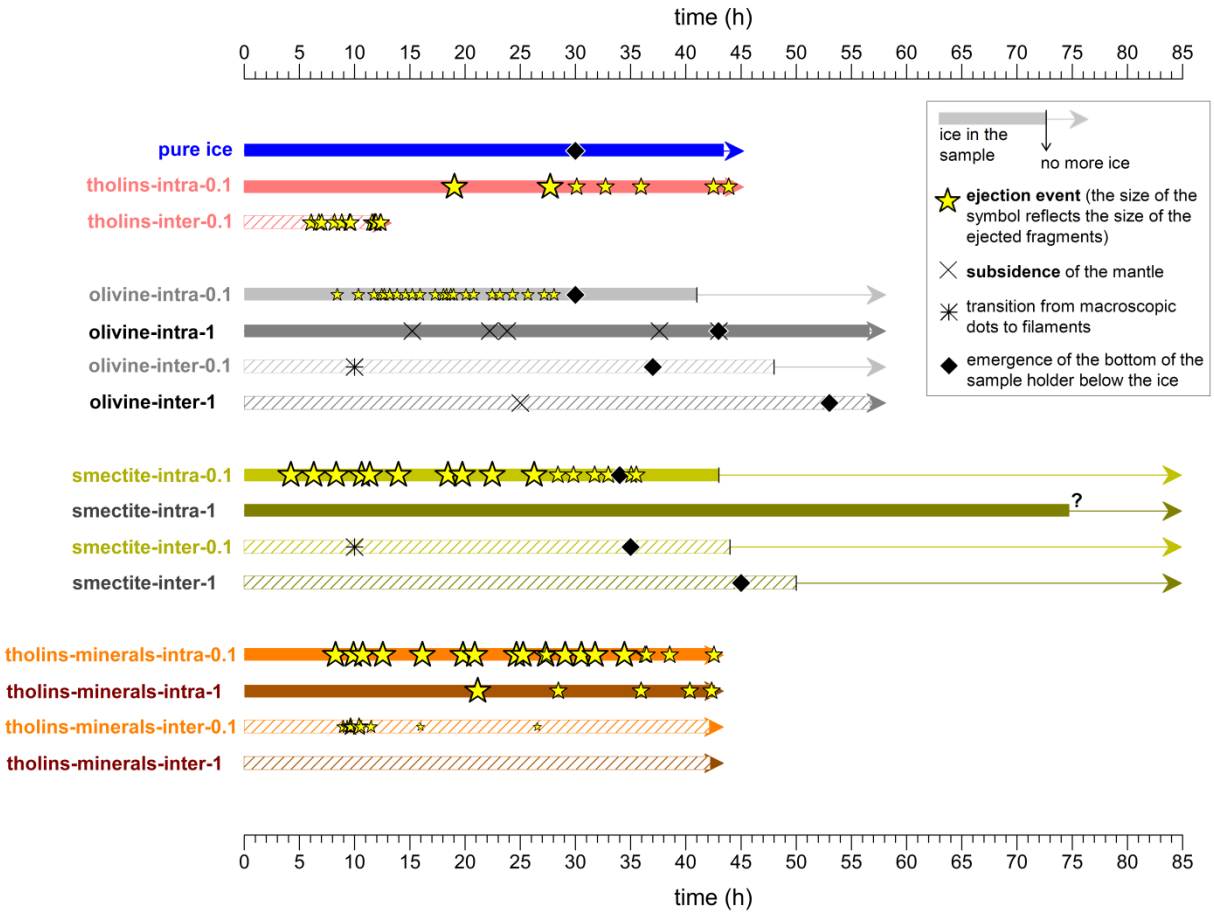

Supplementary Figure 2 : Timelines of the evolution of the surface of all the samples during their sublimation, as seen on Videos 1, 2 and 3. Overall, the temperature and pressure variations were quite similar for all experiments (see Figure 1 and Supplementary Figure 1), allowing a simultaneous comparison of the evolution of the surface morphology of all the samples. The data from "pure ice", "tholins-intra-0.1" and "tholins-inter-0.1" samples are from Poch *et al.*, (in press).

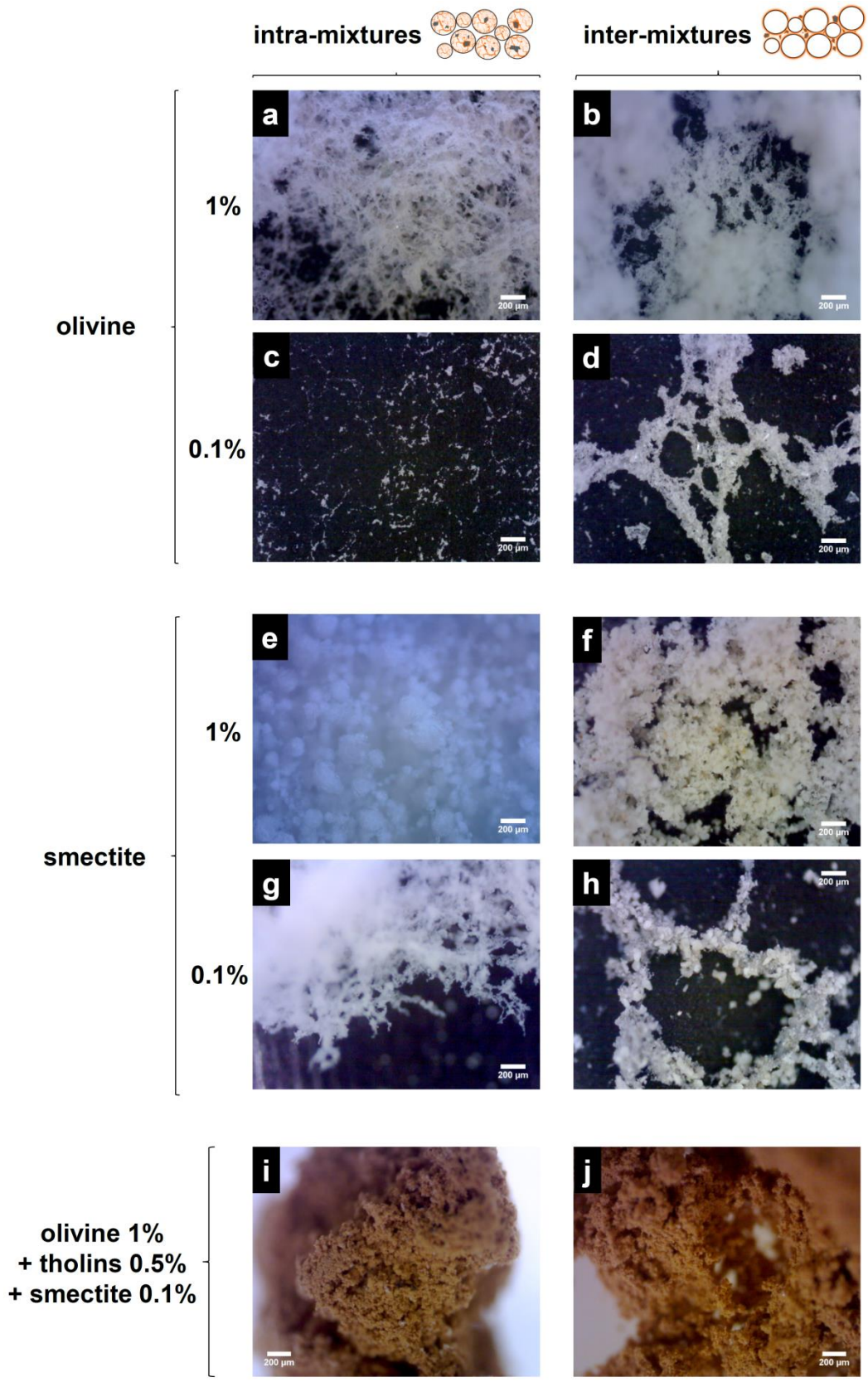

Supplementary Figure 3 : Visible microscope images of the water-free residues collected after sublimation of the samples in the simulation chamber. These images were taken *ex situ*, after the

simulation. Tholins-minerals samples of low concentration (0.1%) have not been imaged by microscopy.

B.1. Evolution of the morphology of samples made of a 1% intra-mixture

The sublimation of the intra-mixture 1% samples results in a very specific evolution dependent upon composition, as seen on Figure 2.

The sublimation mantle formed over the olivine-intra-1 sample appears clearly on Video 1 after 15.22 h. This mantle, not clearly distinguishable from the ice before 14.87 h, appears to have subsided between 14.87 h and 15.22 h. The mantle structure resembles a veil over the ice (see Figure 2a and Figure 3a). A local break of the mantle probably causes a release of water vapour accumulated below the mantle during the sublimation of the ice, explaining the subsidence of the mantle. No ejection of mantle fragment is observed. Several events of subsidence occurred during the sublimation, until the gentle deposition of the veil-like mantle at the bottom of the sample holder when most of the ice had sublimed after about 58h.

The mantle formed over the smectite-intra-mixture-1 sample has a completely different structure. It has the morphology of a foam with the shape of the initial ice surface (see Figure 2e and Figure 3e). The mantle is seen to inflate from t = 3 to t = 67 h, developing a dome shape traversed by a fracture that gets larger and larger. These deformations are caused by the gas produced from the sublimation of the ice, inflating the mantle structure. From 67 h to the end of the experiment, the mantle deflates and vibrates as the remaining ice completes sublimation below the mantle. No mantle fragment is ejected during the sublimation of this sample.

Finally, the mantle formed over the tholins-minerals-intra-mixture-1 sample (Figure 2i) resembles a foam similar to that formed from the smectite-intra-mixture-1 sample. From t = 0 to t = 21.13 h, the surface of the sample is not receding, and no inflation is seen. Between 21.13 and 21.15 h, an ejection event occurs, releasing foam-like fragments of the mantle and exposing ice at the surface. Several other ejection events occur between 28.42-28.44 h, 40.34-40.36 h and 42.33-42.34 h. Also, from 36.43 to 37.7 h, the mantle is seen to vibrate as a result of the flow of water vapour produced from the ice sublimation. Immediately after the ejection events at 21.13 h and 28.42 h, the temperature measured by a sensor located inside the

tholins-minerals-intra-mixture-1 sample dropped by 3.8 and 2.5 K respectively in less than 10 minutes (see Figure 1). Pressure spikes can also be correlated to these ejection events. We hypothesize that the breakage of the surface mantle produced a sharp decrease of pressure in the ice sample, resulting in a quick increase of the sublimation rate and therefore of an absorption of heat by the sample (latent heat of sublimation). After this event, a surface mantle is built again on the ice, increasing the pressure in the sample and reducing its sublimation rate. This may explain why the temperature measured inside the sample increased slowly during the hours following the ejection events (see Figure 1).

A supplementary experiment was conducted to gather more details on the dynamics of the ejection events. Video 7 shows the evolution of a larger tholins-minerals-intra-mixture-1 sample (seen in the upper part of the video frame) during its sublimation. A first ejection event occurred between 8.70-8.72 h, a second between 10.27-10.29 h, a third between 10.44-10.45 h and a fourth between 10.58-10.60 h. Each of these ejection events produced a quasi-circular feature on the surface of the sample. Until t=15 h, all the next ejection events occurred again in the same areas, resulting in their deepening. Using a high-speed camera, we monitored several ejection events. Video 8 shows the local deformation of the mantle (because of development of a bubble of gas below it), followed by ejection of several fragments of this mantle. From this video, the speed of this ejection event has been estimated to be about 0.4±0.1 m s^{-1}. Video 9 shows another ejection event occurring later, after the production of a thicker mantle. The surface of the mantle is seen to vibrate more and more strongly until the ejection of several millimetre- to centimetre-sized fragments.

The fact that such ejection events are only observed in presence of tholins indicates that tholins build a mantle more impervious to the water vapour than the mantles of pure olivine or smectites. The over-pressure, caused by the accumulation below the mantles of water vapour produced from the sublimation, is more efficiently dissipated through the olivine and smectite mantles than through a tholins mantle. The higher over-pressure eventually results in catastrophic breakup and ejection of this mantle.

B.2 Evolution of the morphology of samples made of a 0.1% intra-mixture

From all the mixture types, the intra-mixture 0.1% samples were the most active ones, exhibiting numerous ejections of mantle during their sublimation, irrespective of their composition (see Videos 1, 2, 3 and Supplementary Figure 1).

The expulsion of a fragment of mantle occurred first on the smectite-intra-mixture-0.1 sample between 3.87 and 4.22 h. This type of event occurred later for the tholins-minerals-intra-mixture-0.1 and the olivine-intra-mixture-0.1 samples (between 7.90-8.26 h and 8.42 - 8.43 h respectively). The mantle formed after the sublimation of these samples resembles a thin veil, having a consistency like a dense spider's web (see Figure 3c, g, k). Videos 1, 2, and 3 show that fragments of the mantle still attached to the ice are continuously shaking because of the drag force of the water vapour flow produced by the sublimation of the ice. The surface area of these fragments of mantle is larger for the smectite-intra-mixture-0.1 sample, and smaller for the tholins-minerals-intra-mixture-0.1 and olivine-intra-mixture-0.1 samples (see Videos 1, 2, 3). Moreover, the smectite-intra-0.1 sample accumulates some remains of mantle adhering all around the borders of the sample holder, while it is less the case for the tholins-minerals-intra-mixture-0.1 sample and not at all for the olivine-intra-mixture-0.1 sample (see Figure 2c, g, k).

Taken together, all these observations clearly show a difference of cohesion between these mantles. The rankings reported above indicate that the mantle built from 0.1% smectite appears to have a greater cohesion than the mantle of 0.1% olivine, with or without 0.05% tholins. From these observations, it also clear that tholins play a role in producing a more cohesive mantle: the addition of 0.05% tholins (and 0.01% smectite) to the 0.1% olivine ice mixture significantly changes the mechanical properties of the mantle.

From a photometric point of view, the continuous release of mantle fragments on samples containing tholins results in high albedo contrasts between the active areas (water ice exposed) and the surrounding water-free mantle. This contrast is higher when the ice contains 0.05% tholins (tholins-minerals-intra-mixture-0.1) compared to when it contains 0.5% tholins (tholins-minerals-intra-mixture-1) (see Video 3 between 21.13 and 21.15h). The photometry of the surface is discussed in detail in section 3.2.3.

The dark bottom of the sample holder becomes visible at the centre of the samples after about 30h for the olivine-intra-mixture-0.1 sample and after 34h for the smectite-intra-

mixture-0.1 sample. All the ice constituting the samples seems to have sublimated after around 41h for the olivine-intra-mixture-0.1 sample and after 45h for the smectite-intra-mixture-0.1 sample. The tholins-minerals-intra-mixture-0.1 sample still contains some ice after more than 43h of sublimation. This ranking suggests that the build-up of a more cohesive sublimation mantle above the ice results in a lower sublimation rate of this ice.

B.3 Evolution of the morphology of samples made of a 1% inter-mixture

At a macroscopic scale, the sublimation of the tholins-minerals-inter-mixture-1 and smectite-inter-mixture-1 samples did not produce any particular feature at the surface of the samples (see Figure 2j, f). Smectite grains, apparently randomly deposited at the surface of the sample after the sublimation of the ice, are visible after around 10 hours (see Video 2, Figure 3f). Then they deposit at the bottom of the sample holder as the water ice completely sublimates after about 60 hours (see Video 2, Figure 2f). The tholins-minerals-inter-mixture-1 sample did not exhibit any ejection event or surface change (see Video 3, Figure 2j). However, the supplementary experiment, performed on a similar "tholins-minerals-inter-mixture-1" sample but with a higher irradiation flux (sample positioned closer to the chamber window), did show ejection events on this type of sample (triggered by an external stress, namely the movement of the sample holder), as seen on the Video 7 (the tholins-minerals-inter-mixture-1 is the sample located in the bottom part of the video frame). The speed of the millimetre sized particles ejected during this event has been estimated to be around 1.0±0.1 m s^{-1}, two to three times faster than the fragments of the tholins-minerals-intra-mixture-1 sample.

For the olivine-inter-mixture-1 sample, the deposit of olivine produced after sublimation is a very uniform and flat layer, resembling a crust (see Figure 3b and central part of Figure 2b), which appears to lead to a characteristic evolution of this sample (see Video 1). Starting around 25h, one can clearly see that the sublimation is faster on the periphery of this sample rather than at its centre. On the other hand, for all the other samples analysed here, the sublimation preferentially occurred from the centre to the periphery of the sample. The opposite behaviour observed for the olivine-inter-mixture-1 sample appears to be caused by the "crusty" consistency of the mantle of olivine, which is *de facto* reducing the sublimation

rate of the ice located beneath the mantle. At around 29h, a temperature sensor initially buried in the olivine-inter-mixture-1 sample emerges from this crust (see Video 1). The ice continues to sublimate from the periphery of the sample and all around the temperature sensor and its cable, until 58h. While sublimating, the ice causes the fall of the upper crust of olivine, exposing fresh ice which consequently sublimates (see Video 1 and Figure 3b). This sample shows a mechanism of mass wasting induced by the sublimation process.

B.4 Evolution of the morphology of samples made of a 0.1% inter-mixture

From t = 0h to around 10h, the olivine-inter-mixture-0.1 and smectite-inter-mixture-0.1 samples get covered by numerous dark dots smaller than 1mm (see Videos 1 and 2) which are aggregates of olivine and smectite, respectively, formed after the sublimation of the water ice. After around 10h, these dots progressively increase in size and connect to each other, forming a network of filaments over the ice. As the sublimation continues, the thickness and the length of these filaments increase (see Figure 3d, h). They slightly move toward the centre of the sample because of the concave shape of the surface. This movement is due to dragging force of the gas flow coming from the ice located at the border of the sample holder. The initially flat sample surface gets excavated in a bowl-shape as the ice sublimes, the sublimation rate being slower at the border of the sample holder. After about 39h, the dark bottom of the sample holder becomes visible at the centre of the olivine-inter-mixture-0.1 and smectite-inter-mixture-0.1 samples and all the ice constituting these samples seems to have sublimated after 45h (see Figure 2d, h).

In the presence of tholins, the evolution is significantly different and no millimetre-sized dots or filaments are seen (see Video 3, Figure 2l and Figure 3l). Instead, a homogeneous darkening of the whole surface is observed at the surface of the tholins-minerals-inter-mixture-0.1 sample from t = 0h to around 9h. Between 8.97 and 11.5h, ejections of localised fragments of mantle are observed, whereas no such ejection event was spotted on the olivine-inter-mixture-0.1 and smectite-inter-mixture-0.1 samples. After the ejections, the areas from where the fragments of mantle were released appear brighter on the visible images (see Figure 2l). This bright material is made of the mixture of water ice and tholins, initially located below the sublimation mantle, which is now exposed to the top of the

sample. After about 5 hours, these areas become dark again as the ice sublimates, rebuild-up the tholins mantle at the surface (see Video 3).

B.5 Evolution of the light scattering properties of the surfaces monitored by *in situ* optical coherence tomography (OCT)

Supplementary Figure 7 shows in situ optical coherence tomography (OCT) images of intra- and inter- mixtures of tholins and minerals. These data reveal that the optical properties of the surfaces of these mixtures differ very early in the simulation (t = 1.3-1.7h). As soon as the sublimation starts: at the surface of the intra-mixture the light appears to diffuse in larger and rounder scatterers than in the surface of the inter-mixture. At this time, only a very limited thickness of mantle has been produced and the reflection due to the icy grains might still be visible below the sublimation mantle (white arrows in Supplementary Figure 7a,b). After t = 15h the difference between the two surfaces is even more pronounced: the intra-mixture surface exhibits a residue having the rounded shape of the initial ice particles and a high roughness (see Supplementary Figure 7c and also Video 11). On the opposite, the inter-mixture surface did not retain the shape of the ice particles and is much more compact than the intra-mixture (see Supplementary Figure 7d and also Video 12). In the inter-mixture surface, the light is reflected more strongly by the very first microns of the surface (brighter pixels), whereas in the intra-mixture, the light is reflected equally from the top as well from deeper in the thickness of the deposit (equal intensity of the pixels within the whole optical thickness). These OCT observations are consistent with the difference of densities and porosity discussed above for intra- and inter- mixtures.

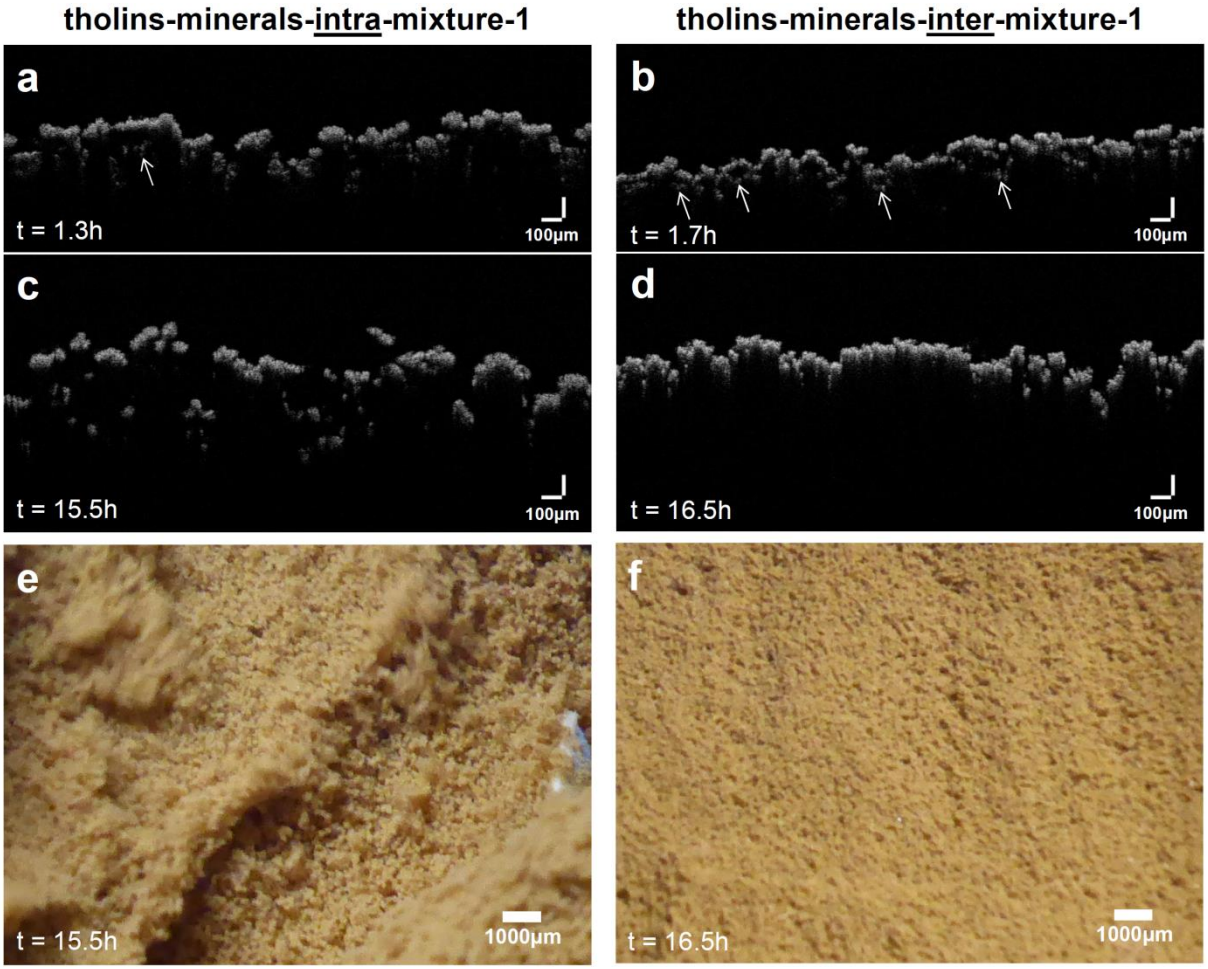

Supplementary Figure 7: Optical Coherence Tomography images of the surface of the tholins-minerals-intra-mixture-1 (left) and tholins-minerals-inter-mixture-1 (right) samples obtained *in situ* during the sublimation of the samples inside the simulation chamber, at t = 1.3-1.7h **(a,b)** and t = 15.5-16.5h **(c,d)** (see also the Video 11 and 12 showing the 3D reconstruction of the surfaces). At t = 1.3-1.7h the surface of the samples consists of water ice particles and of some layer of sublimation residues. At t = 15.5-16.5h, the surface of the samples is completely water-free: the images show the sublimation residue. High resolution images of the surface of the samples obtained *in situ* are shown in **(e)** and **(f)**. (see Table 1 for an explanation of the sample names)

Appendix C:

Long-term spectral evolution of the smectite and olivine samples (without tholins)

The Supplementary Figure 8 and Supplementary Figure 9 show the reflectance at 0.40 μm and the depth of the water absorption band at 1.51 μm for the mixtures of water ice and pure minerals (olivine or smectite). Olivine and smectite absorb at 0.40 μm (charge transfer absorption), but much less than tholins. Similarly to what is observed for tholins-minerals samples, the reflectance at 0.40 μm appears to depend more on the mixture type (intra- or inter- mixture) whereas the band depth of water ice is more sensitive to the concentration of the minerals (0.1 or 1%). For a given concentration, intra-mixtures have higher reflectance at 0.40 μm than inter-mixtures. This difference increases as the concentration increases. The formation of a mantle consisting of a foam of smectite, as seen for the smectite-intra-mixture-1 sample (see Figure 2e), results in a very slow decrease of reflectance at 0.40 μm compared to the other mineral samples (Supplementary Figure 9a). Concerning the water absorption band at 1.51 μm, 0.1% mixture samples exhibit a decrease close to that observed for the sublimation of pure water. Only the 0.1% inter-mixture that includes tholins produces a strong decrease of water bands. At the concentration of 1%, all minerals and tholins mixtures exhibit a decrease of the water absorption bands faster by a factor of 2 to 4 than at 0.1%, until these bands are completely masked.

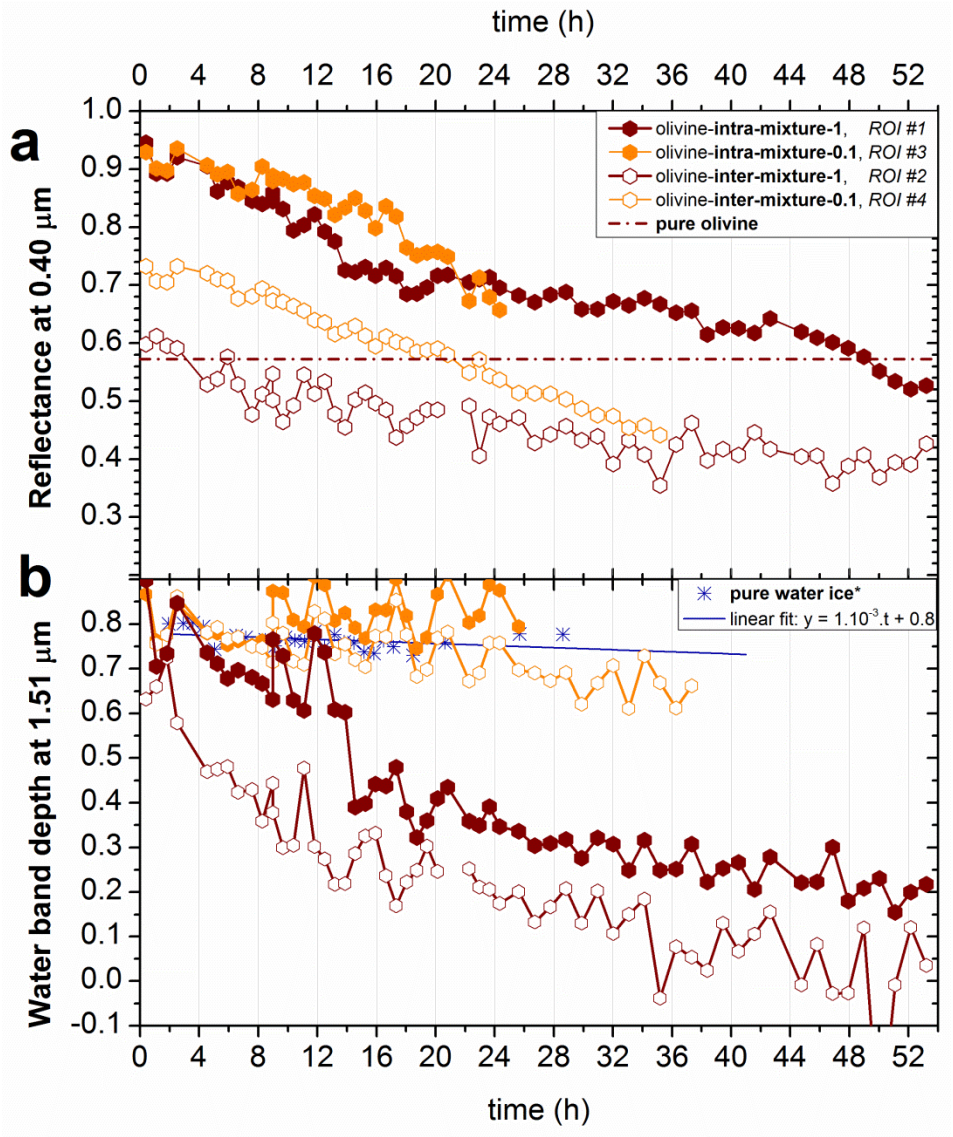

Supplementary Figure 2 : *In situ* spectral evolution of the samples of **olivine mixed with water ice** particles as intra- or inter- mixtures and at different concentrations. Temporal evolution of **(a)** the reflectance at 0.40 µm where olivine absorbs, and **(b)** the band depth of the water absorption band at 1.51 µm (see Eq. 2). These data have been obtained from spectra acquired in ROI #1 (olivine-intra-mixture-1), ROI #3 (olivine-intra-mixture-0.1), ROI #2 (olivine-inter-mixture-1) and ROI #4 (olivine-inter-mixture-0.1) located in Figure 2a,b,c,d and Video 4 (see Table 1 for the explanation of the samples names). *The pure water ice data are from ROI #0 of Poch *et al.* (in press).

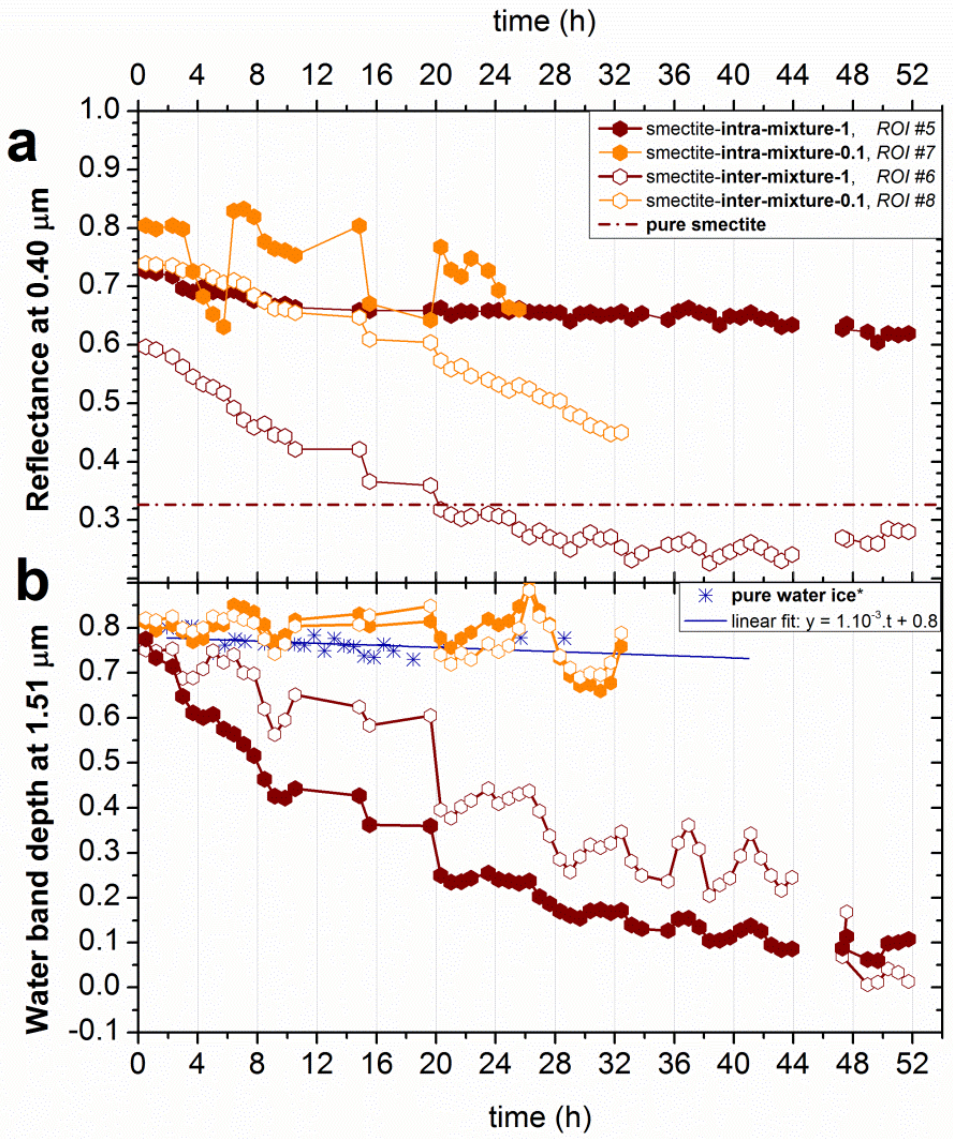

Supplementary Figure 3 : *In situ* spectral evolution of the samples of **smectite mixed with water ice** particles as intra- or inter- mixtures and at different concentrations. Temporal evolution of **(a)** the reflectance at 0.40 µm where smectite absorbs the most, and **(b)** the band depth of the water absorption band at 1.51 µm (see Eq. 2). These data have been obtained from spectra acquired in ROI #5 (smectite-intra-mixture-1), ROI #7 (smectite-intra-mixture-0.1), ROI #6 (smectite-inter-mixture-1) and ROI #8 (smectite-inter-mixture-0.1) located in Figure 2e,f,g,h and Video 5 (see Table 1 for the explanation of the samples names). *The pure water ice data are from ROI #0 of Poch *et al.* (in press).

References:

Beck, P., Pommerol, A., Schmitt, B., Brissaud, O., **2010**. Kinetics of water adsorption on minerals and the breathing of the Martian regolith. *Journal of Geophysical Research: Planets (1991–2012)* 115.

Belton, M.J.S., Thomas, P., Veverka, J., Schultz, P., A'Hearn, M.F., Feaga, L., Farnham, T., Groussin, O., Li, J.Y., Lisse, C., McFadden, L., Sunshine, J., Meech, K.J., Delamere, W.A., Kissel, J., **2007**. The internal structure of Jupiter family cometary nuclei from Deep Impact observations: The "talps" or "layered pile" model. *Icarus* 187, 332-344.

Bernard, J.-M., Quirico, E., Brissaud, O., Montagnac, G., Reynard, B., McMillan, P., Coll, P., Nguyen, M.-J., Raulin, F., Schmitt, B., **2006**. Reflectance spectra and chemical structure of Titan's tholins: Application to the analysis of Cassini–Huygens observations. *Icarus* 185, 301-307.

Bonnet, J.-Y., Quirico, E., Buch, A., Thissen, R., Szopa, C., Carrasco, N., Cernogora, G., Fray, N., Cottin, H., Roy, L.L., Montagnac, G., Dartois, E., Brunetto, R., Engrand, C., Duprat, J., **2015**. Formation of analogs of cometary nitrogen-rich refractory organics from thermal degradation of tholin and HCN polymer. *Icarus* 250, 53-63.

Bradley, J.P., **1988**. Analysis of chondritic interplanetary dust thin-sections. *Geochimica et Cosmochimica Acta* 52, 889-900.

Brown, A.J., **2014**. Spectral bluing induced by small particles under the Mie and Rayleigh regimes. *Icarus* 239, 85-95.

Brownlee, D., Tsou, P., Aléon, J., Alexander, C.M.D., Araki, T., Bajt, S., Baratta, G.A., Bastien, R., Bland, P., Bleuet, P., **2006**. Comet 81P/Wild 2 under a microscope. *Science* 314, 1711-1716.

Capaccioni, F., Coradini, A., Filacchione, G., Erard, S., Arnold, G., Drossart, P., De Sanctis, M.C., Bockelee-Morvan, D., Capria, M.T., Tosi, F., Leyrat, C., Schmitt, B., Quirico, E., Cerroni, P., Mennella, V., Raponi, A., Ciarniello, M., McCord, T., Moroz, L., Palomba, E., Ammannito, E., Barucci, M.A., Bellucci, G., Benkhoff, J., Bibring, J.P., Blanco, A., Blecka, M., Carlson, R., Carsenty, U., Colangeli, L., Combes, M., Combi, M., Crovisier, J., Encrenaz, T., Federico, C., Fink, U., Fonti, S., Ip, W.H., Irwin, P., Jaumann, R., Kuehrt, E., Langevin,

Y., Magni, G., Mottola, S., Orofino, V., Palumbo, P., Piccioni, G., Schade, U., Taylor, F., Tiphene, D., Tozzi, G.P., Beck, P., Biver, N., Bonal, L., Combe, J.-P., Despan, D., Flamini, E., Fornasier, S., Frigeri, A., Grassi, D., Gudipati, M., Longobardo, A., Markus, K., Merlin, F., Orosei, R., Rinaldi, G., Stephan, K., Cartacci, M., Cicchetti, A., Giuppi, S., Hello, Y., Henry, F., Jacquinod, S., Noschese, R., Peter, G., Politi, R., Reess, J.M., Semery, A., **2015**. The organic-rich surface of comet 67P/Churyumov-Gerasimenko as seen by VIRTIS/Rosetta. *Science* 347.

Carrasco, N., Schmitz-Afonso, I., Bonnet, J.Y., Quirico, E., Thissen, R., Dutuit, O., Bagag, A., Laprévote, O., Buch, A., Giulani, A., Adandé, G., Ouni, F., Hadamcik, E., Szopa, C., Cernogora, G., **2009**. Chemical Characterization of Titan's Tholins: Solubility, Morphology and Molecular Structure Revisited†. *The Journal of Physical Chemistry A* 113, 11195-11203.

Clark, R.N., **1999**. Spectroscopy of Rocks and Minerals, and Principles of Spectroscopy, In: Rencz, A.N. (Ed.), Manual of Remote Sensing, Volume 3, Remote Sensing for the Earth Sciences. John Wiley and Sons, New York, pp. 3-58.

Cooper, C.D., Mustard, J.F., **1999**. Effects of very fine particle size on reflectance spectra of smectite and palagonitic soil. *Icarus* 142, 557-570.

de Bergh, C., Schmitt, B., Moroz, L.V., Quirico, E., Cruikshank, D.P., **2008**. Laboratory Data on Ices, Refractory Carbonaceous Materials, and Minerals Relevant to Transneptunian Objects and Centaurs, In: Barucci, A. (Ed.), The Solar System Beyond Neptune. University of Arizona Press.

Dobrovolsky, O., Kajmakow, E., **1977**. Surface phenomena in simulated comet nuclei, In: Delsemme, A.H. (Ed.), Comets, Asteroids, Meteorites, pp. 37-46.

Duprat, J., Dobrica, E., Engrand, C., Aleon, J., Marrocchi, Y., Mostefaoui, S., Meibom, A., Leroux, H., Rouzaud, J.-N., Gounelle, M., **2010**. Extreme deuterium excesses in ultracarbonaceous micrometeorites from central Antarctic snow. *Science* 328, 742-745.

Fomenkova, M., Kerridge, J., Marti, K., McFadden, L., **1992**. Compositional trends in rock-forming elements of comet Halley dust. *Science* 258, 266-269.

Fomenkova, M.N., **1999**. On the Organic Refractory Component of Cometary Dust. *Space Science Reviews* 90, 109-114.

Fornasier, S., Hasselmann, P. H., Barucci, M.A., Feller, C., Besse, S., Leyrat, C., L. Lara, P. J. Gutierrez, N. Oklay, C. Tubiana, F. Scholten, H. Sierks, C. Barbieri, P. L. Lamy, R. Rodrigo, D. Koschny, H. Rickman, H. U. Keller, J. Agarwal, M. F. A'Hearn, J.-L. Bertaux, I. Bertini, G. Cremonese, V. Da Deppo, B. Davidsson, S. Debei, M. De Cecco, M. Fulle, O. Groussin, C. Güttler, S. F. Hviid, W. Ip, L. Jorda, J. Knollenberg, G. Kovacs, R. Kramm, E. Kührt, M. Küppers, F. La Forgia, M. Lazzarin, J. J. Lopez Moreno, F. Marzari, K.-D. Matz, H. Michalik, F. Moreno, S. Mottola, G. Naletto, M. Pajola, A. Pommerol, F. Preusker, X. Shi, C. Snodgrass, N. Thomas, J.-B. Vincent, **2015**. Spectrophotometric properties of the nucleus of comet 67P/Churyumov-Gerasimenko from the OSIRIS instrument onboard the ROSETTA spacecraft. *Astronomy and Astrophysics*, in press.

Gautier, T., Carrasco, N., Buch, A., Szopa, C., Sciamma-O'Brien, E., Cernogora, G., **2011**. Nitrile gas chemistry in Titan's atmosphere. *Icarus* 213, 625-635.

Gombosi, T.I., Houpis, H.L.F., **1986**. An icy-glue model of cometary nuclei. *Nature* 324, 43-44.

Greenberg, J.M., **1998**. Making a comet nucleus. *Astronomy and Astrophysics* 330, 375-380.

Greenberg, J.M., Li, A., **1999**. Morphological structure and chemical composition of cometary nuclei and dust. *Space Science Reviews* 90, 149-161.

Gundlach, B., Skorov, Y.V., Blum, J., **2011**. Outgassing of icy bodies in the Solar System–I. The sublimation of hexagonal water ice through dust layers. *Icarus* 213, 710-719.

Hanner, M.S., **1999**. The silicate material in comets. *Space Science Reviews* 90, 99-108.

Hapke, B., **1993**. Theory of Reflectance and Emittance Spectroscopy, Cambridge, United Kingdom.

Hartmann, W.K., Tholen, D.J., Cruikshank, D.P., **1987**. The relationship of active comets, "extinct" comets, and dark asteroids. *Icarus* 69, 33-50.

Herbst, E., Van Dishoeck, E.F., **2009**. Complex organic interstellar molecules. *Annual Review of Astronomy and Astrophysics* 47, 427-480.

Huebner, W., **2003**. Composition of Comets: Observations and Models, In: Boehnhardt, H., Combi, M., Kidger, M.R., Schulz, R. (Eds.), Cometary Science after Hale-Bopp. Springer Netherlands, pp. 179-195.

Jessberger, E.K., Christoforidis, A., Kissel, J., **1988**. Aspects of the major element composition of Halley's dust. *Nature* 332, 691-695.

Jessberger, E.K., Kissel, J., Rahe, J., **1989**. The composition of comets, Origin and evolution of planetary and satellite atmospheres, pp. 167-191.

Jewitt, D., **2015**. Rosetta mission: When the dust has settled. *Nature Physics* 11, 96-97.

Jewitt, D., Chizmadia, L., Grimm, R., Prialnik, D., **2007**. Water in the small bodies of the solar system, Protostars and Planets V, pp. 863-878.

Johnson, R.E., Cooper, J.F., Lanzerotti, L.J., Strazzulla, G., **1988**. Radiation formation of a non-volatile comet crust, In: Grewing, M., Praderie, F., Reinhard, R. (Eds.), Exploration of Halley's Comet. Springer Berlin Heidelberg, pp. 889-892.

Jost, B., Pommerol, A., Poch, O., Gundlach, B., Leboeuf, M., Dadras, M., Blum, J., Thomas, N., Experimental characterization of the opposition surge in fine-grained water-ice and high albedo analogs, *Icarus* 264, 109-131.

Kissel, J., Krueger, F.R., **1987**. The organic component in dust from comet Halley as measured by the PUMA mass spectrometer on board Vega 1. *Nature* 326, 755-760.

Kochan, H., Ratke, L., Theil, K., Grun, E., **1990**. Particle emission from artificial cometary surfaces-Material science aspects, Lunar and Planetary Science Conference Proceedings, pp. 401-411.

Kochan, H., Roessler, K., Ratke, L., Heyl, M., Hellmann, H., Schwehm, G., **1989**. Crustal strength of different model comet materials, Physics and Mechanics of Cometary Materials, pp. 115-119.

Kofman, W., Herique, A., Barbin, Y., Barriot, J.-P., Ciarletti, V., Clifford, S., Edenhofer, P., Elachi, C., Eyraud, C., Goutail, J.-P., Heggy, E., Jorda, L., Lasue, J., Levasseur-Regourd, A.-C., Nielsen, E., Pasquero, P., Preusker, F., Puget, P., Plettemeier, D., Rogez, Y., Sierks, H., Statz, C., Svedhem, H., Williams, I., Zine, S., Van Zyl, J., 2015. Properties of the 67P/Churyumov-Gerasimenko interior revealed by CONSERT radar. Science 349.

Kömle, N.I., Steiner, G., Dankert, C., Dettleff, G., Hellmann, H., Kochan, H., Baguhl, M., Kohl, H., Kölzer, G., Thiel, K., Öhler, A., **1991**. Ice sublimation below artificial crusts: Results from comet simulation experiments. *Planetary and Space Science* 39, 515-524.

Kossacki, K., Kömle, N., Leliwa-Kopystyński, J., Kargl, G., **1997**. Laboratory investigation of the evolution of cometary analogs: Results and interpretation. *Icarus* 128, 127-144.

Kuppers, M., Bertini, I., Fornasier, S., Gutierrez, P.J., Hviid, S.F., Jorda, L., Keller, H.U., Knollenberg, J., Koschny, D., Kramm, R., Lara, L.-M., Sierks, H., Thomas, N., Barbieri, C., Lamy, P., Rickman, H., Rodrigo, R., The, O.t., **2005**. A large dust/ice ratio in the nucleus of comet 9P/Tempel 1. *Nature* 437, 987-990.

Lignell, A., Gudipati, M.S., **2014**. Mixing of the Immiscible: Hydrocarbons in Water-Ice near the Ice Crystallization Temperature. *The Journal of Physical Chemistry A* 119, 2607-2613.

Lisse, C., Kraemer, K., Nuth, J., Li, A., Joswiak, D., **2007**. Comparison of the composition of the Tempel 1 ejecta to the dust in Comet C/Hale–Bopp 1995 O1 and YSO HD 100546. *Icarus* 187, 69-86.

Lisse, C., VanCleve, J., Adams, A., A'hearn, M., Fernández, Y., Farnham, T., Armus, L., Grillmair, C., Ingalls, J., Belton, M., **2006**. Spitzer spectral observations of the Deep Impact ejecta. *Science* 313, 635-640.

Mahjoub, A., Carrasco, N., Dahoo, P.-R., Gautier, T., Szopa, C., Cernogora, G., **2012**. Influence of methane concentration on the optical indices of Titan's aerosols analogues. *Icarus*.

Mermut, A.R., Cano, A.F., **2001**. Baseline studies of the clay minerals society source clays: chemical analyses of major elements. *Clays and Clay Minerals* 49, 381-386.

Nakamura, K., Messenger, S., Keller, L., **2005**. TEM and NanoSIMS Study of Hydrated/Anhydrous Phase Mixed IDPs: Cometary or Asteroidal Origin?, 36th Annual Lunar and Planetary Science Conference, p. 1824.

Oehler, A., Neukum, G., **1991**. Visible and near IR albedo measurements of ice/dust mixtures. *Geophysical Research Letters* 18, 253-256.

Pat-El, I., Laufer, D., Notesco, G., Bar-Nun, A., **2009**. An experimental study of the formation of an ice crust and migration of water vapor in a comet's upper layers. *Icarus* 201, 406-411.

Pernot, P., Carrasco, N., Thissen, R., Schmitz-Afonso, I., **2010**. Tholinomics—Chemical analysis of nitrogen-rich polymers. *Anal. Chem.* 82, 1371-1380.

Poch, O., Pommerol, A., Jost, B., Carrasco, N., Szopa, C., Thomas, N., Sublimation of ice tholins mixtures: A morphological and spectro-photometric study. Icarus, in press. http://dx.doi.org/10.1016/j.icarus.2015.11.006

Pommerol, A., Jost, B., Poch, O., El-Maarry, M.R., Vuitel, B., Thomas, N., **2015a**. The SCITEAS experiment: Optical characterizations of Sublimating icy planetary analogues. *Planetary and Space Science* 109, 106-122.

Pommerol, A., Schmitt, B., Beck, P., Brissaud, O., **2009**. Water sorption on martian regolith analogs: Thermodynamics and near-infrared reflectance spectroscopy. *Icarus* 204, 114-136.

Pommerol, A., Thomas, N., Affolter, M., Portyankina, G., Jost, B., Seiferlin, K., Aye, K.M., **2011**. Photometry and bulk physical properties of Solar System surfaces icy analogs: The Planetary Ice Laboratory at University of Bern. *Planetary and Space Science* 59, 1601-1612.

Pommerol, A., Thomas, N., El-Maarry, M.R., Pajola, M., Groussin, O., Auger, A.-T., Oklay, N., Fornasier, S., Feller, C., Davidsson, B., Gracia, A., Jost, B., Marschall, R., Poch, O., Barucci, M.A., Bertaux, J.-L., La Forgia, F., Keller, H.U., co-authors, **2015b**. OSIRIS observations of meter-size exposures of H2O ice at the surface of 67P/Churyumov-Gerasimenko and interpretation using laboratory experiments. *A&A*.

Prialnik, D., Mekler, Y., **1991**. The formation of an ice crust below the dust mantle of a cometary nucleus. *The Astrophysical Journal* 366, 318-323.

Protopapa, S., Sunshine, J.M., Feaga, L.M., Kelley, M.S.P., A'Hearn, M.F., Farnham, T.L., Groussin, O., Besse, S., Merlin, F., Li, J.-Y., **2014**. Water ice and dust in the innermost coma of comet 103P/Hartley 2. *Icarus* 238, 191-204.

Quirico, E., Montagnac, G., Lees, V., McMillan, P.F., Szopa, C., Cernogora, G., Rouzaud, J.N., Simon, P., Bernard, J.M., Coll, P., **2008**. New experimental constraints on the composition and structure of tholins. *Icarus* 198, 218-231.

Ratke, L., Kochan, H., **1989**. Fracture mechanical aspects of dust emission processes from a model comet surface, Physics and Mechanics of Cometary Materials, pp. 121-128.

Rietmeijer, F., Mukhin, L., Fomenkova, M., Evlanov, E., **1989**. Layer silicate chemistry in P/comet Halley from PUMA-2 data, Lunar and Planetary Science Conference, p. 904.

Roessler, K., Hsiung, P., Kochan, H., Hellmann, H., Duren, H., Theil, K., Kolzer, G., **1990**. A model comet made from mineral dust and H2O-CO2 ice: Sample preparation development, Lunar and Planetary Science Conference Proceedings, pp. 379-388.

Rosenthal, W., Saleta, J., Dozier, J., **2007**. Scanning electron microscopy of impurity structures in snow. *Cold Regions Science and Technology* 47, 80-89.

Sagan, C., Khare, B.N., **1979**. Tholins: organic chemistry of interstellar grains and gas. *Nature* 277, 102-107.

Salisbury, J.W., Wald, A., **1992**. The role of volume scattering in reducing spectral contrast of reststrahlen bands in spectra of powdered minerals. Icarus 96, 121-128.

Saunders, S.R., Fanale, F.P., Parker, T.J., Stephens, J.B., Sutton, S., **1986**. Properties of filamentary sublimation residues from dispersions of clay in ice. *Icarus* 66, 94-104.

Sears, D.W.G., Kochan, H.W., Huebner, W.F., **1999**. Laboratory simulation of the physical processes occurring on and near the surfaces of comet nuclei. *Meteoritics & Planetary Science* 34, 497-525.

Seiferlin, K., Spohn, T., Benkhoff, J., **1995**. Cometary ice texture and the thermal evolution of comets. *Advances in Space Research* 15, 35-38.

Storrs, A.D., Fanale, F.P., Saunders, R.S., Stephens, J.B., **1988**. The formation of Filamentary Sublimate Residues (FSR) from mineral grains. *Icarus* 76, 493-512.

Sunshine, J.M., Groussin, O., Schultz, P.H., A'Hearn, M.F., Feaga, L.M., Farnham, T.L., Klaasen, K.P., **2007**. The distribution of water ice in the interior of Comet Tempel 1. *Icarus* 190, 284-294.

Szopa, C., Cernogora, G., Boufendi, L., Correia, J.J., Coll, P., **2006**. PAMPRE: A dusty plasma experiment for Titan's tholins production and study. *Planetary and Space Science* 54, 394-404.

Thiel, K., Koelzer, G., Kochan, H., Ratke, L., Gruen, E., Koehl, H., **1989**. Dynamics of crust formation and dust emission of comet nucleus analogues under isolation, Physics and Mechanics of Cometary Materials, pp. 221-225.

Thiel, K., Koelzer, G., Kohl, H., **1991**. Dust emission of mineral/ice mixtures: Residue structure and dynamical parameters. *Geophysical Research Letters* 18, 281-284.

Thomas, N., Sierks, H., Barbieri, C., Lamy, P.L., Rodrigo, R., Rickman, H., Koschny, D., Keller, H.U., Agarwal, J., A'Hearn, M.F., Angrilli, F., Auger, A.-T., Barucci, M.A., Bertaux, J.-L., Bertini, I., Besse, S., Bodewits, D., Cremonese, G., Da Deppo, V., Davidsson, B., De Cecco, M., Debei, S., El-Maarry, M.R., Ferri, F., Fornasier, S., Fulle, M., Giacomini, L., Groussin, O., Gutierrez, P.J., Güttler, C., Hviid, S.F., Ip, W.-H., Jorda, L., Knollenberg, J., Kramm, J.-R., Kührt, E., Küppers, M., La Forgia, F., Lara, L.M., Lazzarin, M., Moreno, J.J.L., Magrin, S., Marchi, S., Marzari, F., Massironi, M., Michalik, H., Moissl, R., Mottola, S., Naletto, G., Oklay, N., Pajola, M., Pommerol, A., Preusker, F., Sabau, L., Scholten, F.,

Snodgrass, C., Tubiana, C., Vincent, J.-B., Wenzel, K.-P., **2015**. The morphological diversity of comet 67P/Churyumov-Gerasimenko. *Science* 347.

Weber, C., Heuser, M., Stanjek, H., **2014**. A collection of aspect ratios of common clay minerals determined from conductometric titrations. *Clay Minerals* 49, 495-498.

Weissman, P.R., **1986**. Are cometary nuclei primordial rubble piles? *Nature* 320, 242-244.

Wooden, D.H., **2008**. Cometary Refractory Grains: Interstellar and Nebular Sources. *Space Science Reviews* 138, 75-108.

Wozniakiewicz, P., Ishii, H., Kearsley, A., Burchell, M., Bradley, J., Teslich, N., Cole, M., **2010**. Survivability of cometary phyllosilicates in Stardust collections and implications for the nature of comets, Lunar and Planetary Science Conference, p. 2357.

Yoldi, Z., Pommerol, A., Jost, B., Poch, O., Gouman, J., Thomas, N., **2015**. VIS-NIR reflectance of water ice / regolith analogue mixtures and implications for the detectability of ice mixed within planetary regoliths. *Geophysical Research Letters* 42, 6205-6212.

Zolensky, M., Bland, P., Brown, P., Halliday, I., **2006**. Flux of Extraterrestrial Materials. *Meteorites and the Early Solar System II*, 869-888.